SYNTHESIS AND CHARACTERIZATION OF ZSM TYPE PENTASIL ZEOLITES

A THESIS

SUBMITTED TO THE

UNIVERSITY OF POONA

FOR THE DEGREE OF

DOCTOR OF PHILOSOPHY

BY

ARVIND NARAYAN KOTASTHANE
M. Sc.

PHYSICAL CHEMISTRY DIVISION
NATIONAL CHEMICAL LABORATORY
PUNE – 411 008 (INDIA)

SEPTEMBER 1984

Dedicated

To My Son

COMPUTERISED

Certified that the work incorporated in the thesis SYNTHESIS AND CHARACTERIZATION OF ZSM TYPE PENTASIL ZEOLITES submitted by Shri Arvind Narayan Kotasthane was carried out under my supervision. Such materials as has been obtained from other sources are duly acknowledged in the thesis.

S. B. Kulkarni

Dr. Miss S. B. Kulkarni
Supervisor

A C K N O W L E D G E M E N T

I gratefully acknowledge the persistent guidance of Dr. Miss S. B. Kulkarni in completion of this work. As a Supervisor, she had spared no pains in helping me to make this investigation a success.

I express my deep gratitude to Dr. Paul Ratnasamy for his valuable advise and suggestions from time to time. Without his help, I would not have been able to complete the work.

It is my pleasant duty to thank Dr. A.P. B. Sinha, Head, Physical Chemistry Division, NCL, for his constant encouragement.

I sincerely thank my colleagues Dr. V. P. Shiralkar, Dr. S. G. Hegde and Mr. I. Balakrishnan for their friendly help and untiring cooperation during the experimental part of the thesis.

I thank Mr. S. M. Kulkarni who completed the typing work in a decent manner and in the shortest possible time.

Lastly, I wish to thank Director, NCL, for allowing me to submit this investigation in the form of a Ph.D. Thesis.

A. N. Kotasthane

C H A P T E R - I

GENERAL INTRODUCTION

CONTENTS

1.1. INTRODUCTION

Zeolites are microporous, crystalline, hydrated aluminosilicates having a framework structure composed of AlO_4 and SiO_4 tetrahedra, linked through oxygen atoms forming a rigid three-dimensional structure. Zeolites may be represented by the empirical oxide formula,

$$M_{2/n}O.Al_2O_3.xSiO_2.yH_2O$$

where $x \geq 2$ and n is the cation valence. The charge deficiency resulting from the tetrahedral coordination of trivalent aluminium atoms is compensated by the exchangeable cations M^{n+} in the structure. In general, the structural formula of the crystallographic unit cell of a zeolite is expressed as,

$$M_{p/n}[(AlO_2)_x(SiO_2)_y].zH_2O$$

where n is the charge on p valent cation and z is the water of hydration. In general, the ratio $y/x > 1$ and $(x + y)$ is the total number of tetrahedra in the unit cell. The square bracket represents the framework composition.

1.2. HISTORICAL BACKGROUND

The history of zeolites began with the discovery of Stilbite in 1756 by Cronstedt[1]. He first recognized the group of minerals consisting of hydrated aluminosilicates.

Because the minerals exhibited intumescence when heated in a blowpipe flame, he named them ZEOLITES, a Greek word meaning 'Boiling Stone'. In 1840, Damour[2] observed reversible dehydration exhibited by the crystals of zeolites without any apparent change in their morphology. In 1925, Weigel and Steinhoff[3] studied the adsorption properties of dehydrated chabazite crystals. They found that dehydrated chabazite rapidly adsorbed vapors of water, methyl alcohol and ethyl alcohol; however, when exposed to acetone, ether and benzene no adsorption occurred. To account for this phenomenon of selective sorption, McBain[4] interpreted these results in terms of molecular size difference and proposed the term 'Molecular Sieves'.

1.3. THE EVOLUTION IN MATERIALS

The year 1979 marked the twenty-fifth anniversary of the commercial birth of molecular sieve zeolites as a new class of industrial materials. They were introduced in late 1954 as adsorbents for industrial separations and purifications. Milton[5] reviewed the beginning and development of molecular sieve zeolites in 1967. An in-depth coverage of zeolite molecular sieves is given by Barrer[6] and Breck[7]. Recent up-to-date review articles on the applications of molecular sieve zeolites[8] as adsorbents[9], catalysts[10,11] and ion-exchangers[12] cover the persistant development in these areas. It is of interest to note that the success of

molecular sieve zeolites has been due primarily to the discovery of new materials. An attempt is made in the following paragraphs, to trace the changes in those discoveries as they were evolved and developed.

1.3.1. Low Silica Zeolites or Aluminium-rich Zeolites

The discovery of zeolites A and X by Milton[13] at the Union Carbide Corporation Laboratories marked their lasting commercial prominence. Both A and X zeolites are nearly 'saturated' in the aluminium in the framework composition with a molar ratio of $Si/Al \simeq 1$. As a consequence, they contain the maximum number of cation exchange sites and thus the highest exchange capacity. These characteristics give them the most highly heterogeneous surface. Their surface is highly selective for water, polar and polarizable molecules which finds its use in drying and purification. Their pore volumes of $\simeq 0.5$ cm^3/cm^3 are the highest known for zeolites and give them a distinct economic advantage in bulk separation and purifications. The pore sizes achievable by cation exchange of types A and X span the entire range from the smallest pore-sized zeolite known, Cs-A at 0.2 nm in size[14] through the 0.3 nm potassium A, the 0.4 nm sodium-A, the 0.5 nm calcium-A, to the largest known which is about 0.8 nm in sodium-X. This large pore of zeolite X was a key to its introduction as a catalytic cracking catalyst.

1.3.2. Intermediate Silica Zeolites

The next evolution in zeolite materials was an impetus to synthesize more siliceous zeolites, to improve stability characteristics, both thermal and acid. It was recognized by the scientists in the early 1950s that the tetrahedral framework aluminium provided a site of instability for attack by acid and water vapor or steam. Also, the siliceous mineral zeolite mordenite was known with Si/Al = 5, possessing superior stability characteristics. Breck[15] provided the first success in this quest with the discovery of the third commercially important molecular sieve zeolite type Y, with Si/Al = 1.5-3.0, and a framework topology like that of X.

The next important synthetic zeolite introduced in early 1960s was a large pore mordenite made by the method of Sand[16] and marketed as ZEOLON by the Norton Company[17]. Other zeolites with intermediate Si/Al composition of 2 to 5 which have achieved commercial status, are the zeolite minerals mordenite, erionite, chabazite and clinoptilolite, and the synthetic zeolite Omega[18].

1.3.3. High-Silica Zeolites

The recent development for more siliceous molecular sieve composition was achieved in the late 1960s and the early 1970s. High-Silica zeolites synthesized at

the Mobil Research and Development Laboratories, exemplified first by zeolite beta discovered by Wadlinger, Kerr and Rosinki[19], and latter ZSM-5 (Zeolite Socony Mobil) discovered by Argauer and Landolt[20]. Subsequently, ZSM-11[21], ZSM-12[22] and ZSM-34[23] were reported. The generic name 'Pentasil Zeolite' has been used to encompass the members of a family of high-silica zeolites[24]. The pentasil zeolites have Si/Al ratios from 10 to 100 or higher. In contrast to the 'low' and 'intermediate' silica zeolites, they have heterogeneous hydrophilic surfaces within a porous crystal. In addition to this, they contain a small concentration of aluminium in the framework and the accompanying stoichiometric cation exchange sites. This allows introduction of acidic OH groups via ion exchange reactions, essential to the development of acid hydrocarbon catalysis properties.

1.3.4. Silica Molecular Sieve

The ultimate in siliceous molecular sieve, silicalite[25], was synthesized in the 1970s containing essentially no aluminium or cation sites. Silicalite exhibits a high degree of organophilic-hydrophobic character. Silicalite reportedly[26] has the same framework topology as zeolite ZSM-5.

A summary of the evolution of molecular sieve materials is given in Table 1.1 with framework Si/Al variation.

T A B L E - 1.1

The Evolution of Molecular Sieve Materials[a]

Low Si/Al Zeolites (1 to 1.5)

A, X

Intermediate Si/Al Zeolites (~2 to 5)

(A) Natural Zeolites

Erionite, Chabazite, Clinoptilolite, Mordenite.

(B) Synthetic Zeolites

Y, L, large-port mordenite, Omega.

High Si/Al Zeolites (~10 to 100, or even more)

(A) By thermochemical modification

Highly siliceous variants of Y, mordenite, erionite.

(B) By direct synthesis

ZSM-5.

Silica Molecular Sieves

Silicalite

---

a : Flanigen, E.M., Pure and Appl. Chem., Vol. 52, 9, p. 2193, 1980.

Since the present thesis is concerned with the "Synthesis and Characterization of ZSM type Pentasil Zeolites", further discussion is limited to ZSM-5 zeolites only.

1.4. ZEOLITE SYNTHESIS

1.4.1. Synthesis of aluminosilicate zeolite

Progress in zeolite synthesis in the last several years has been mostly in experimental realm and has covered a voluminous patent literature[27]. Most of the work has been conducted empirically, and although a few guidelines have been given, there is not, as yet, a quantitative basis for this type of synthesis. Zeolites are synthesized by crystallizing reactive aluminosilicate gels with alkali and alkaline earth metal hydroxides, under hydrothermal conditions. The essential process underlying the hydrothermal synthesis of most zeolites is the conversion of an amorphous solid into a crystalline one in the presence of an alkaline aqueous solution. An excellent review on synthesis and crystallization of zeolites by Zhdanov[28] and Flanigen[29] includes the synthesis conditions, compositions and other properties.

The early discovery of synthetic zeolites with low silica to alumina ratios (< 10) involves typically very high pH (> 13) of the synthesis gels which were usually crystallized at 100°C or less. Well-known examples of such a group are zeolites A, X, Y, L and synthetic mordenite. In the early 1960s,

the tetramethylammonium cation (TMA) was introduced as the first organic cation to be used in zeolite synthesis. There are various examples of zeolite formation in presence of TMA-hydroxide. The use of organic bases as replacements for inorganic bases was initiated in 1961 by Barrer and Denny[30] and by Kerr and Kokotailo[30a]. As a result, more siliceous materials were synthesized, for example, N-A[31], ZK-4[32] and ∝[33], all having A type structure but with higher silica to alumina ratio. The member of the high-silica zeolite (SiO_2/Al_2O_3 > 20) family, Zeolite β, was synthesized using tetraethylammonium cation (TEA)[34]. The use of other quaternary ammonium ions in zeolite synthesis clearly had a major impact. Shortly after these discoveries the synthesis of ZSM-5(Zeolite Socony Mobil) using tetrapropylammonium cation (TPA) was disclosed in a patent publication[20]. Subsequently, the other members of high-silica zeolite compositions, ZSM-11[19],-12[35],-21[36], -34[37] and-39[38] were reported.

Erdem and Sand[38a] emphasized the essential role of Na^+ (or K^+) ions, added as hydroxides, in the formation of ZSM-5 and reported that the latter could not be obtained in the absence of alkali.

The success in synthesizing a pure silica molecular sieve, by Grose and Flanigen[25] led to yet another class of

interesting materials. Silicalite-1, Silicalite-2[39], TEA-silicate[40], and Holdslite[41] are examples of pure silica molecular sieve compositions.

1.4.2. Zeolite Synthesis with Isomorphous Substitution

Considerable work has been performed in producing clay minerals in which isomorphous replacements are effected by elements not usually found in naturally occurring clay minerals, under high pressures[42]. Similarly, Group I-VIII elements can replace other elements such as aluminium in zeolite framework has been demonstrated under high-temperature conditions[43,44]. In another series of high temperature preparations, Eitel et al[45] introduced Y, La and Nd in place of aluminium in synthetic nepheline type phases. Besides, all these replacements refer to synthesis at high temperatures in the absence of water. Zeolite formation at low temperatures under alkaline aqueous conditions poses a very different situation. It is of interest to examine claims[46] that the zeolites bearing such metallic elements in the framework of zeolites have been made. Zeolites having the ZSM-5 topology were synthesized, in which iron and chromium were considered to occupy some of the tetrahedral framework sites. The iron-bearing ZSM-5 was prepared from reaction mixture containing silica, ferric-oxide and caustic soda, with incorporation of hexamethylene diamine as the organic base. This was

crystallized in the low temperature range, 140-160°C for 2 to 4 days. The chromium-bearing ZSM-5 was also prepared under similar conditions. In another study, Barrer et al[47] synthesized iron-bearing cancrinite from kaolinite by heating at 80°C for 5 days. The Mössbauer spectrum showed the presence of Fe^{III} in cancrinite.

An important family of molecular sieve materials, aluminophosphate was synthesized recently by Wilson et al[48]. These represent the first family of framework oxide molecular sieve without silica and designated as 'ALPO'.

Thus, it is observed from the above literature survey that, variation in two important parameters; cation-base system and silica to alumina ratio, has generally been used in the synthesis of zeolites. However, their synthesis still uses the basic reactive gel crystallization method developed by Milton[5] in the late 1940s. The use of a variety of quaternary ammonium ions has made possible the extension of zeolite science into the high-Si/Al region. Secondly, many other structure types e.g. β, ZSM-4,-11, -8,-12,-34,-39 have been made with the use of organic base (Table 1.2 Modification of zeolite framework by isomorphous substitution is also possible, particularly under low temperature and aqueous alkaline conditions.

TABLE - 1.2

Organic Zeolite Structure Relationship[104]

Organic	Structure	Structure type
TEA	β	?
	ZSM-8	ZSM-5
	ZSM-12	?
	ZSM-20	Faujasite
	Mordenite	Mordenite
	ZSM-25	?
Methyltriethyl ammonium	ZSM-12	?
TPA	ZSM-5	ZSM-5
n-Propylamine	ZSM-5	ZSM-5
TBA	ZSM-11	ZSM-11
Choline	ZSM-38	Ferrierite
	ZSM-34	Erionite-offretite
	ZSM-43	?
	CZH-5	?
TMA + TEA	ZSM-39	ZSM-39
TMA + n-propylamine	ZSM-39	ZSM-39
	ZSM-48	ZSM-12?
Pyrrolidine	ZSM-35	Ferrierite
	ZSM-21	Ferrierite
	ZSM-23	?
1,2-Diaminoethane	ZSM-5	ZSM-5
	ZSM-21	Ferrierite
	ZSM-35	Ferrierite
1,3-Diaminopropane	ZSM-35	Ferrierite, ZSM-5
	ZSM-5	
1,4-Diaminobutane	ZSM-35	Ferrierite, ZSM-5
1,5-Diaminopentane	ZSM-5	ZSM-5
1,6-Diaminohexane	ZSM-5	ZSM-5
1,7-Diaminoheptane	ZSM-11	ZSM-11

Table 1.2 .. continued

1,8-Diaminooctane	ZSM-11	ZSM-11
	ZSM-48	
1,9-Diaminononane	ZSM-11	ZSM-11
1,10-Diaminodecane	ZSM-11	ZSM-11
DDO	ZSM-10	?
	ZK-5	?
MDO	ZK-20	Levynite
MQ	LZ-132	Levynite
	NU-3	Levynite
TQA	ZSM-18	?
BP	LOSOD	LOSOD
Dihexamethylene-triamine	ZSM-30	?
Neopentylamine	Mordenite	Mordenite

1.5. STRUCTURE OF ZSM-5 ZEOLITES

ZSM-5 is a member of a new class of shape-selective zeolite with a unique channel structure. This structure is distinctly different from the familiar wide-pore faujasite and the narrow-pore zeolites (Fig. 1.1(a)).

The crystal structure of ZSM-5 was reported in 1978[26]. The framework of ZSM-5 pentasil zeolite contains a novel configuration of linked tetrahedra consisting of eight five-membered rings. The channel system, which is three-dimensional and defined by ten-membered rings of tetrahedra, consists of intersecting straight [010] and sinusoidal (zig-zag) [100] channels as shown in Fig. 1.1(d). Straight channels has elliptical openings of free diameter of 0.52 x 0.58 nm and the Sinusoidal channel has near circular openings of free diameter of 0.54 x 0.56 nm. A similar framework structure has been found in silicalite[24], which is an alumina-free three dimensional crystalline SiO_2.

The as-synthesized, uncalcined ZSM-5 zeolite, generally exhibits orthorhombic symmetry with lattice parameters a = 20.1Å, b = 19.9Å, and c = 13.4Å. However, a reversible transformation to monoclinic symmetry has been observed due to certain treatments, such as calcination, ion-exchange etc.[49]. The framework density of Si + Al per $1000Å^3$ is 17.9 while unit cell volume is $5363\ A^{\circ 3}$.

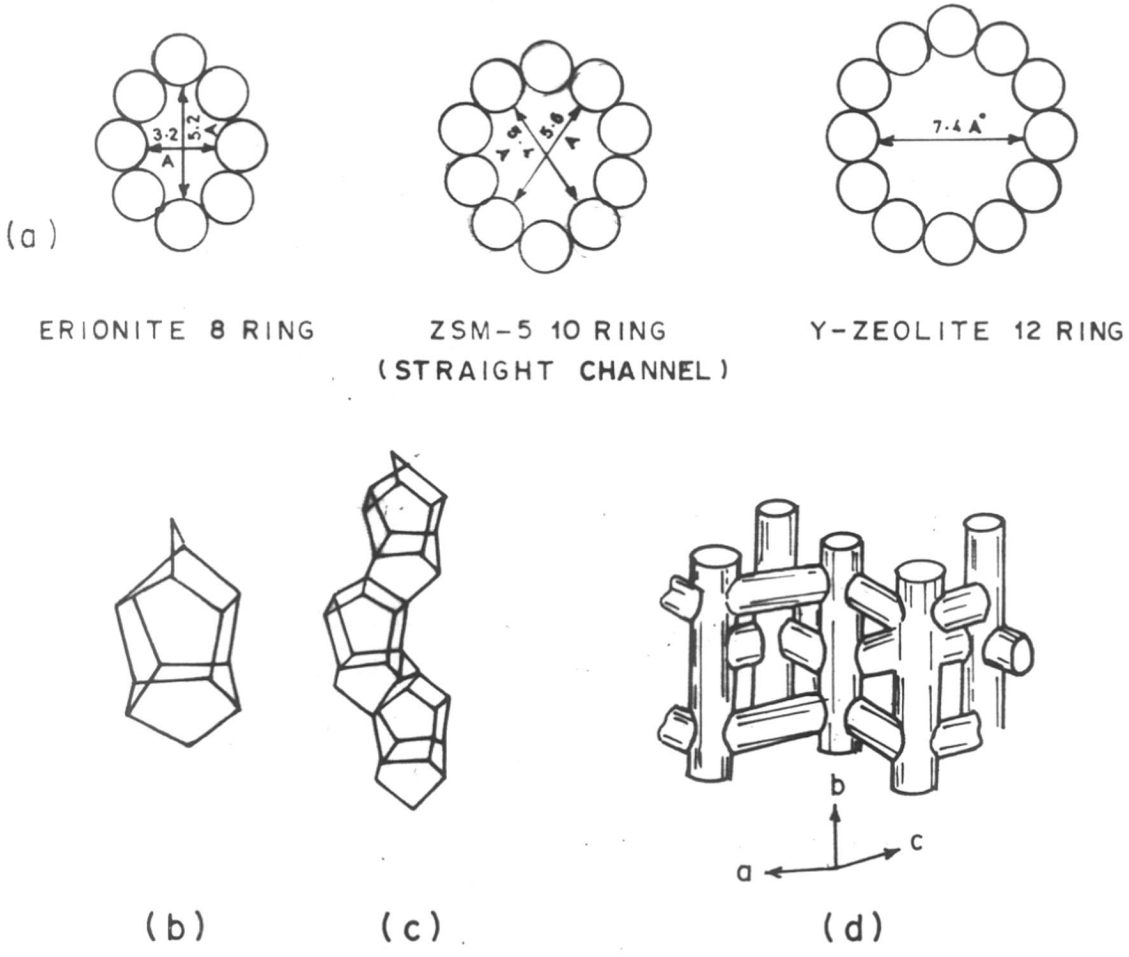

FIG. 1·1. STRUCTURE OF ZSM-5 PENTASIL ZEOLITE

(a) TYPICAL ZEOLITE PORE GEOMETRIES
(b) CHARACTERISTIC CONFIGURATION OF ZSM-5
(c) LINKAGE OF ZSM-5
(d) CHANNEL STRUCTURE OF ZSM-5

The composition of the unit-cell in Na form is,

$$Na_nAl_nSi_{96-n}O_{192}\cdot 16H_2O$$

where n < 27 and typically about 3[20]. The number of aluminium atoms per unit-cell is obtained from the relation[26]

$$N_{Al} = \frac{96}{1 + R}$$

where $R = N_{Si}/N_{Al}$ and N_{Si}, N_{Al} are gm atoms of silicon and aluminium respectively.

1.6. PHYSICO-CHEMICAL CHARACTERIZATION OF ZEOLITES

1.6.1. X-ray Diffraction

X-ray diffraction is one of the most important classical techniques which has been utilised not only to determine the zeolite structures but also employed for quantitative phase identification and to understand the kinetics of crystallization[15,50-53a]. The apparent framework symmetry change with small change in lattice parameters has been reported[49] for ZSM-5 zeolites using X-ray diffraction technique. Wu et al[49] observed a reversible transformation of framework symmetry on increasing Si/Al ratio in ZSM-5 framework. Bibby et al[54] reported the use of X-ray diffraction technique for estimating the average alumina content in the ZSM-5 crystals. The X-ray diffraction technique has been developed[55] to provide a rapid method for estimating SiO_2/Al_2O_3 ratios over a range of 30 to 150.

1.6.2. Infrared Spectroscopy

Infrared spectroscopy is a sensitive analytical technique and has been employed to investigate the structural features of zeolite framework. Infrared data on the fundamental vibrations in mid-ir (200-1300 cm^{-1}) region of the framework structure have been published[56-58] for many mineral and synthetic zeolites. Systematic investigations[59] on the framework structure of zeolites A, N-A, X, Y, ZK-5, Omega, in mid-infrared region have been reported. Flanigen and Grose[60] have used mid-infrared spectroscopy to characterize the framework of phosphate zeolites and to establish a proof of phosphorus substitution. Because of the shorter tetrahedral P-O bond distance of 1.54Å, compared to a distance of 1.61Å for Si-O and 1.75Å for Al-O, a shift to a higher frequency for the main asymmetric stretch band was observed as a function of phosphorus substitution in the zeolite framework. Wu et al[61] studied the decomposition of tetramethylammonium Y-zeolite and observed that the absorption bands, typical of the amine near 3028, 2965, 2930 and 1480 cm^{-1} decreased and absorption bands near 3735, 3637 and 3550 cm^{-1}, typical of decationized Y appeared.

The acidic properties of OH groups in zeolites, as well as properties of Lewis and Brönsted acid centres of HZSM-5 have been extensively investigated[62-64]. The types of

hydroxyl groups are characterized by the presence of absorption band at 3600 and 3720 cm^{-1}, corresponding to strong and weak Brönsted acid sites respectively[64]. Registering IR spectra after adsorption of base molecules like pyridine and ammonia on HZSM-5, has revealed the presence of Brönsted and Lewis acid sites[65]. With increase in temperature of calcination, above 675 K, dehydroxylation takes place and the number of Brönsted acid sites decreases while that of strong Lewis acid sites increases.

1.6.3. Nuclear Magnetic Resonance Spectroscopy (NMR)

The knowledge of the intimate structure of crystalline alumino-silicates possessing corner-sharing SiO_4 and AlO_4 tetrahedra is of paramount importance to rationalize and predict their catalytic properties. Since the advent of high-resolution solid state n.m.r. technique, different types of nuclei can easily be detected. The existence of discrete sites in zeolite samples, characterized by different environments can be detected with the help of high-resolution solid state ^{27}Al and ^{29}Si n.m.r. spectroscopy.

A recent high resolution solid state ^{13}C n.m.r. study, using cross-polarization (CP) and magic angle spinning (MAS), has proved that the occluded organic species were chemically intact in as-synthesized ZSM-5

zeolite channels[66]. Nagy et al[67] also confirmed this by using only ^{13}C n.m.r. magic angle spinning technique and showed that two types of methyl groups could be distinguished by ^{13}C n.m.r. By employing magic angle spinning proton n.m.r. for H-ZSM-5, two adsorbing sites were detected from the differences in the proton chemical shift[68]. The low field resonance was assigned to protons at the Si-OH-Al sites, and the high field resonance at the ≡ SiOH sites. In another ^{29}Si n.m.r. measurements, two types of spectra were obtained for ZSM-5; a broad, featureless spectrum and a well resolved one[69]. This behaviour was attributed to the fact that orthorhombic symmetry always exhibits a featureless ^{29}Si n.m.r. spectrum whereas for monoclinic symmetry zeolite samples, a well resolved ^{29}Si n.m.r. spectrum was observed. Lippman and coworkers[70] have demonstrated that in zeolite minerals, chemically distinct Si species produce resonance with intensities proportional to their multiplicity in the unit cell. The application of this technique to the study of synthetic zeolites has been reported for ZSM-5[71] and faujasites[72].

Because of the complex nature of zeolite structures which often exhibit low symmetry and a relatively large number of tetrahedral sites, their n.m.r. spectra are difficult to interprete. However, measurements

with high resolution ^{29}Si n.m.r. spectroscopy for ZSM-39 zeolite sample, Higgins et al.[73] reported that possible deviations from ideal crystallographic symmetry may be detected under certain conditions.

1.6.4. TEMPERATURE PROGRAMMED DESORPTION (TPD)

Acidic properties of ZSM-5 type pentasil zeolites have been reported by Vedrine et al.[65,74]. Anderson et al.[75] studied TPD of ammonia on NaZSM-5, HZSM-5, and silicalite to assess the energetic distribution of sorption sites for the bases. They observed two desorption peaks for chemisorbed ammonia on HZSM-5 with maxima at about 403 K and 773 K. Only the 773 K peak was thought to be connected with the active sites in the methanol conversion processes. Jacobs et al.[76] studied the ammonia desorption from US-Y and ZSM-5 zeolites and observed that both the zeolites released ammonia over a large temperature range, indicating the existence of weak, medium and strong acid sites. The amount of ammonia desorbed above 753 K clearly indicated the abundance of very strong acid sites on HZSM-5.

Topsøe et al.[77] investigated acidic properties of HZSM-5 by TPD of ammonia from fresh and partially deactivated catalysts. Three different states α, β and γ of chemi-adsorbed ammonia in the

range 333-373, 423-473, and 693-778 K were observed for fresh catalyst. In case of partially deactivated sample (for the reaction methanol to hydrocarbon at 645 K) the β state was absent and α-state was strongly reduced. The activation energies for the desorption of ammonia from α, β and γ states were found to be 84.6, 96.7 and 162.3 KJ $mole^{-1}$ respectively.

1.6.5. THERMAL STABILITY OF ZEOLITES

The importance of thermal stability and the interest in high temperature properties of zeolites is largely related to their use in petroleum catalytic cracking reactions. Thermal properties can be related to other physico-chemical characteristics of zeolites and thus provide some predictive utility. For example, the DTA structural collapse temperature of several stabilized type Y samples is related to the structure-sensitive symmetrical stretching frequency in the framework infrared region investigated by Flanigen and coworkers[59].

It is known that the thermal stability of zeolite framework structure increases with the Si/Al ratio[78]. The crystal structure of ZSM-5 transforms from orthorhombic to monoclinic symmetry on calcination[79], when SiO_2/Al_2O_3

ratio is greater than 170. The monoclinic symmetry remained unchanged by NH_4^+ ion-exchange, however, it was reformed to orthorhombic by protonation. The SiO_2/Al_2O_3 ratio was found to play major role on the symmetry change of ZSM-5. Zeolite ZSM-5 possesses exceptionally high degree of thermal and hydrothermal stability. Silicalite, the end member of ZSM-5 pentasil family is stable in air upto 1373 K and is converted slowly to amorphous silica at 1573 K[25].

1.6.6. Sorption and Diffusion Studies

Zeolites are highly porous, crystalline adsorbents with pore opening of fixed and uniform dimensions. The channels and cavities which uniformly occupy the entire volume of the adsorbent provide the essential internal surface for adsorption. The molecular sieving properties of the zeolites are uniquely determined by their pore dimensions. The synthetic zeolites have been characterized by their sorption capacities for various organic compounds. The molecular exclusion properties of these zeolites have been used to estimate their pore opening and shape selective properties.

Sorption of various gases and vapours on natural as well as synthetic zeolites have been extensively studied by Barrer and coworkers[80-82]. They estimated[83,84] various thermodynamic parameters such as entropy, heat and free energy of sorption. Sorption of various hydrocarbons on ZSM-5

pentasil zeolites have been reported[85,86]. From the knowledge of critical dimensions of adsorbed molecules, channel length occupied per unit cell by adsorbates has been evaluated. A theoretical channel length has been calculated for ZSM-5 zeolites, amounting to total value of 0.88 nm for both type of channels and 0.55 nm for elliptical channels[85].

Anderson et al.[75] compared the sorption behaviour of some hydrocarbons with more than six carbon atoms on HZSM-5, Na-ZSM-5, and silicalite at 298 K and P/P_o = 0.5. The lower accessibility to the inner pore structure of Na-ZSM-5 was attributed to the blocking of channels by the Na^+ ions. They concluded that the openings of HZSM-5 and silicalite should fall in between 0.58 nm and 0.61 nm, and for Na-ZSM-5 between 0.43 nm and 0.56 nm. The sorption property of silicalite has also been studied by Flanigen et al.[25]. They reported that in addition to its ability to serve as a molecular sieve by adsorbing benzene (0.585 nm) and rejecting neopentane (0.62 nm), silicalite also shows surface adsorption selectivity. Silicalite exhibits a distinct preference for adsorbing organic molecules (organophilic) rather than water molecules (hydrophobic). The relative intracrystalline mobility of hydrocarbons in ZSM-5 channel system have been investigated by Meisel et al.[87] who found that n-paraffins and monomethylparaffins diffuse more rapidly than dimethyl substituted prraffins. The activation

energies for diffusion for some alkyl benzenes in sodium-ZSM-5 at 523 K and 623 K have been reported by Weisz[88]. Olson et al.[89] reported some composition dependent properties of ZSM-5. They observed that the ion-exchange capacity, the catalytic activity and the hydrophobicity are linearly dependent on the aluminium content in the framework.

1.7. CATALYTIC REACTIONS OVER ZEOLITES

Small, uniform intracrystalline cavities and pores characterize zeolite catalyst. Crystalline zeolites are best known as heterogeneous catalysts. The use of zeolite as a catalyst is based on its characteristic properties such as high resistance to coke formation and thermal degradation associated with shape selectivity. Shape selectivity was first described by Weisz and coworkers[90]. Recently, several review articles discussing shape selectivity in catalysis have been published[91,92].

Most shape selective catalysts are acidic. Acid sites are introduced in the Na- or K-zeolites by acid treatment, by ammonium exchange and subsequent deammoniation or exchanging with multivalent cations, such as alkaline earth or rare earth ions.

After the successful performance of sodium and calcium X zeolites in cracking of paraffins, olefins and alkylaromatics[90,93], large number of catalytic conversion

processes have been developed and were disclosed in patent literature. A novel class of high-silica ZSM-5 pentasil zeolite has received much attention[94,95]; and has caused breakthrough in the field of catalysis. Soon after, large number of processes were developed based on ZSM-5 zeolite catalysts, which include the isomerization[96] of C_8 aromatics to produce isomerically pure xylenes, especially para-xylene for polyester manufacture; ethyl benzene synthesis for styrene production; and catalytic dewaxing[97]. The conversion of methanol to gasoline[98] as a new route from coal or natural gas to motor fuel is entirely based on high-silica ZSM-5 zeolite catalyst. More recently, Mobil Research and Development Corporation has also reported[99] a similar conversion of other oxygenated hydrocarbon compounds obtained from biomass to gasoline.

These initial commercial applications for ZSM-5 appear to be elegant examples of shape selective catalysis[90,92] reflecting its unique crystal structure with 0.6 nm pores outlined by 10-membered rings of oxygen. In addition they depend upon the other specific properties of highly acidic sites as in HZSM-5 catalyst, and substrate or reactant concentration effect. The novel organophilic-hydrophobic selectivity also appears to contribute to the unique selectivity of ZSM-5 for the conversion of oxygenated hydrocarbons to paraffins

and aromatics. Synthesis gas (CO + H_2) conversion to gasoline or olefins over ZSM-5 and silicalite impregnated with Group VIII metals has been reported[100].

Table 1.3 summarises important industrial applications of shape selective catalysts.

1.8. SCOPE OF THE PRESENT WORK

In view of the above brief literature review, it appears that the discovery of new shape selective catalyst material of the ZSM-5 type pentasil zeolite among the known synthetic zeolites, has led to their applications as potential catalysts for hydrocarbon conversion reactions. The properties which are responsible to make the choice of ZSM-5 for industrial applications are shape selectivity associated with high resistance to coke formation and thermal degradation, and their amenability to modification by ion-exchange and acid treatment.

The purpose of this study was to delineate the synthesis conditions for the crystalline zeolite, ZSM-5 in the Na-TEBA organic cation and mixed alkyl amine, alkyl bromide systems, to understand the nature of active sites in the zeolite, ZSM-5 needed for catalytic hydrocarbon conversion reactions. The present study has a scope mainly in the following areas :

TABLE - 1.3

Industrial Processes based on Shape Selective Zeolites[88]

Process	Objective	Major chemical process characterisation
Selectoforming	Octane number is increased in gasoline LPG production	Selective n-paraffin cracking.
M-forming	High yield, octane number increases in gasoline	Cracking depending on degree of branching aromatic alkylation and cracking fragments.
Dewaxing	Light fuel from heavy fuel oil. Lube oil with low temperature pour point	Cracking of high molecular weight, n- and monomethyl paraffins.
Xylene isomerisation	High yield of p-xylene product	High throughput, long cycle life, suppression of side reactions.
Ethylbenzene	High yield of ethylbenzene eliminating $AlCl_3$ handling	
Toluene disproportionation	Benzene and xylenes from toluene	
Methanol to gasoline	Methanol (from coal or natural gas) conversion to high grade gasoline	Synthesis of hydrocarbons only, restricted to gasoline range (C_4 to C_{10}) including aromatics

1. Hydrothermal synthesis of new or known zeolite structures with different chemical compositions, e.g. isomorphous substitution of Fe^{3+} in place of Al^{3+}.

2. The use of mixed alkyl amines and alkyl bromides in-situ during synthesis of zeolite ZSM-5, to produce corresponding organic template.

3. To understand the mechanism of zeolite nucleation and crystallization during hydrothermal synthesis.

4. To study the effect of thermal treatment on the structural and textural properties of ZSM-5 zeolites by IR, XRD, XPS and sorption of nitrogen, hydrocarbon and water.

5. To correlate the surface acidity of Al/HZSM-5 and Fe/HZSM-5 zeolites with their catalytic activity and selectivity.

The first three problems are interrelated in many aspects, which are important in understanding the crystallization process as well as for providing specimens needed for many aspects of zeolite research. Last two areas are related to the use of zeolite ZSM-5 as potential catalyst material in variety of important hydrocarbon conversion processes.

C H A P T E R - II

SYNTHESIS OF ZSM-5 PENTASIL ZEOLITE

C O N T E N T S

2.1. INTRODUCTION

Zeolites, a class of microporous crystalline aluminosilicate materials, have been extensively studied and synthesized over the last 30 years[7]. Zeolites are usually crystallized by producing high supersaturated aqueous solutions of appropriate compositions at relatively low temperatures in the range of 298 to 473 K. Although, the experimental procedures are quite simple, they are dependent on a host of parameters and the chemistry of the reaction system is extremely complex. The synthesis conditions of important zeolites using Na_2O-Al_2O_3-SiO_2-H_2O systems have been reviewed[101-103]. Due to lack of thermodynamic equilibrium, there is a large scope to modify the reaction composition and other conditions to produce new zeolites and vary the chemical composition and physical properties such as size and shape of the zeolite crystals. Instead of equilibrium phase diagrams, reaction diagrams are used to record the product of the synthesis[51].

Zeolite synthesis utilizes highly unstable coprecipitated gel, in aqueous solution containing an alkali hydroxide at high pH. Under hydrothermal synthesis conditions, the zeolite stabilizes the structural units with linked AlO_4 or SiO_4 tetrahedra, with associated cations and water molecules. In many instances, achieving the right-gel often becomes the initial requirement for obtaining crystalline material.

Lok et al.[104] recently examined the 'gel-chemistry' in detail. They traced the importance of gel-aging in zeolite synthesis. Usually the aging process is carried out at room temperature (298 K) during which the bulk physical nature and consequently intimate atomic linkages change.

Starting with highly reactive gel-mixtures, the probability of metastable crystallization, as Fyte[105] pointed out, is particularly high. In such systems, the initial maximum free energy excess must be high with respect to the final stable state. With increasing temperature of the synthesis, more compact zeolites are formed because of the greater reaction rates towards the true equilibrium. Frequently, a change in starting material alone changes the final product as well as the yield of zeolite even for the same bulk composition and temperature[106,107].

Recently, Lowe[108] proposed a simple equilibrium model to explain the change in pH which occurs when high silica zeolites are crystallized from gel. The model is based on the assumption that in the initial reaction gel-mix, the amorphous solid is in true or quasi equilibrium with the solution phase, and on completion of the crystallization a similar equilibrium is established between the zeolite and its mother liquor.

Since it is not possible to observe the detailed atomic movements during gel formation and crystallization,

and all theories are speculative, but data on hydrated cations occurring in zeolite structures and incorporation of various elements like phosphorus by simultaneous co-precipitation of all components into the intermediate gel, support theories of structural inheritance during zeolite crystallization[11].

2.2. SYSTEM FOR CRYSTALLIZATION OF ZEOLITE ZSM-5

The hydrothermal synthesis of high-silica zeolites in the presence of organic cations have been extensively studied during the last 15 years. The use of quaternary ammonium ions in zeolite synthesis of the type ZSM-5 pentasil family clearly had two major impacts. First is the extension of zeolite science into the high silica to alumina ratio ($SiO_2/Al_2O_3 > 20$) region. Secondly, great variety of other structure types, is possible through the synthesis route. The synthesis of ZSM-5 zeolite has been disclosed in number of patents. The system for ZSM-5 crystallization is,

$$M_{2/n}O\text{-}(R_4N)_2O - Al_2O_3\text{-}SiO_2\text{-}H_2O$$

where R_4N^+ is the quaternary ammonium cation and M is the alkali metal cation of valence n. In general, R_4N^+ can be selected from tetramethylammonium (TMA), tetra-ethylammonium (TEA), tetrapropylammonium (TPA),

triethyl-n-butylammonium (TEBA) and tetrabutylammonium (TBA) ions, alkylamines + alkyl bromides, and from the alkali metal or ammonium cation[38a,120,120a].

Zeolite ZSM-5 can best be synthesized by preparing a solution containing organic cation, sodium oxide, an oxide of aluminium, an oxide of silicon, and water, having composition in terms of mole ratios of oxides, falling within the range shown in Table 2.1.

TABLE - 2.1

Range of Composition of Reaction Mixtures in terms of mole ratios of Oxides[20,133]

Ratio	Broad range	Preferred	Particularly preferred
OH^-/SiO_2	0.07-10	0.1-0.8	0.20-0.75
H_2O/OH^-	10-300	10-300	10-300
SiO_2/Al_2O_3	5-100	10-60	10-40
$R^+/R^+ + Na^+$	0.2-0.95	0.3-0.9	0.4-0.9
R_4N^+/SiO_2	0.01-0.6	0.015-0.4	0.02-0.2
Na_2O/R_2O	0.17-150	10-75	5-30

Zeolite ZSM-5 is conventionally formed as aluminosilicate. The composition can be prepared by utilizing materials which supply the appropriate oxides. Such compositions include for an aluminosilicates, sodium aluminate, aluminium salts, alumina, sodium silicate, silica hydrosol, silica gel, silicic acid, sodium hydroxide and quaternary ammonium compounds. It has been found that each oxide composition utilized in the reaction mixture for synthesizing a member of the ZSM-5 pentasil family, can be mixed together in any order.

Typical reaction conditions consist of heating the reaction mixture, containing TEBA-Br/TEA + B.Br, Na_2O, Al_2O_3, SiO_2 and H_2O or TEBA-Br, Na_2O, Fe_2O_3, SiO_2 and H_2O to a temperature of about 373 to 473 K for a period of time of about 6 hours to 60 days. A more preferred temperature range is from 423 to 473 K. When the temperature is in this range the crystallization time is reported to be less than 5 days[20]. Crystal size and crystallization time of ZSM-5 will vary with the nature of the reactants employed.

In this Chapter, factors influencing the synthesis of ZSM-5 zeolite using mixed alkyl ammonium cations of the type $R^1_x R^2_y$ where R^1 and R^2 are different alkyl groups and $x + y = 4$, as well as, producing the requisite alkyl ammonium cation in-situ by mixing the corresponding alkyl amines and alkyl bromides, have been investigated.

2.3. EXPERIMENTAL

2.3.1. Synthesis of triethyl-n-butyl ammonium bromide (TEBA-Br)

TEBA-Br was prepared by refluxing equimolar solutions of triethylamine, TEA (SDS 99.5% pure) and n-butyl bromide (SDS 99.5% pure) in dry alcohol for 24 hours. The excess alcohol was distilled off and TEBA-Br crystals were separated by filteration, washed with cold-dry ethyl ether and dried at 363 K overnight. The micro-analysis of the dry product for C, N and Br agreed with the theoretical values within $\pm$ 0.5%. The product is highly hygroscopic, hence need to be preserved in air-tight container.

2.4. SYNTHESIS OF ZSM-5 PENTASIL ZEOLITE

Synthesis runs were carried out for the following systems, at various temperatures in stainless steel autoclaves (shown in Fig. 2.1) of 250 ml capacity at autogeneous pressure.

2.4.1. Procedure

In system A' (essentially based on addition of alkyl amines and alkyl bromides in-situ), a solution of aluminium sulphate, prepared by dissolving appropriate amounts of pure aluminium sulphate [$Al_2(SO_4)_3.16H_2O$, BDH AR]

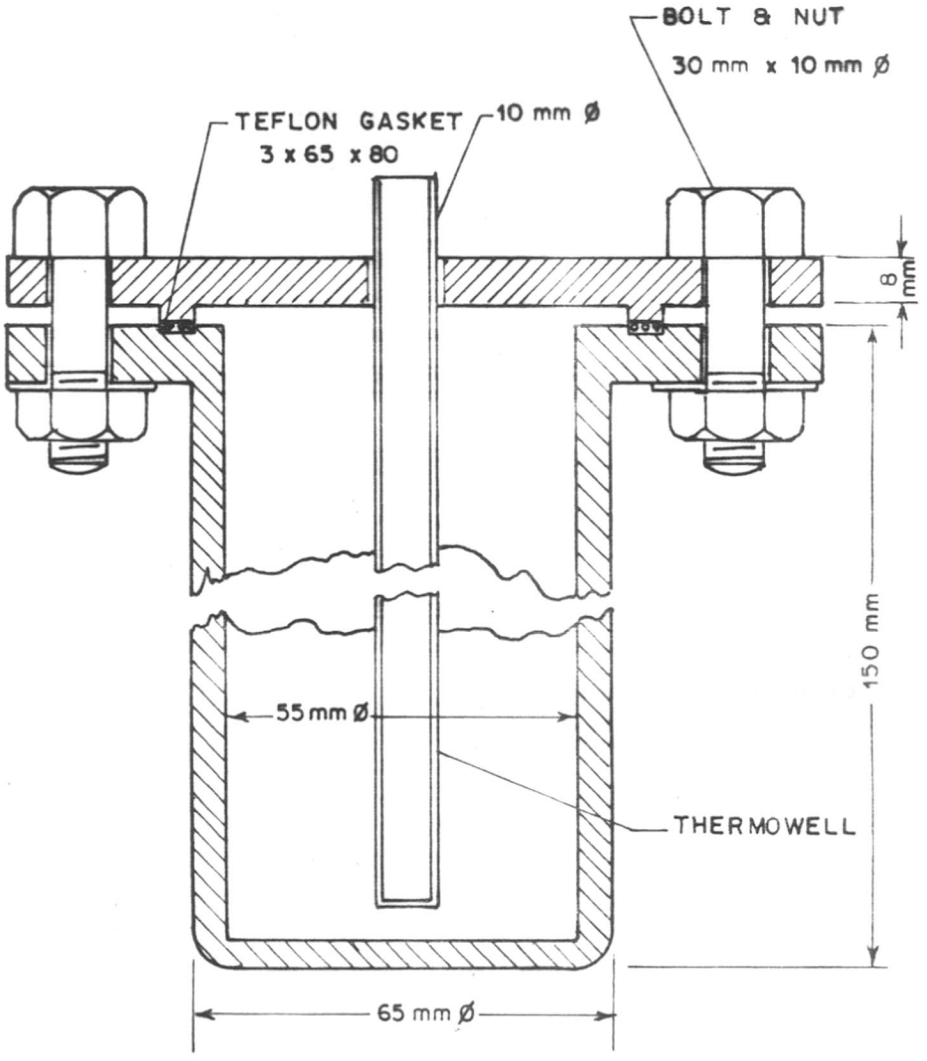

FIG. 2·0. STAINLESS-STEEL (316) AUTOCLAVE WITH TEFLON-GASKET FOR HYDROTHERMAL SYNTHESIS

in a known quantity of H_2SO_4 solution (98% H_2SO_4, BDH AR), is added to a basic solution of aqueous sodium silicate (27.17 % SiO_2, 8.41% Na_2O, 64.42% H_2O), preliminarily mixed with TEA (SDS, pure) and n-B-Br (SDS, pure), under vigorous stirring. The gel so obtained (~pH 10.7) is stirred for ten minutes before closing the autoclave and subjecting it for heating at controlled temperature in an air oven.

In system A (essentially based on incorporation of synthesized TEBA.Br product), an acidic solution, prepared by mixing appropriate amounts of aluminium sulphate [$Al_2(SO_4)_3.16H_2O$, BDH AR] and H_2SO_4 (98 % H_2SO_4, BDH AR) in water, is added to a basic solution of aqueous sodium silicate (27.17% SiO_2, 8.41% Na_2O, 64.42% H_2O), initially mixed with a solution of previously prepared TEBA-Br under vigorous stirring. The gel so obtained (~pH 10.2) is stirred for ten minutes before closing the autoclave and subjecting it for heating at controlled temperature in an air oven.

In system B (essentially for isomorphous substitution in the framework), a solution of an appropriate amount of ferric sulphate hexahydrate [$Fe_2(SO_4)_3.6H_2O$, LOBA, GR], is used in place of aluminium sulphate solution using all the other ingredients as in A.

When the required temperature was attained (measured by chromel-alumel thermocouple inserted in a thermowell of the autoclave) the time was noted as zeroth hour. On the termination of the reaction, the autoclaves were quenched in cold-water to stop the crystallization process. The solid product was separated by filteration, washed and dried in the air oven at 393 K for 24 hours.

2.5. CHARACTERIZATION

2.5.1. X-ray Diffraction

The synthesized samples of different time of crystallization were analysed by X-ray powder diffraction method for quantitative zeolite phase identification. Philips X-ray diffractometer, Model PW 1730 and Ni filtered CuKα radiation (λ = 1.5405Å) was used for the analysis of the sample. For quantitative phase identification, selected reference sample was used and the per cent crystallization was calculated from the sum of areas of the peaks between 2θ = 22 to 25°. The extent of crystallization was estimated by using the formula[53]

$$\% \text{ Crystallization} = \frac{\text{Peak area between } 2\theta = 22 \text{ to } 25^{\circ} \text{ of the product}}{\text{Peak area between } 2\theta = 22 \text{ to } 25^{\circ} \text{ of the reference sample}} \times 100$$

2.5.2. Infrared Spectroscopy

The ir-spectra were recorded in the frequency range 200-1300cm^{-1} on PYE UNICAM SP-300 Spectrophotometer using KBr pellets, hexachlorobutadieneand/or nujol mulls of the sample. For quantitative phase identification, a selected reference sample was used and per cent crystallization was calculated from the area under the band at 550 cm^{-1}. The extent of crystallization was estimated using the formula[109]

$$\% \text{ Crystallization} = \frac{\text{Peak area of the band at } 550\ cm^{-1} \text{ of the product}}{\text{Peak area of the band at } 550\ cm^{-1} \text{ of the reference sample}} \times 100$$

KCN was used as an internal standard.

2.5.3. Thermal Analysis

Simultaneous TG-DTA-DTG analysis of intermediate phases were performed on an automatic derivatograph (MOM-Budapest, Type 00-102B) described by Paulik et al.[110]. The thermograms of the samples were recorded under the following conditions

Weight of the sample	- 100 mg
Heating rate	- 10 K min^{-1}
Sensitivity	
TG	- 100
DTA	- 1/5
DTG	- 1/5
Atmosphere	- Flowing air.

preheated and finely powdered α-alumina was used as a reference material.

. . . Scanning Electron Microscopy

The morphology of ZSM-5 zeolites and representative intermediate phases was investigated using the scanning electron microscope, Sterioscan Model 150 Cambridge, U.K. The sample was dusted on aluminium pegs and coated with an Au-Pd evaporated film.

2.5.4. Chemical Analysis

Known quantity of zeolite sample was heated at high temperature in a platinum crucible in duplicate for 6 hours to constant weight. The ignited zeolite powder was treated with hydrofluoric acid and evaporated to dryness. The HF treatment was repeated three times. From the loss in weight silica was estimated. The residue was fused in potassium pyrosulfate and dissolved in hot water and made into a standard volume. The solution was used for estimation of sodium by flame photometry, and aluminium and iron by atomic absorption spectroscopy. The results have been tabulated in Table 3.1, Chapter III.

2.6. RESULTS AND DISCUSSION

The preliminary synthesis runs were made in the systems A, A' and B (as already described) for one selected batch composition with SiO_2/M_2O_3 = 85 (where M = Al^{3+}, or Fe^{3+}) using TEBA-Br and TEA + n-Bu bromide as the source of organic cations. Further detailed study was carried out with TEBA-Br as the source of organic cation. The molar composition of the reaction mixtures are given in Table 2.2.

TABLE - 2.2

Composition of Reaction Mixtures

SiO_2/M_2O_3 (M = Al^{3+} or Fe^{3+})	$(Et_3\text{-}Bu\text{-}N)_2O^*/SiO_2$	Na_2O/SiO_2	OH^-/H_2O
35	0.054	0.30	6.36×10^{-3}
85	0.054	0.30	6.0×10^{-3}
200	0.054	0.30	5.8×10^{-3}
600	0.054	0.30	5.6×10^{-3}
∞ (silicalite)	0.054	0.30	4.1×10^{-3}

* $Et_3Bu.N^+$ = triethyl-n-butylammonium ion.

The X-ray diffraction patterns of crystalline products of synthesis systems A,A' and B are illustrated in Fig. 2.1. The peak height I and position of the X-ray diffraction peak as a function of 2θ, where θ is the Bragg angle were read from diffractograph. From these, the relative intensities ($I/I_o \times 100$, where I and I_o are the intensities of the strongest line or peak of the sample and the reference respectively) and d the interplanar spacing in $\mathring{A}$, corresponding to recorded lines were calculated. The values of interplanar spacings (d values) and relative intensities are given in Table 2.3.

In each case, it was noticed that the crystallization products matched with the reported d values and relative intensities of crystalline ZSM-5 zeolite[20,38a,110], except in synthesis A' system, where phase transformation to α-quartz was identified. α-quartz was identified in the ZSM-5 zeolite (peak at $2\theta = 26.7^o$ and 20.8^o) from x-ray diffractograms[53,53a]. The more detailed discussion and treatment on α-quartz formation will be dealt later.

The range of composition of reaction mixtures in terms of their molar ratios and comparison with suggested range for synthesis systems A, A' and B are given in Table 2.4.

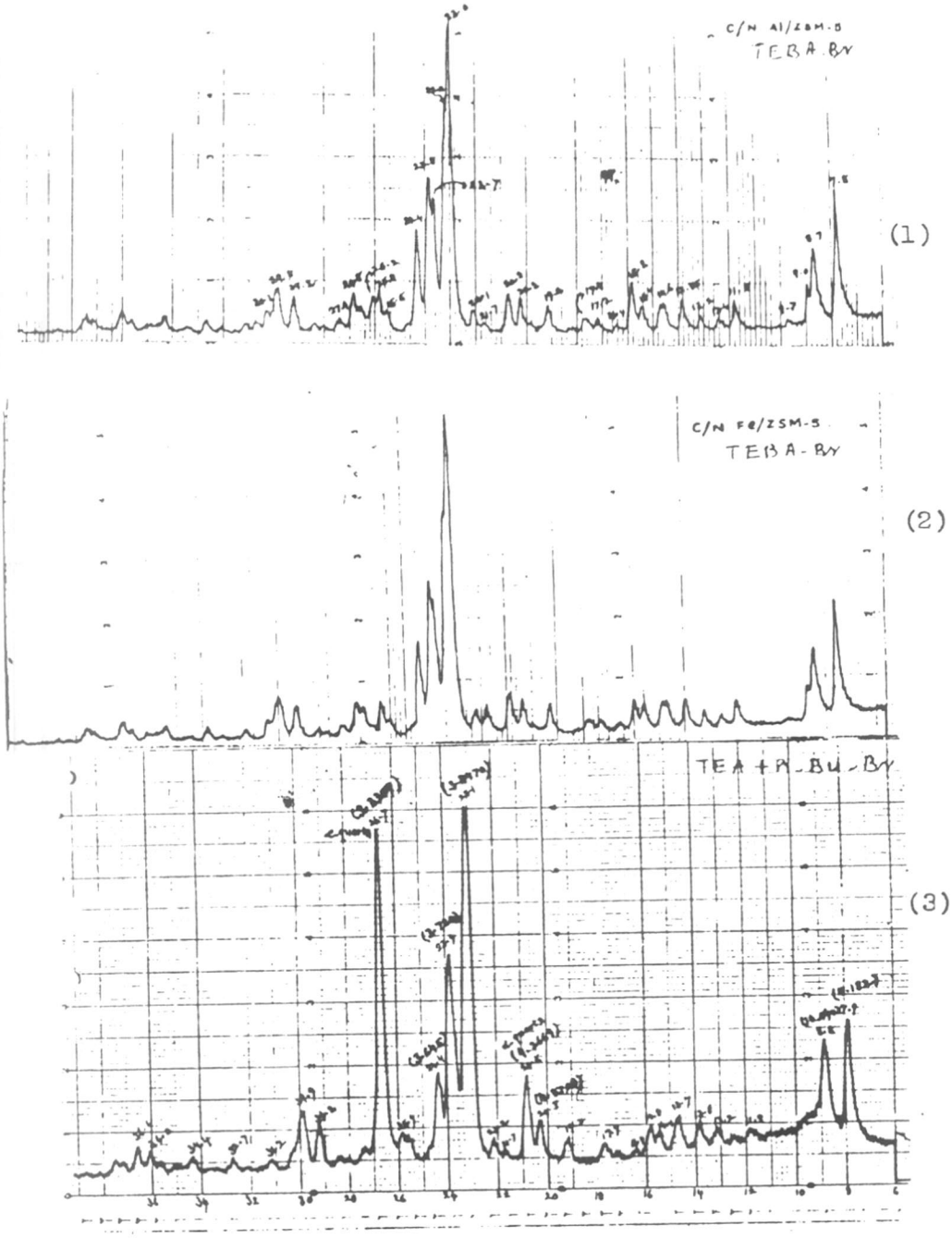

Fig.2.1: X-RAY DIFFRACTION PATTERNS OF ZSM-5 ZEOLITES FOR SYNTHESIS SYSTEMS (1) A(TEBA-Br) (2) B: (TEBA-Br), (3) A' (TEA + n.Bu-Br)

TABLE - 2.3

d-Spacings and relative intensities for ZSM-5 zeolites synthesized using TEBA-Br

TEBA-Al/ZSM-5 (synthesis system B)		TEBA-Fe/ZSM-5 (synthesis system B)	
d(Å)	(I/I_o) 100	d(Å)	(I/I_o) 100
11.32	48.0	11.04	41.9
10.16	30.7	9.93	28.5
9.81	19.2	9.71	15.2
9.11	7.6	-	-
7.49	13.8	7.40	11.4
7.13	8.6	7.08	7.6
6.70	9.6	6.70	9.5
6.39	14.4	6.32	11.5
6.06	13.0	6.01	11.6
5.75	11.5	5.68	11.5
5.60	19.2	5.54	12.3
5.40	6.1	5.37	1.9
5.15	7.7	5.12	3.8
4.98	7.7	4.98	3.8
4.62	12.5	4.60	11.4
4.39	14.4	4.35	12.3
4.27	15.3	4.25	15.2
4.09	6.1	4.07	11.4
4.02	10.5	4.00	9.5
3.86	100.0	3.85	100.0
3.83	74.0	3.81	70.4
3.75	46.1	3.74	43.8

Table 2.3 continued

3.72	51.9	3.72	49.5
3.64	34.9	3.65	31.4
3.45	9.6	3.47	5.7
3.40	16.3	3.43	13.3
3.36	14.8	-	-
3.32	15.3	3.32	9.5
-	-	3.31	12.3
3.25	6.7	3.24	3.8
3.14	14.8	-	-
3.06	17.3	3.05	11.4
2.99	9.6	2.98	15.2
2.75	6.7	-	-
2.92	5.7	2.92	5.7
2.87	3.8	2.86	3.8
2.79	6.7	2.78	0.9
2.74	1.9	-	-
2.61	7.6	2.60	3.8
2.52	6.7	2.51	3.8
2.49	9.6	2.49	2.8
2.42	5.7	-	-
2.40	8.6	2.40	3.8
2.01	13.4	2.01	10.4
1.99	13.4	-	-
1.95	3.8	-	-
1.91	5.7	1.90	10.4
1.87	6.7	-	-

TABLE 2.4

Comparison of the molar ratios for synthesis systems with suggested range[20,133]

Ingredient molar ratios	Synthesis system			Suggested range		
	A	A'	B	Broad	Preferred	Particularly preferred
OH^-/SiO_2	0.27	0.27	0.27	0.07-10	0.1-0.8	0.2-0.75
H_2O/OH^-	141.75	141.66	141.14	10-300	10-300	10-300
SiO_2/M_2O_3	85	85	85	5-100	10-60	10-40
H_2O/SiO_2	38.5	38.5	38.45	5-200	15-50	20-45
Et_3BuN^+/SiO_2	0.10	0.094	0.10	0.01-06	-	0.02-02
$Na_2O/(Et_3BuN)_2O$	5.74	6.30	5.74	0.17-150	10-75	5-30

Et_3BuN^+ = triethyl n-butyl ammonium ion

2.6.1. Kinetics of crystallization

A kinetic study was undertaken for a selected batch composition to determine the apparent energy of activation for nucleation and crystallization. The crystallization curves in the temperature range 433-473 K using TEBA-Br as the source of organic cation for both the synthesis systems A and B are illustrated in Fig. 2.2A. The reaction gel composition used was

$$4.41(TEBA)_2O - 25.32\ Na_2O - Al_2O_3 \overset{or}{(}Fe_2O_3 - 85\ SiO_2 - 3276\ H_2O.$$

Fig. 2.2B represents the crystallization curves at 433, 453, and 473 K, for the same batch composition. Instead of aluminium-sulphate, ferric-sulphate was used to obtain the resulting oxide Fe_2O_3 in the molar composition, the zeolite being designated as Fe/ZSM-5. The curves show that the rate of zeolite crystallization significantly depends on the temperature and that the reaction temperature strongly influences the kinetics of the process. Increasing the temperature of the zeolite crystallization, raises the solubility of the solid aluminosilicate phase and hence the composition of the liquid phase in such heterogeneous system has a beneficial effect on the crystallization process. The crystallization curves exhibit sigmoid nature characteristic of processes involving two distinct stages, viz :

a) an induction period when nuclei are formed, and

b) a crystal growth period when nuclei grow into crystals.

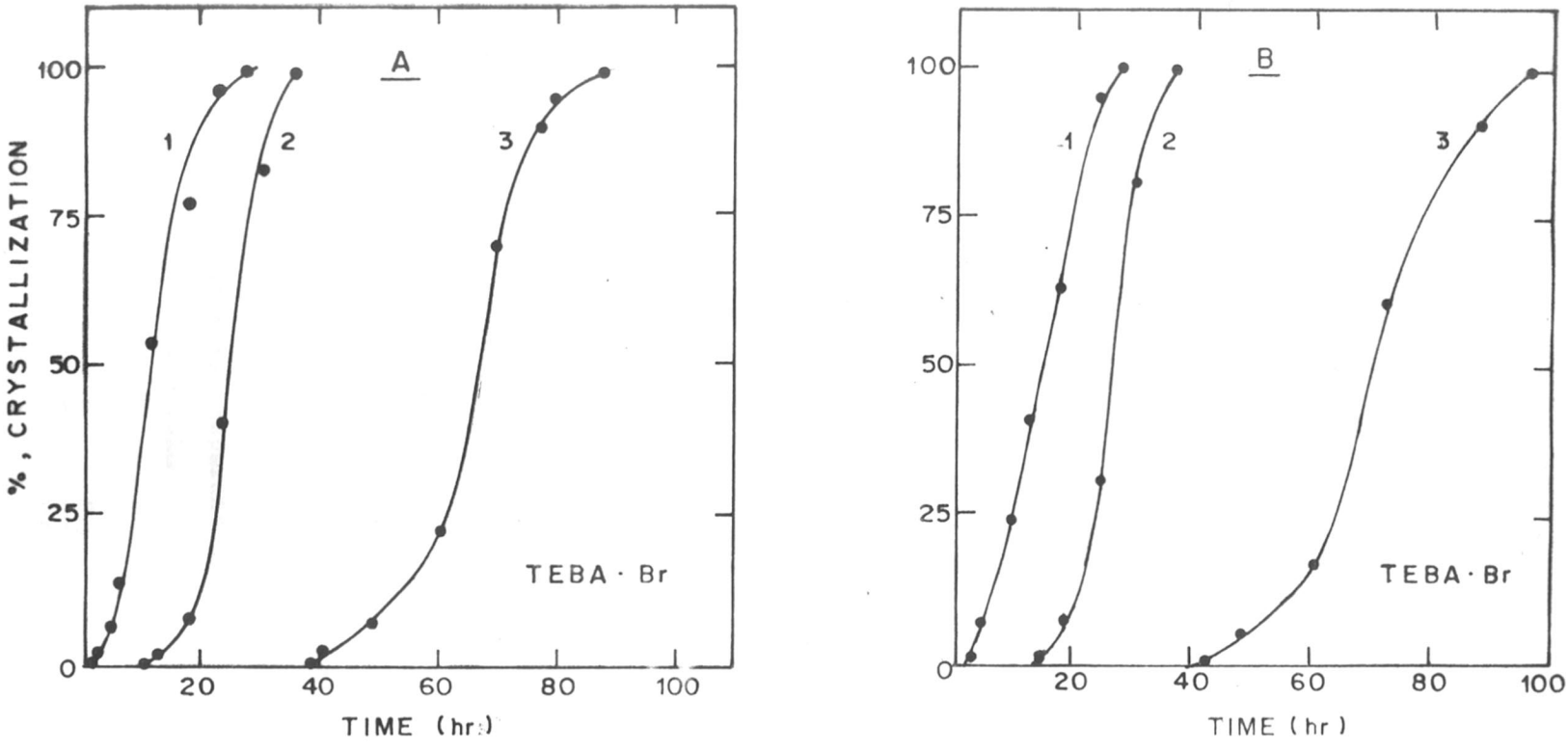

FIG. 2·2. THE KINETICS OF CRYSTALLIZATION AT (1) 473 K (2) 453 K (3) 433 K
(A) Al / ZSM-5 ZEOLITE (B) Fe / ZSM-5 ZEOLITE

The induction period may be defined as the time required for providing the condition for the nuclei formation, and the crystal growth period as the time which is necessary for the growth of nuclei to a critical size[52].

The rate of any crystallization process is determined by the rate of nuclei formation and the rate of crystal growth. Obviously, the observed accleration of crystallization must be connected with the increase in the rate of nuclei formation. The crystallization rate is defined as the rate of conversion at 50% of total conversion level in terms of per cent conversion per hour. The decrease in the rate of crystallization observed above 60% conversion can be caused by the decrease in reactant concentration in the solution.

Assuming that the formation of nuclei during the induction period is an energetically activated process and since nucleation is the rate determining step during the induction period, the apparent energy of activation for nucleation, E_n was calculated from the temperature dependance of the rate of nucleation. The rate of nucleation has been assumed to be inversely proportional to the nucleation period. Temperature dependance of the rate of nucleation was expressed by Arrhenius equation and apparent activation energy for nucleation was calculated from

$$\frac{d \ln (1/\theta)}{d(1/T)} = \frac{-E_n}{RT} \qquad \ldots (1)$$

where θ is induction period, that is point on the crystallization curve where conversion to the crystalline phase is just starting, and T is the absolute temperature and R is gas constant.

Similarly, E_c, the apparent activation energy for crystal growth was calculated from the temperature dependance of the rate of crystallization and was obtained from the point on the crystallization curves where the crystallization is 50%. The rate equation may be represented as

$$\frac{d \ln (K)}{d (1/T)} = \frac{-E_c}{RT} \qquad \ldots 2$$

where K is the point on the crystallization curves (hours), where 50% crystallization is complete, T the absolute temperature and R, the gas constant. Fig. 2.3 illustrates the temperature dependance of the rate of nucleation and crystallization for synthesis of A and B systems. The calculated values of E_n and E_c are given in Table 2.5, together with the reported values for ZSM-5 synthesized using TPABr and TEPABr as the organic cations. Chao et al[53] using TPAOH (SiO_2/Al_2O_3 = 70, OH^-/H_2O = 2.2 x 10^{-3}) had obtained values of E_n and E_c of 25 and 29 kJ $mole^{-1}$ respectively. Erdem and Sand[38a] (TPAOH, SiO_2/Al_2O_3 = 28, OH^-/H_2O = 26.7 x 10^{-3}), however, obtained values of E_n = 107.5 and E_c = 81.5 kJ $mole^{-1}$. Also, Mostowich and Sand (TPABr,

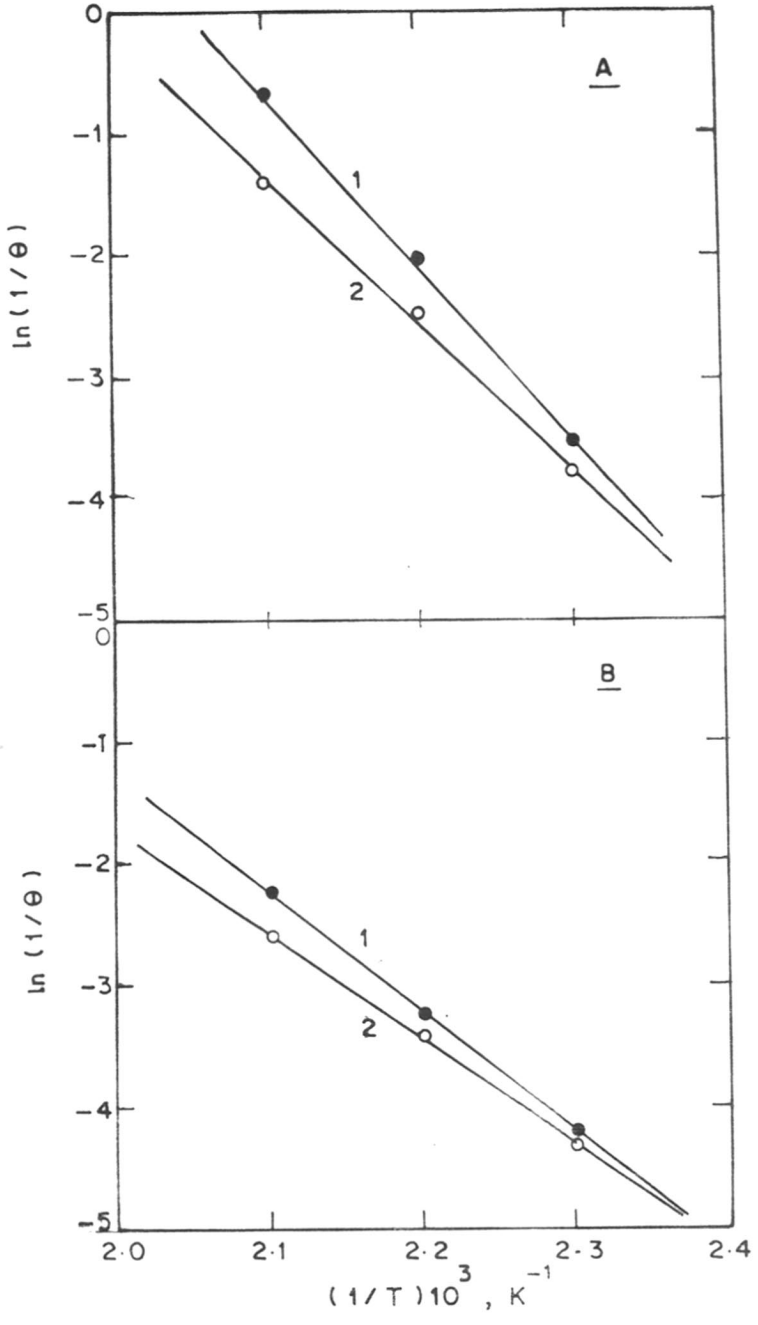

FIG. 2-3. ARRHENIUS PLOTS FOR (A) NUCLEATION (B) CRYSTALLIZATION

(1) TEBA. Br, SiO_2 / Al_2O_3 = 85

(2) TEBA. Br, SiO_2 / Fe_2O_3 = 85

Table 2.5

Activation energies for nucleation and crystallization

Source of organic	SiO_2/M_2O_3	E_n, kJ mole^{-1}	E_c, kJ mole^{-1}
TEBA-Br	85	272	181
*TEBA-Br	85	226	167
TPA-Br[53a]	86	199.5	236.6
TEPA-Br[53a]	86	270.5	206.8
TPA-Br[38a]	90	35.5	83.6
TPA-Br[111]	70	133.7	-
TPA-OH[53]	70	104.5	121.2
*TPA-Br[113a]	85	177.8	198.2

* isomorphous substitution Fe^{3+} in place of Al^{3+} in the framework.

SiO_2/Al_2O_3 = 90, OH^-/H_2O = 12 x 10^{-3}) reported values of E_n = 35.5 and E_c = 86.6 kJ $mole^{-1}$. Kulkarni et al[53a] have reported for TPABr and TEPABr systems the values of E_n = 199.5, E_c = 236.6 kJ $mole^{-1}$ and E_n = 270.5, E_c = 206.8 kJ $mole^{-1}$ respectively. These variety of values and their large variations indicate the complex function of the kinetic parameters, which, in turn, is dependent on many reaction variables.

To check if the zeolite formation in our systems confirms the above general picture, the data of Fig. 2.2 were fitted to the Avarami-Erofeev[112] equation, that is,

$$\ln\left[\frac{1}{1-\alpha}\right] = (kt)^m \qquad \ldots(3)$$

where α and t are fractional conversion and time respectively and k and m are the constants. The results are shown in Fig. 2.4 and values of k and m, obtained at 433, 453 and 473 K using the template TEBA-Br are compared in Table 2.6.

TABLE - 2.6

Avarami-Erofeev parameters for ZSM-5 synthesis

Synthesis temp. K	TEBA-Br synthesis system A : Al/ZSM-5		TEBA-Br synthesis system B : Fe/ZSM-5	
	10^2K	m	10^2K	m
433	1.52	7.5	1.25	7.68
453	3.95	4.33	4.10	7.60
473	8.11	2.13	6.45	2.15

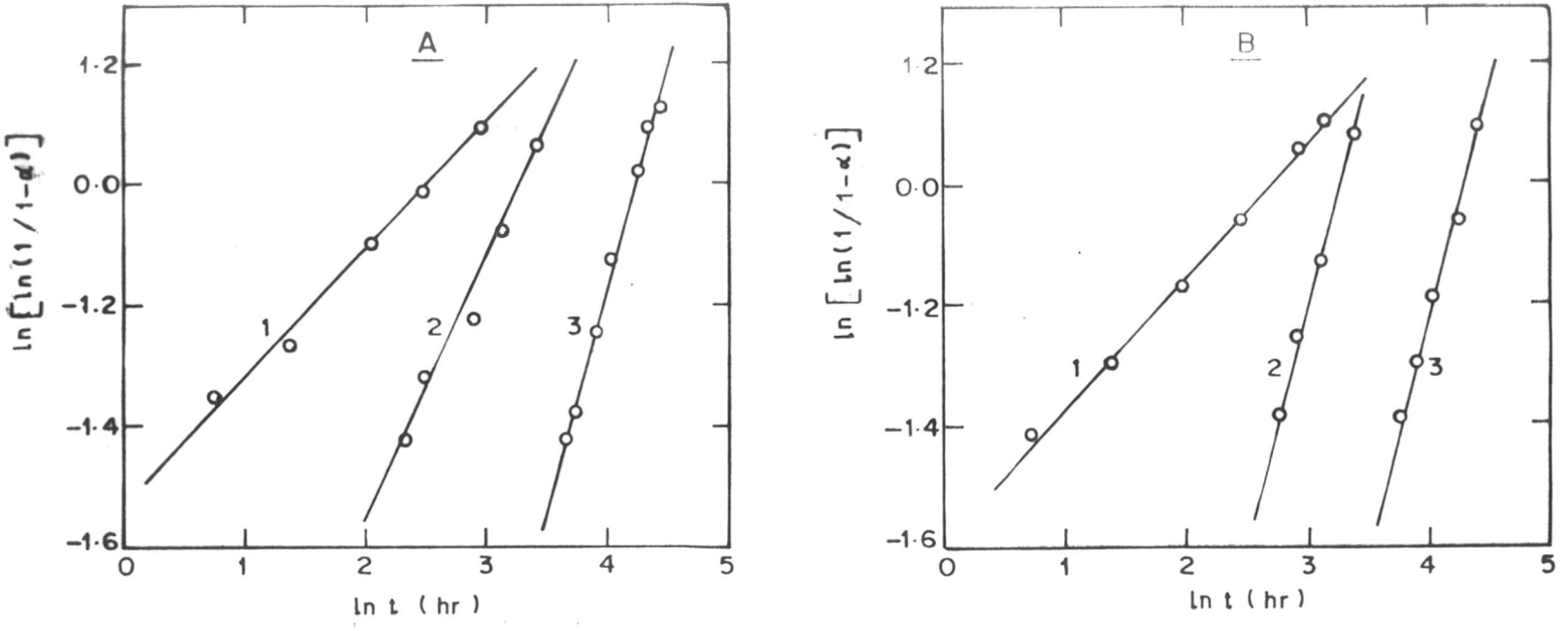

FIG. 2-4. FIT OF EXPERIMENTAL DATA TO AVARAMI-EROFEEV EQUATION AT 1) 473 K 2) 453 K 3) 433 K

A) Al / ZSM-5, $SiO_2 / Al_2O_3 = 85$ B) Fe / ZSM-5, $SiO_2 / Fe_2O_3 = 85$

From the good fit of the data, it is concluded that the crystallization process can be described, at least mathematically, by Avarami-Erofeev equation involving nucleation and growth of crystalline zeolite ZSM-5 phase.

2.6.2. Effect of SiO_2/M_2O_3 (M = Al^{3+} or Fe^{3+}) ratio on the kinetics of crystallization of pentasil zeolite, ZSM-5

Zeolite ZSM-5 was synthesized as crystalline phase over the temperature range 433-473 K with SiO_2/M_2O_3 (M = Al^{3+} or Fe^{3+}) ratios varying from 85 to Al and Fe-free batch compositions. Figs. 2.5 and 2.6 illustrate the typical crystallization curves at 453 K for Na-TEBA aluminosilicate gel compositions of varying SiO_2/M_2O_3 mole ratios, at constant (fixed) $(TEBA)_2O/SiO_2$ mole ratio. These curves show typical sigmoid nature characteristic of processes involving nucleation and crystal growth. The increase in SiO_2/M_2O_3 ratio enhances the crystallization of ZSM-5, that is ZSM-5 is formed faster in the reaction mixture of higher SiO_2/M_2O_3 ratio. It was observed that the rate of crystallization of ZSM-5 in Na-TPA and Na-TEPA systems also decreased with increasing aluminium content in synthesis mixture[53,113]. Gamami et al.[114] and Nakamoto et al.[115] also reported that the rate of crystallization decreased at higher Al content in the synthesis mixture of ZSM-5. These results have enabled to

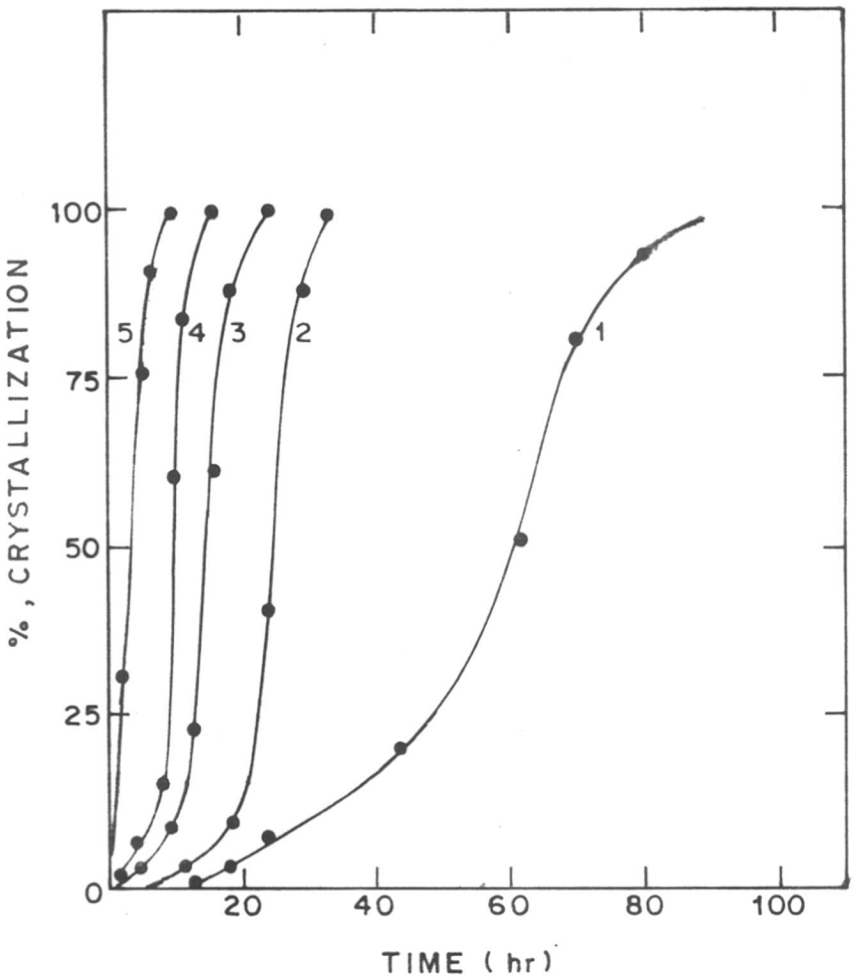

FIG. 2·5. INFLUENCE OF SiO_2/Al_2O_3 RATIO ON CRYSTALLIZATION OF ZSM-5, AT 453 K. CURVES 1-5 REFER TO SiO_2/Al_2O_3 MOLAR RATIOS OF 35, 85, 200, 600 AND SILICALITE RESPECTIVELY

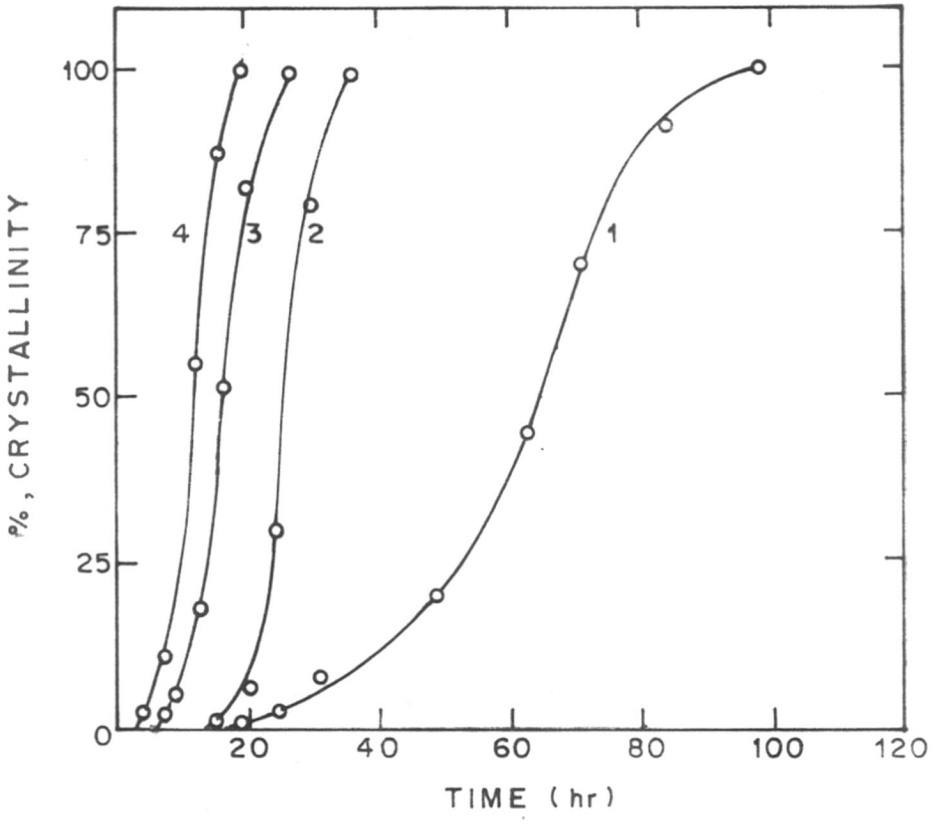

FIG. 2·6. INFLUENCE OF SiO_2 / Fe_2O_3 RATIO ON CRYSTALLIZATION OF Fe / ZSM-5 AT 453 K. CURVES 1-4 REFER TO SiO_2 / Fe_2O_3 MOLAR RATIO OF 35, 85, 200, AND 600 RESPECTIVELY

to explain the observation that higher concentration of aluminate species "blocks" as a gel or the solution, larger amounts of silica monomers which are needed for nucleation.

Further increase in the crystallization period leads to decrease in crystallinity of the product (detected by XRD, decrease in crystallinity on further crystallization is not shown in Fig. 2.5 and 2.6). However, no phase transformation or α-quartz formation was observed on further increase in the crystallization period for these systems using TEBA-Br. The decrease in zeolite crystallinity is related to the decrease in reactant concentration after attaining 100 per cent crystallinity in the product.

2.6.3. Effect of $(TEBA)_2O/SiO_2$ ratio

Crystallization of zeolites is a nucleation controlled process occurring from molecularly inhomogeneous, aqueous aluminosilicate gel . The product is strongly dependent on the cation distribution in these mixtures. The addition of quaternary ammonium cation to a reaction mixture can induce effect as

(i) a different zeolite structure is obtained,

(ii) a zeolite crystallizes where the reaction mixture would otherwise remain amorphous indefinitely, or

(iii) the same zeolite is obtained as without quaternary ammonium cations, but it possesses different chemical composition.

Unless crystallization is markedly accelerated, only (i) and (ii) represent "template effects" which is attributable to quarternary ammonium cations, and (i) is by far more common of the two effects. In case of high-silica molecular sieves a true "templating" pervades wherein the alkylammonium cation forms complexes with silica via hydrogen bonding interactions. These complexes cause replication of the structure via a stereo specific hydrogen-bonding interaction of the quaternary ammonium cations with the framework oxygens[25,116,117]. The concept of cation templating in zeolite synthesis has been discussed by Flanigen[118] and summarized and further developed by Rollman[119]. Thus, the concept of templating is the phenomenon occurring during either the gelation or the nucleation process whereby the organic molecule organizes oxide tetrahedra into a particular geometric topology around itself and thus provides the initial building block for a particular structure type. Such an important role is often referred to as the structure directing role.

The nature of pentasil zeolites synthesized in specific conditions by using various tetraalkylammonium cations (TAA^+) or the corresponding trialkylamine (AlK_3N^+) precursors was investigated by Gabelica et al.[120]. Further, the zeolites of the type ZSM-8, ZSM-5, ZSM-11, were synthesized using tetraethylammonium (TEA^+), tetrapropylammonium (TPA^+) and tetrabutylammonium (TBA^+) bromide, respectively, demonstrating the structure directing role of (TAA^+) cations.

Fig. 2.7 shows crystallization curves of zeolite ZSM-5 for both the synthesis systems with varying $(TEBA)_2O/SiO_2$ ratios. The reaction mixture with same batch composition in the mole ratio of SiO_2/M_2O_3 = 85, Na_2O/SiO_2 = 0.297, OH^-/H_2O = 6.0×10^{-3} was selected to study the effect of quaternary ammonium cation on the crystallization of ZSM-5. At low ratios of $(TEBA)_2O/SiO_2$, both, the rates of nucleation and crystallization were found to decrease. At higher concentration of organic template which provides large number of species to form nuclei, as the formation of zeolite takes place around the organic template[117], the rate of nucleation as well as the rate of crystal growth is enhanced.

At constant or fixed H_2O/SiO_2 ratio, the $(TEBA)_2O/SiO_2$ ratio in the reaction mixture indicates the alkalinity of the reactants and increase in alkalinity should enhance the dissolution of solid gel to form soluable reactive species and hence should increase both the rates of nucleation and crystallization. It has been proposed[115,29] that in mixed organic base system, the presence of organic base changes the solid-liquid equilibrium and stabilizes larger sol-like aluminosilicate species. The alkali ion affects the agglomeration of particles to larger amorphous precipitate particles which subsequently crystallize to zeolite. The precipitation and solution phenomena depend on the relative concentration of the organic and alkali cation and on pH. Howden[121] had also

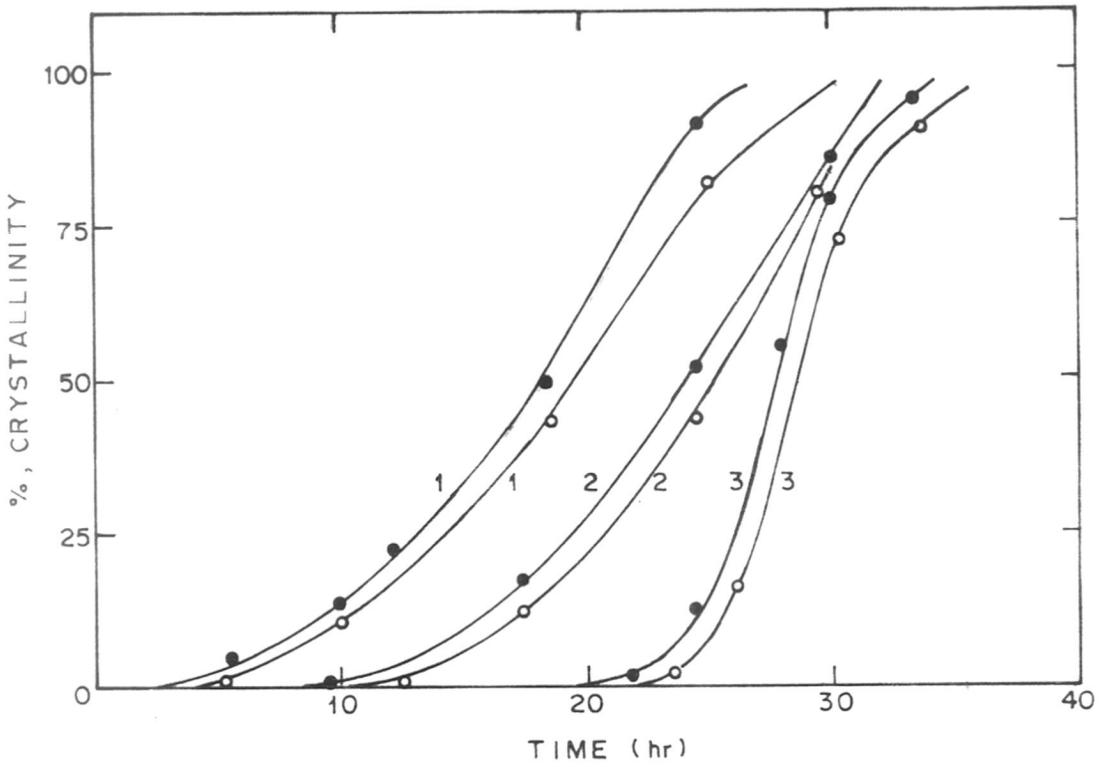

FIG. 2-7. INFLUENCE OF $(TEBA)_2O / SiO_2$ RATIO ON THE CRYSTALLIZATION OF Al-ZSM-5 AND Fe/ZSM-5 ZEOLITE AT 453 K, $SiO_2 / M_2O_3 = 85$, $Na_2O / SiO_3 = 0.297$. CURVES 1-3 REFER TO $(OH^- / H_2O) \times 10^3$ RATIOS OF 0.12, 0.07 AND 0.0121 RESPECTIVELY

- ● Al / ZSM-5, (SYN. SYS. A)
- ○ Fe / ZSM-5, (SYN. SYS. B)

observed that, by keeping other experimental parameters constant, there was a significant decrease in the concentration of ZSM-5 and in the product yield, when the amount of template was reduced to less than 10% of the original.

In view of the above observations, it is concluded that, the crystallization rate in both the synthesis systems, also depends on $(TEBA)_2O/SiO_2$ ratio, and higher the ratio, faster the crystallization of zeolite ZSM-5.

2.6.4. Effect of OH^-/H_2O ratios on the kinetics of crystallization

As OH^-/H_2O ratio in the reaction mixture indicates the alkalinity of the reactants of the system, which influences the polymerization-depolymerization equilibrium of the soluble alumino-[28] and ferrosilicates, the functional dependence of zeolite crystallization kinetics on alkalinity was developed for these synthesis systems. At the same time, it was of interest to study the effect of alkalinity on the metastable phase transformation giving rise to a non-zeolitic material such as ∝-quartz. Such transformation during the synthesis of system A', involving addition of TEA and n-B-Br in situ, ∝-quartz was formed alongwith the ZSM-5 zeolite phase [Fig.2.1 (3)]. Hagiwara[122] et al. had observed such ∝-quartz formation using sodium dodecylbenzenesulphonate in batch composition $SiO_2/Al_2O_3 = 56$, $SiO_2/Na_2O = 2$ at 473 K during ZSM-5 crystallization. They speculated that higher alkalinity of the reactants

at higher synthesis temperature tends to decompose template rapidly giving rise to ∝-quartz phase. It was then assumed, particularly in this system A', that under hydrothermal conditions in presence of higher alkaline reactants Et_3BuN^+ formation may be retarded (even if it forms to operate as structure-directing agent during nucleation stage, it may be forming in traces) which results in rapid decomposition of TEA and n-B-Br entities. ∝-quartz was also identified in ZSM-5 zeolite by Chao et al.[53].

In Fig. 2.8 crystallization curves for system A and B (Al/ZSM and Fe/ZSM respectively) and in Fig. 2.9(B) for system A' are shown. In all these systems the same starting batch compositions are used, only the alkalinity of the system is varied. This was accomplished by adding sulfuric acid.

As can be seen from Fig. 2.8 the change in OH^-/H_2O (alkalinity) ratios in the reaction mixture causes a change in the rate of nucleation and hence presence of hydroxide ions strongly affects the formation of nuclei. When the solutions of aluminate and silicate or polysilicate anions are mixed to form the hydrogels, alkalinity accelerates the dissolution of the gel materials and the formation $Al(OH)_n$ species. The dissolved species (Si and Al) can also undergo a polymerization process to form aluminosilicate or polysilicate ions, and those in turn, in presence of quaternary ammonium ions, condense to

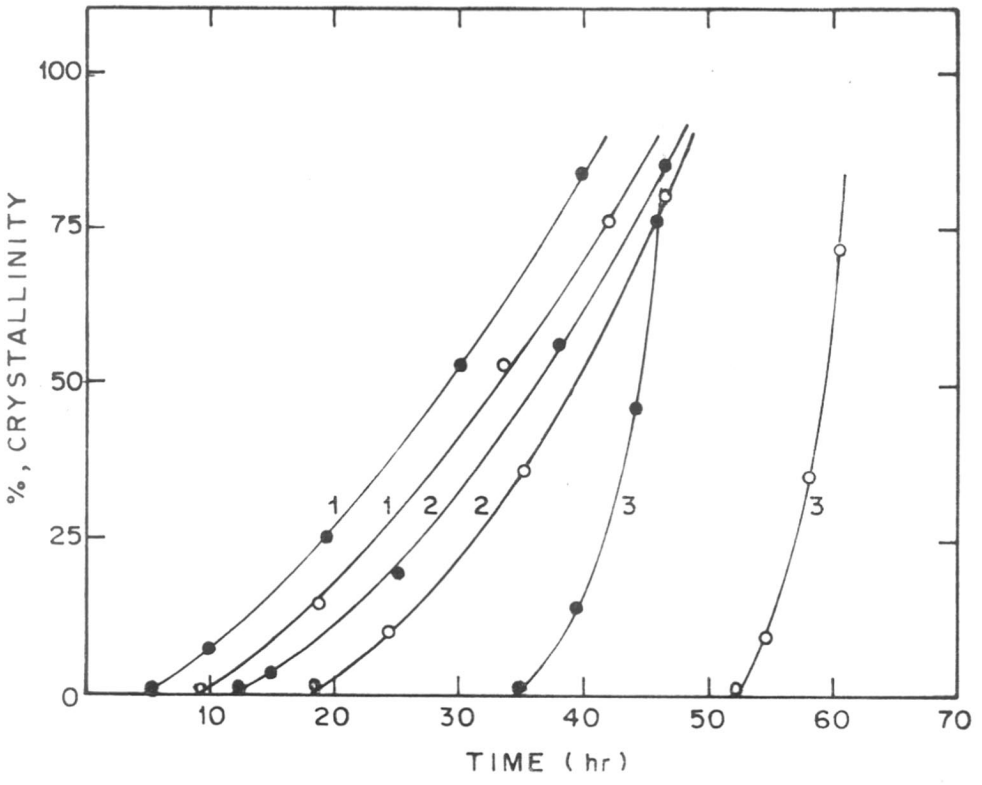

FIG. 2·8. INFLUENCE OF OH^- CONCENTRATION ON CRYSTALLIZATION OF ZSM-5 AT 453 K, $SiO_2 / M_2O_3 = 85$ ($M = Al^{3+}$ or Fe^{3+}). CURVES 1-3 REFER TO $(OH^- / H_2O) \times 10^3$ RATIOS OF 3·05, 1·2 AND 10·50 RESPECTIVELY

- ● Al / ZSM-5, (SYN. SYS. A)
- ○ Fe / ZSM-5, (SYN. SYS. B)

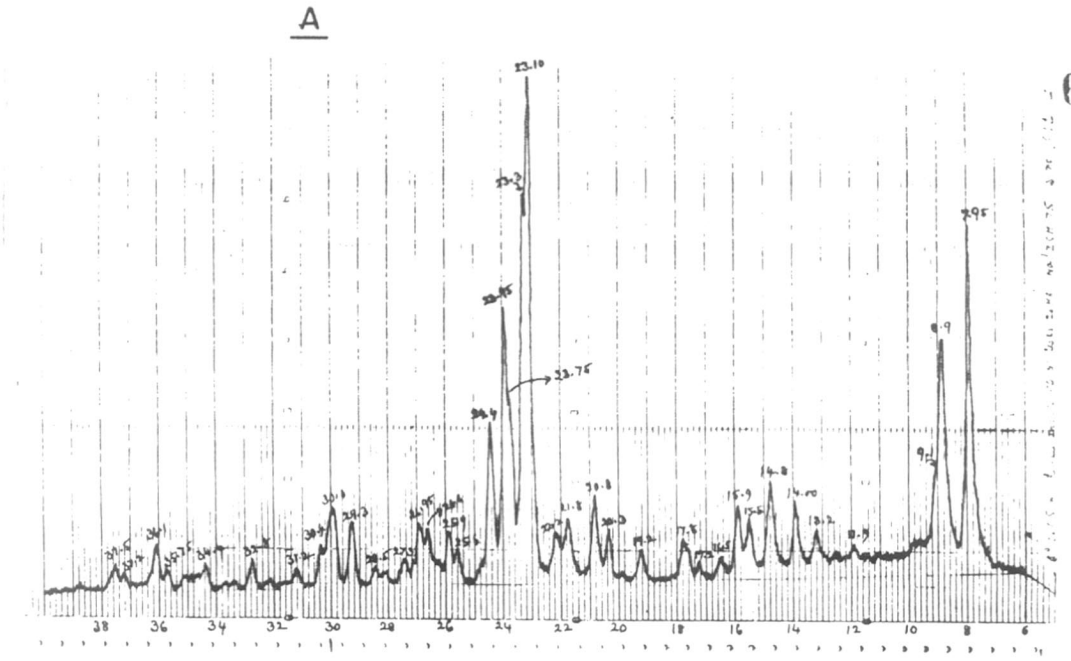

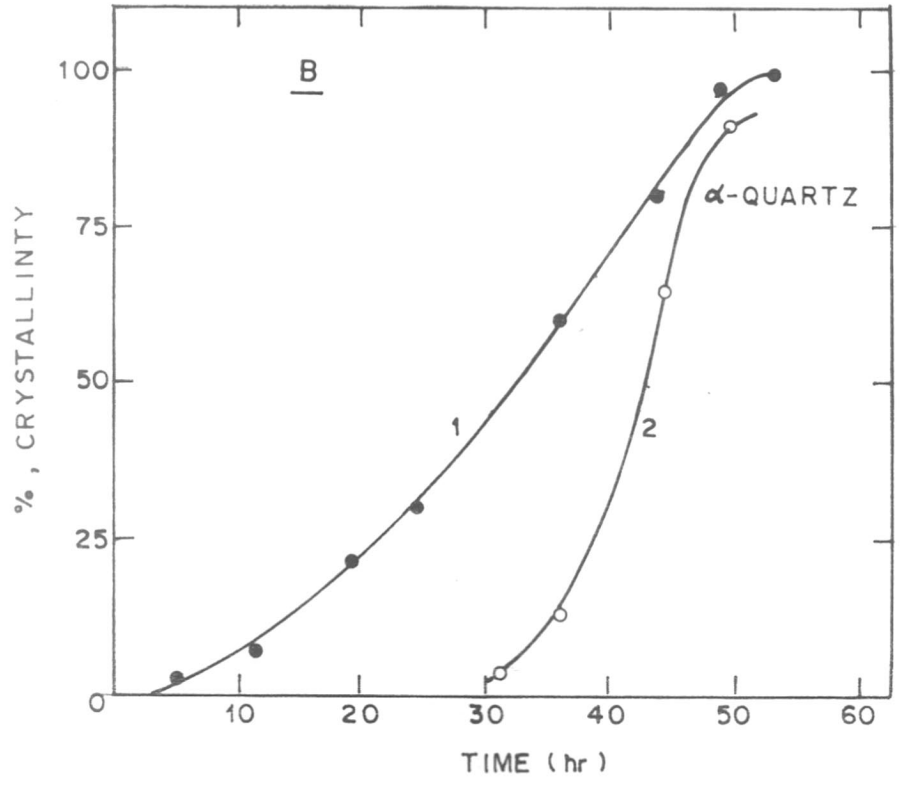

FIG. 2·9. INFLUENCE OF OH^- ION CONCENTRATION ON THE FORMATION OF α-QUARTZ PHASE IN ZSM-5 AT 453 K, $SiO_2 / Al_2O_3 = 85$, OH^- / H_2O RATIO FOR CURVE
1) 3.7×10^{-3} 2) 6.4×10^{-3}

form the nuclei of the ordered zeolite. Thus, an increase in OH^- ion concentration can shorten the nucleation period, but decrease in OH^- ion concentration will prolong the nucleation time. For example, SiO_2/M_2O_3 = 85 (M = Al^{3+} or Fe^{3+}), the nucleation period was shortened from 36 to 5 hours in case of Al/ZSM-5 (system A) and 52 to 10 hours in case of Fe/ZSM-5 (system B), and then prolonged to 10 hours and 20 hours for Al/ZSM-5 and Fe/ZSM-5 systems respectively, when the OH^-/H_2O was first decreased from 10.5 x 10^{-3} to 3.05 x 10^{-3} and then further decreased to 1.2 x 10^{-3}.

This suggest the existence of an optimum OH^- ion concentration for nucleation in synthesis of ZSM-5. Although the alkalinity strongly affects the nucleation, the crystal growth rate is almost independent of OH^- concentration.

Further, it is seen from the Fig. 2.9,(B) as the OH^-/H_2O ratio of the synthesis system A' decreased from 6.04 x 10^{-3} to 3.80 x 10^{-3}, the formation of α-quartz, a non-zeolitic phase subsequently gets suppressed. However, the nucleation and crystallization of the zeolite ZSM-5 is markedly affected, by shortening the nucleation period associated with longer crystallization time. This is evident from the x-ray diffraction pattern of the product [Fig. 2.9(A)], taken after the crystallization was complete. The XRD pattern shows no major peaks at 2θ = 26.7° and 20.9° (I/I_o x 100 values of 93.3 and 46.3 respectively). The 2θ and corresponding d values for α-quartz

have been reported by Hanawalt et al.[123]. It has also been reported in the patent literature[123a] that the use of methylethyl ketone (butanone) and salts retard the growth, or phase transformation to ∝-quartz during the synthesis of ZSM-5. It is, therefore, obvious that methylethyl ketone acts as solvent which facilitates the formation of template in the reaction system and salts help to decrease the OH^-/H_2O ratio, which, in turn, results into suppression of ∝-quartz phase.

Further, the formation of ∝-quartz phase mainly, because of the decomposition of organic cations in the synthesis mixtures at 453 K, was confirmed experimentally and reported by Borade et al.[113b].

2.6.5. Infrared Spectroscopy

The structure of zeolite phase formed from alumino-silicate mixture was studied by infrared technique. An earlier IR studies of lattice vibrational bands (200-1300 cm^{-1}) for different zeolites had revealed[113] that the presence of the bands at 550 cm^{-1} in addition to the one at 450 cm^{-1} showed the formation of zeolite ZSM-5 type material and absence of 550 cm^{-1} band unambiguously confirms that such a zeolite has not been formed. The IR spectra in the framework region (200-1300 cm^{-1}) for synthesis A and B systems at different crystallization time are shown in Fig. 2.10. The spectra were recorded using nujol mull technique with KCN as internal standard (reference peak at 2200 cm^{-1}). The strong absorption band in the 1000-1200 cm^{-1}

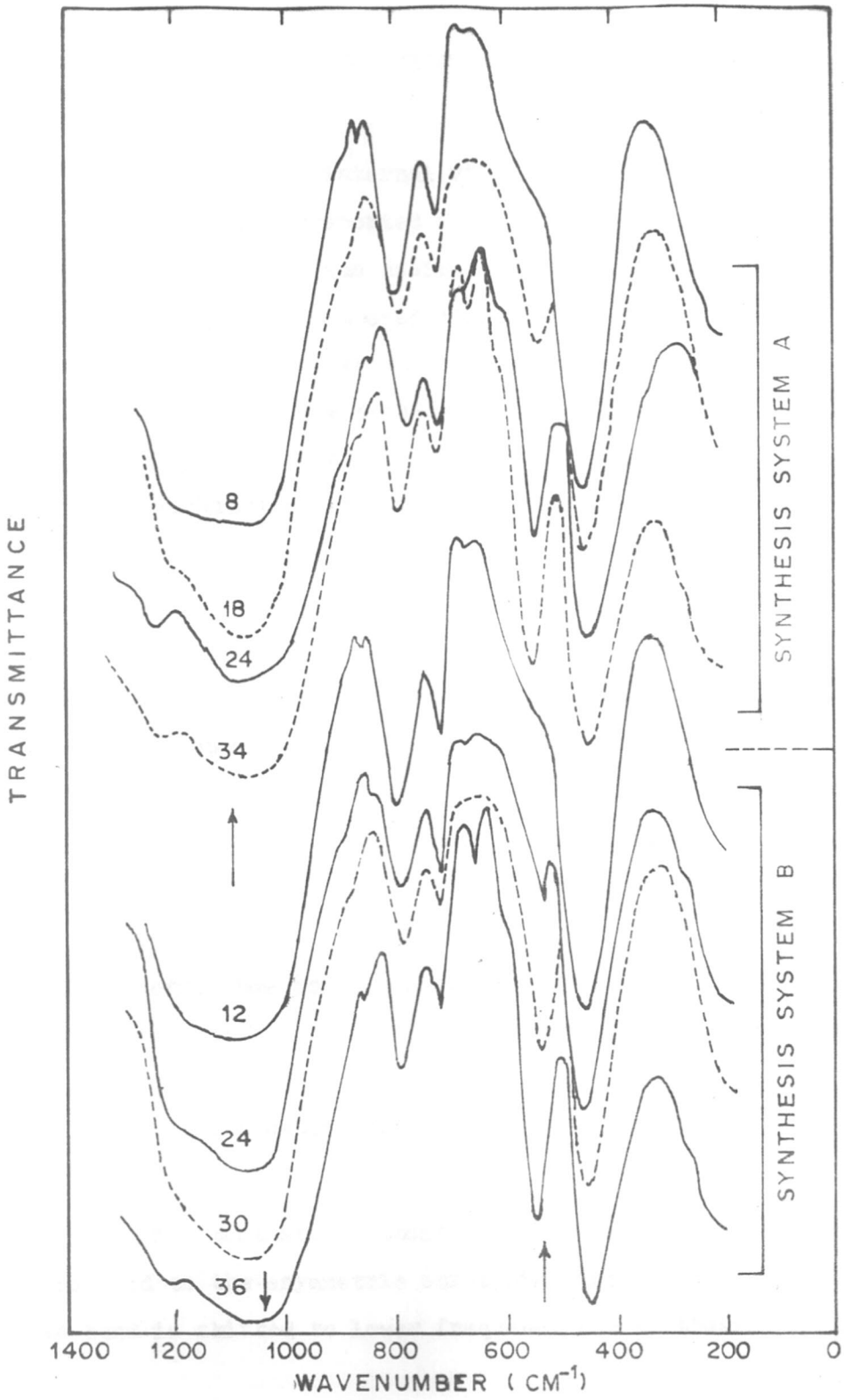

FIG. 2-10. IR SPECTRA OF ZSM-5 PENTASIL ZEOLITES SYNTHESIZED AT T = 453 K, NUMBERS INDICATE SYNTHESIS TIME IN HOURS

region are assigned to internal vibration of Si, AlO_4 tetrahedra, which are also reported for silica and quartz[114]. The absorbance at 550 cm^{-1} was assigned by Jacobs et al.[86] to highly distorted double five membered ring present in zeolite framework structure. The area under the peak at this frequency was employed to estimate the crystallinity of the materials by IR technique[109]. The variation in crystallinity evaluated by both X-ray diffraction and IR technique for ZSM-5 synthesized for both systems at different time, is presented in Fig. 2.11. Both, IR and XRD plots (Fig. 2.11 A) are sigmoid in nature indicating that the nucleation and crystal growth occur successively. The lower value of crystallinity obtained by XRD is attributed to its inability to see crystals smaller than 5 nm[86]. Further, the linear correlation between the two values of crystallinity is also in accordance with above observation. In a recent study, Jacobs et al.[109] showed that although the XRD pattern of the sample was characteristic of an amorphous material, the IR spectra show the material to be ZSM-5 zeolite with crystallite size less than 5 nm[109]. The variation observed in the IR crystallinity was attributed to the difference in the source of organic cation that has been used in the synthesis of ZSM-5[124].

The most strong absorption band at around 1100 cm^{-1} is related to the asymmetric stretching vibrations of T-O bond. This band is shifted to lower frequency for synthesis system B

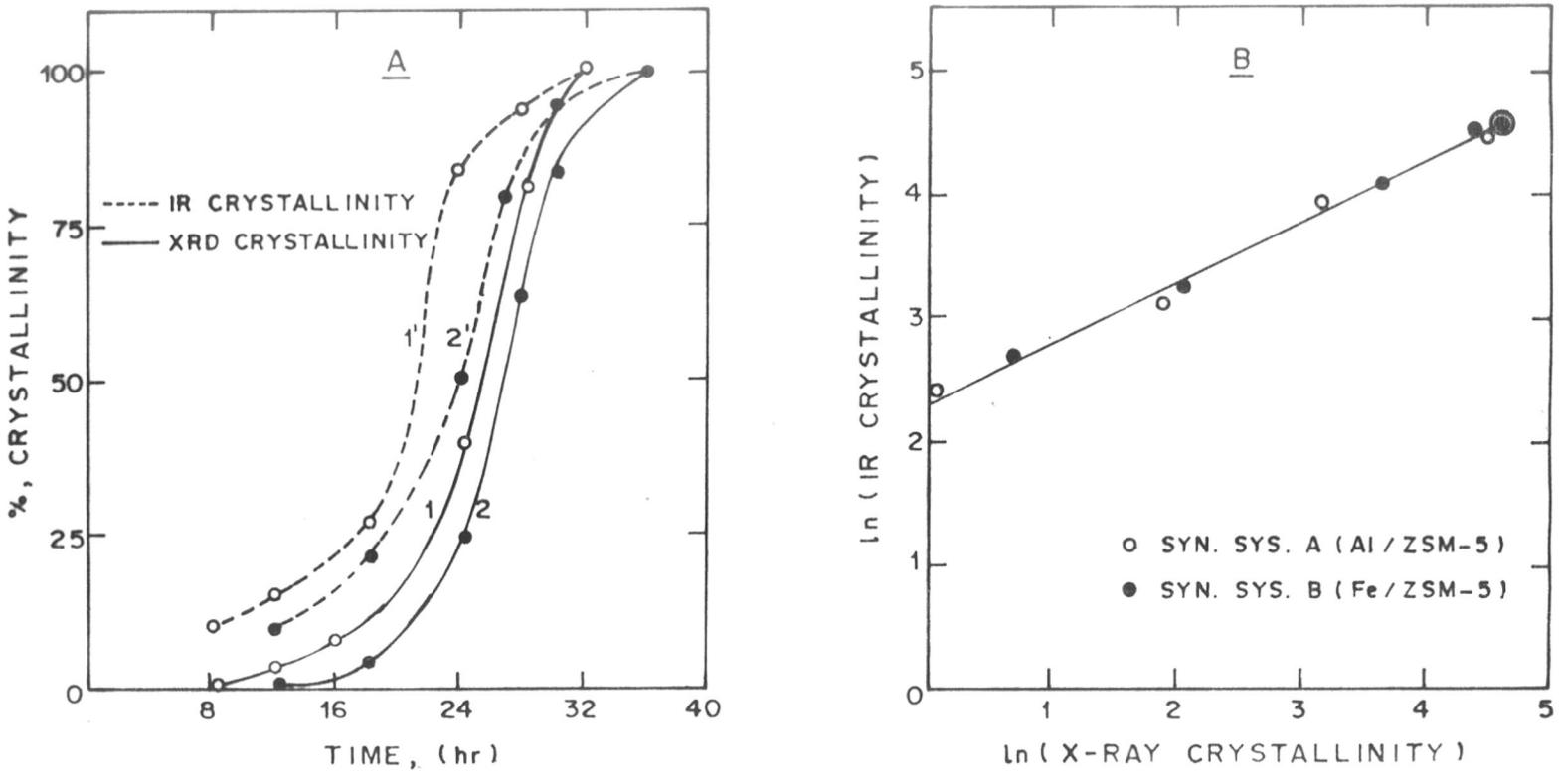

FIG. 2-11. A. CHANGE IN CRYSTALLINITY OF Na-ZSM-5 WITH SYNTHESIS TIME ESTIMATED BY IR-(CURVE 1',2') FOR Al/ZSM-5, SYN. SYS. A AND Fe/ZSM-5, SYN. SYS. B RESPECTIVELY, AND X-RAY DIFFRACTION CURVE (1,2). B. RELATION BETWEEN THE CRYSTALLINITY EVALUATED FROM IR AND X-RAY DIFFRACTION

i.e. for Fe/ZSM-5 (Fig.2.10) as compared to synthesis system A i.e. Al/ZSM-5 samples. The shift in frequency can be explained on the basis of T-O bond distance. In case of stretch frequency, substitution of Al for Si in the framework causes a shift to lower frequency owing to longer Al-O bond distance (1.75 Å) as compared to Si-O bond distance (1-60 Å). Flanigen and Grose[60] have established a proof of phosphorous substitution in the zeolite framework by using IR technique. A substitution of phosphorous in the framework showed the shift in the main asymmetric band towards higher frequency because of shorter tetrahedral P-O bond distance (1.54 Å). Similarly, the substitution of iron (Fe^{3+}) in the zeolite framework should show similar change, however, on account of longer Fe-O bond distance (1.97 Å) the band which occurs around 1100 cm^{-1} shifts towards lower frequency as can be seen in Fig. 2.10.

Additional information is now being obtained on zeolites and their mechanism of decomposition from studies of organic cation containing zeolites by using IR techniques. Wu et al.[61] studied the decomposition of tetramethylammonium (TMA-Y) zeolite by infrared spectroscopy by monitoring the decomposition products at 423-623 K. They observed at about 473 K absorption bands typical of the amine near 3028, 2965, 2930 and 1480 cm^{-1} decreased and absorption bands near 3735, 3637 and 3550 cm^{-1} typical of decationized Y- appeared.

They also suggested decomposition of the cations to give trimethylamine, methanol and decationized zeolite followed by secondary reactions including the formation of a methoxy zeolite at low temperatures.

The infrared spectra of solid TEBA-Br, zeolite incorporated with TEBA-Br and Na/ZSM-5 in hexachlorobutadiene mulls are shown in Fig. 2.12. A medium strong band for pure $N^+(C_2H_5)_3C_4H_9Br^-$ at 3005 cm^{-1} is ascribable to CH_3 asymmetric stretching mode and additional weaker bands below 3005 to 2700 cm^{-1} have their origin in alkyl symmetric stretching modes[124]. Similarly, bands between 1400-1480 cm^{-1} are due to deformed (bending) CH_3, CH_2 asymmetric, symmetric modes respectively. However, in case of ZSM zeolite containing TEBA-Br weak band at 2700 cm^{-1} of alkyl symmetric stretching is absent. This may be due to some change in charge environment of $N^+(C_2H_5)_3C_4H_9Br^-$ taking place as it involves incorporation during synthesis. Further discussion on the aspects of organic cations involvement and their decomposition will be taken up in the next section.

2.6.6. Thermal Analysis

The zeolite ZSM-5 samples synthesized by incorporating TEBA-Br in synthesis system A and synthesis system B (Al/ZSM-5 and Fe/ZSM-5 respectively) are studied by thermogravimetry. Both the weight loss and magnitude of the corresponding thermal effects are utilized to characterize the intermediate phases.

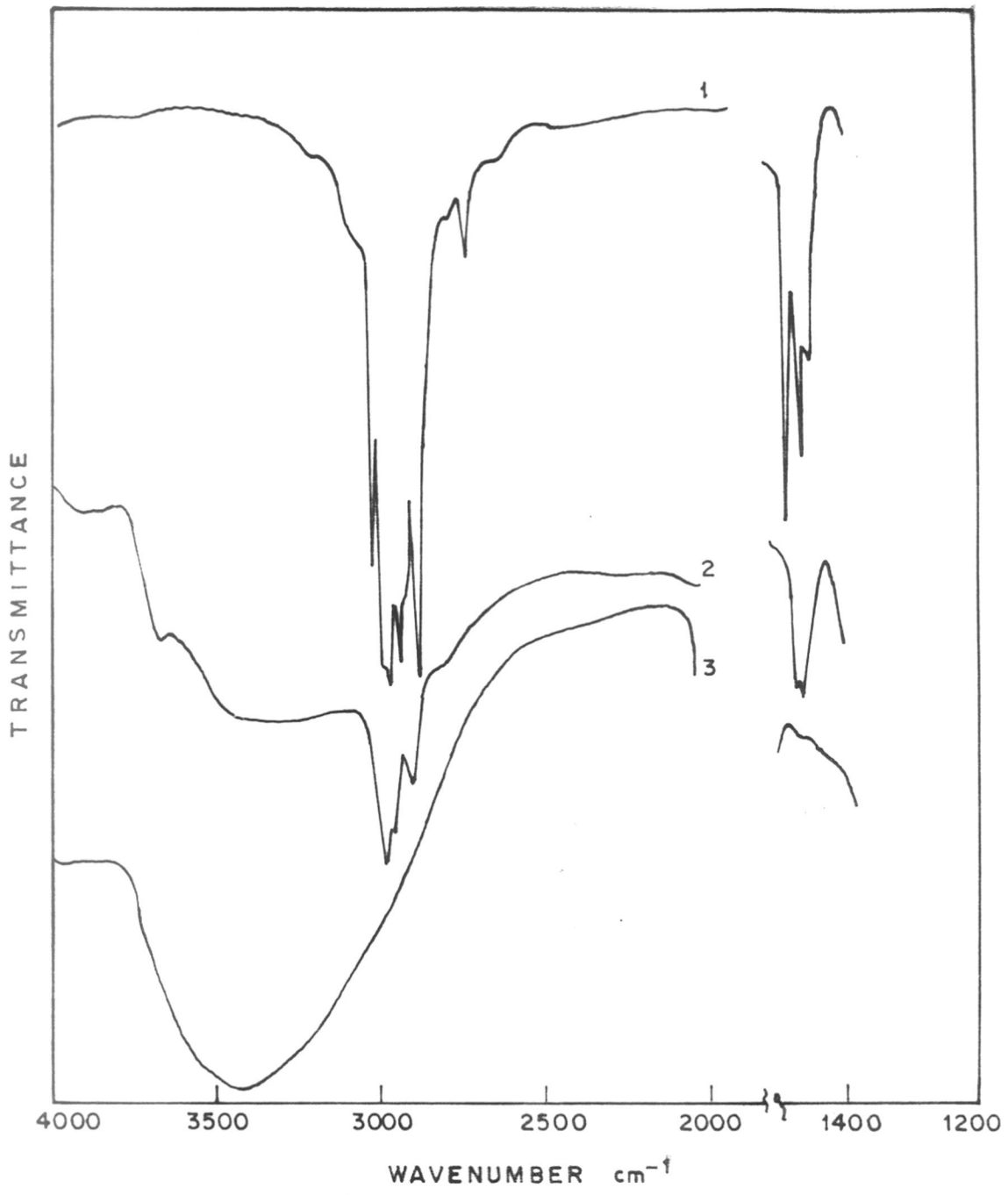

FIG. 2·12. IR SPECTRA IN HCB MULLS;
CURVES 1) TEBA·Br 2) ZEOLITE
SYNTHESIZED USING TEBA·Br AND
3) Na/ZSM-5 ZEOLITE SAMPLE

The TG and DTA curves for dried young gel mix and fully crystalline samples of ZSM zeolite synthesized by both the systems using TEBA-Br as organic cations are shown in Fig. 2.13. The figure reveals an endothermic effect with minimum at 373-383 K and very strong exothermic effect at 623-773 K with two pronounced maximas at 683 K and 743 K. The endothermic effect at low temperature is related to the dehydration of physically adsorbed and occluded water by zeolite, while the inspection of exotherms in the temperature range 623-773 K reveals major transformation. This positive heat effect is related to the oxidative decomposition of organic compound occluded in the zeolite framework. These exothermic transformations were also observed by Chao[125] and Bibby et al.[126].

The decomposition of pure organic compound like tetraalkylammonium salts[127] occurs in the temperature range 450-553 K, but when tetraalkylammonium cations are adsorbed or bound to aluminosilicate framework they decompose at higher temperature range 623-775 K[128,129]. Similarly, the decomposition of pure TEBA-Br was observed between the temperature range 473-553 K, but the decomposition occurred at higher temperature, while it was occluded and stabilized in the ZSM-5 zeolite framework. It was further observed that the exothermic peak has two segments, indicating the oxidative decomposition of the organic species stabilized in the zeolite

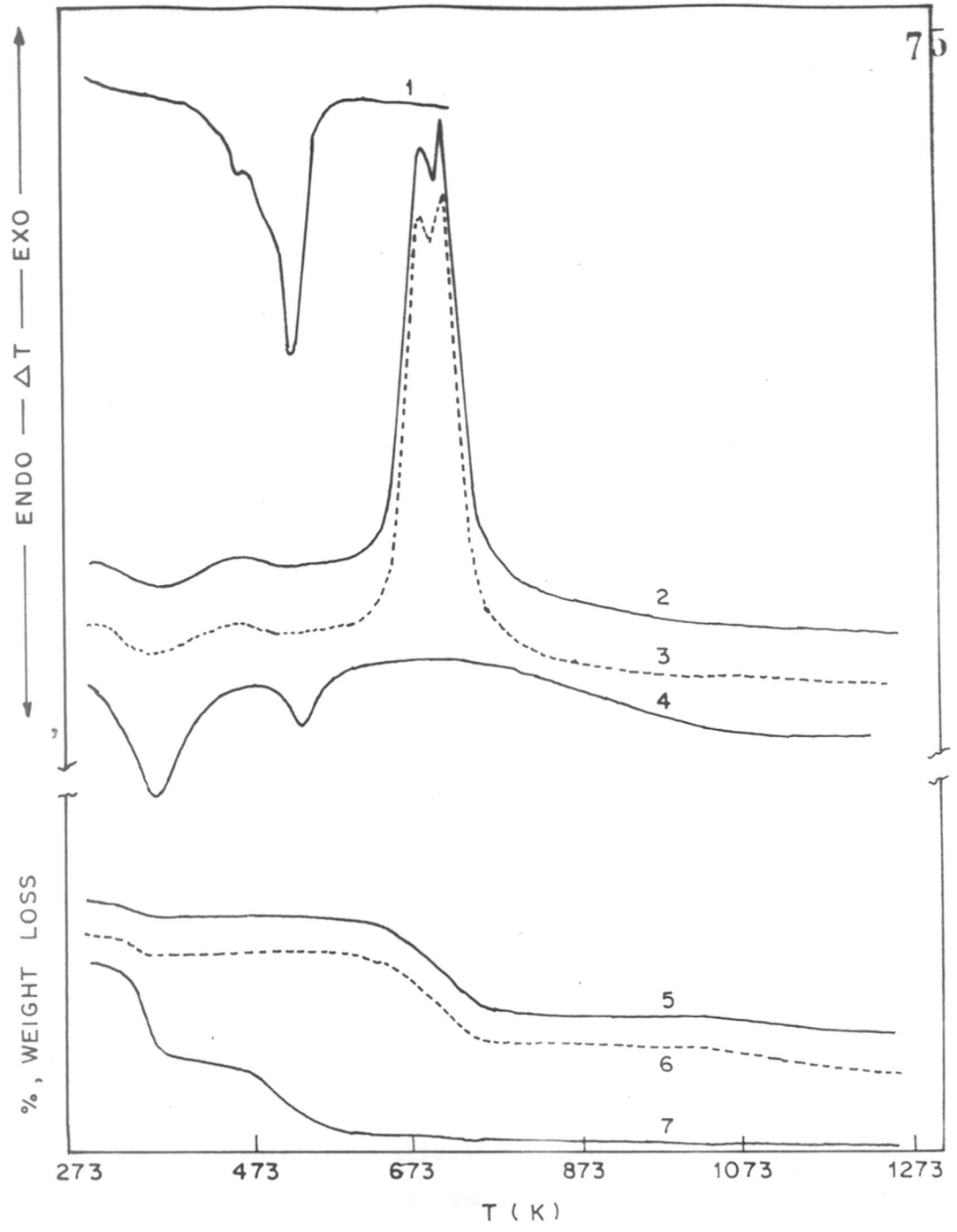

FIG. 2·13. DTA, TG THERMOGRAMS; CURVES 2,3 AND 5,6 FOR 100 % CRYSTALLINE ZSM-5 ZEOLITES, 4 AND 7 FOR YOUNG-GEL OF REACTION MIXTURE AND 1 FOR PURE TEBA. Br

—— Al / ZSM – 5 , --------- Fe / ZSM – 5

framework in two steps. However, presence of two segments on DTA curve reflects that this process is much more complex. Apparently, the organic species or cations which are weakly bonded may undergo oxidative decomposition (exotherm segment around 683 K) early than those which are strongly bonded (exotherm segment around 743 K). As mentioned in the last section (IR spectra, Fig. 2.12) in case of zeolite ZSM-5 incorporated with TEBA-Br sample weak band at 2700 cm^{-1} of alkyl symmetric stretching is absent, which may be due to some change in charge environment of $N^{+}(C_2H_5)_3C_4H_9Br^{-}$. This is quite likely that during synthesis process the organic cation incorporated may undergo such change to balance the electro-negative part of the Al in the tetrahedra. Finally for the sample Na/ZSM-5 (TEBA-Br) (obtained on calcination of as-synthesized zeolite ZSM-5 at 823 K) all the symmetric and asymmetric stretching modes below 3500-2500 cm^{-1} as well as CH_3, CH_2 asymmetric, symmetric modes at 1400-1480 cm^{-1} are absent. This also is obvious since the organic (TEBA) is decomposed at 823 K and removed from the zeolite ZSM-5 framework.

It emerges from the above experimental evidence that the two segments on the DTA curve between 673-773 K are characteristics of this type of pentasil ZSM-5 zeolites, and further they are related to the localization of these organic cations at channel intersections[130], where they can also interact with framework negative charges.

The representative thermoanalytical curves for ZSM-5 in as-synthesized samples, using TEBA as organic cation for both the synthesis systems are shown in Fig. 2.14. It may be seen in both the systems that the amorphous zeolite phase has a continuous weight loss in the temperature range 298 to 1273 K. The observed weight loss in the temperature range 298 to 473 K is due to dehydration of physically adsorbed and occluded water. No major weight loss was observed above 573 K, for the amorphous materials. It is also observed that with increase in synthesis time, the weight loss due to decomposition of organic cations, in the temperature range 525-775 K, increases while corresponding weight loss due to dehydration decreases, indicating that more hydrophobic material is formed as organic species are progressively incorporated during the zeolite crystallization[117]. Table 2.7 summarizes the quantitative data for dehydration and decomposition of ZSM-5 zeolites synthesised using TEBA-Br for synthesis systems A and B.

The weight loss corresponding to decomposition of organic cations as a function of crystallinity, measured by x-ray diffraction is plotted in Fig. 2.15. Linear relations are observed in both the synthetic systems, where they extrapolate to finite ordinate. This may be due to the fact that, in both the systems, the nuclei of ZSM-5 are probably present in amorphous gel, which are not detected by x-ray diffraction on account of their smaller size (< 5 nm). From the weight loss due to decomposition of organic compound, it has been estimated that about four tetraalkylammonium ions are present per unit cell. Since ZSM-5 zeolite structure also contains four channel

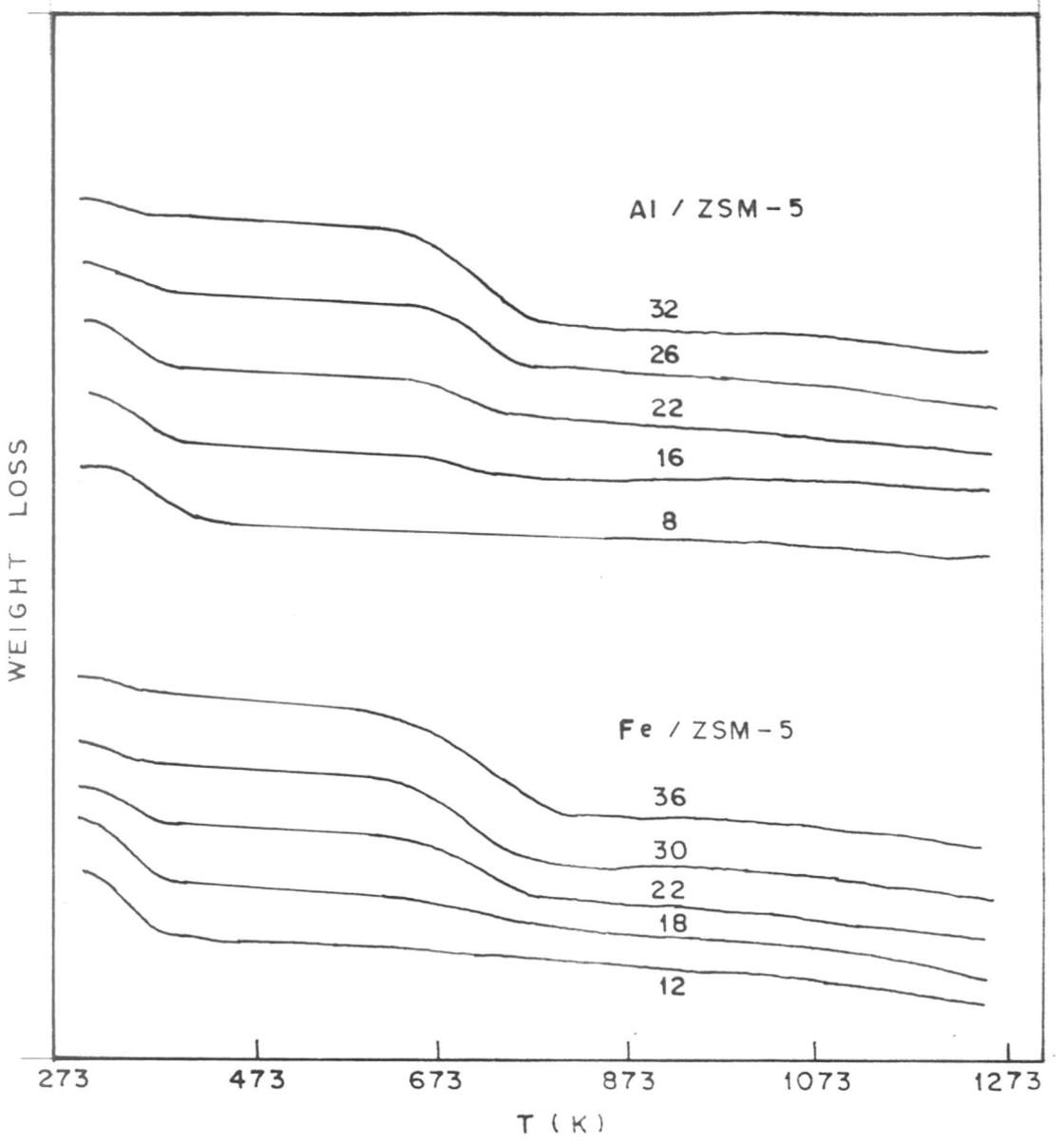

FIG. 2·14. TG CURVES FOR INTERMEDIATE PHASES FOR THE SYNTHESIS SYSTEMS USING TEBA. Br AT 453 K. NUMBERS INDICATE SYNTHESIS TIME IN HOURS

TABLE 2.7

Loss in weight upon dehydration and decomposition in ZSM-5 zeolites

Synthesis system A : Al/ZSM-5			Synthesis system B :Fe/ZSM-5		
% X-ray crystallinity	% Wt.loss upon dehydration	% Wt.loss upon decomposition	% X-ray crystallinity	% Wt.loss upon dehydration	% Wt.loss upon decomposition
4.5	12.4	2.0	2.2	12.6	1.5
9.0	10.2	2.6	11.5	11.7	2.2
27.0	9.3	4.1	25.0	10.0	3.5
65.5	6.6	6.9	90.0	5.5	8.4
100.0	5.0	8.5	100.0	4.8	8.8

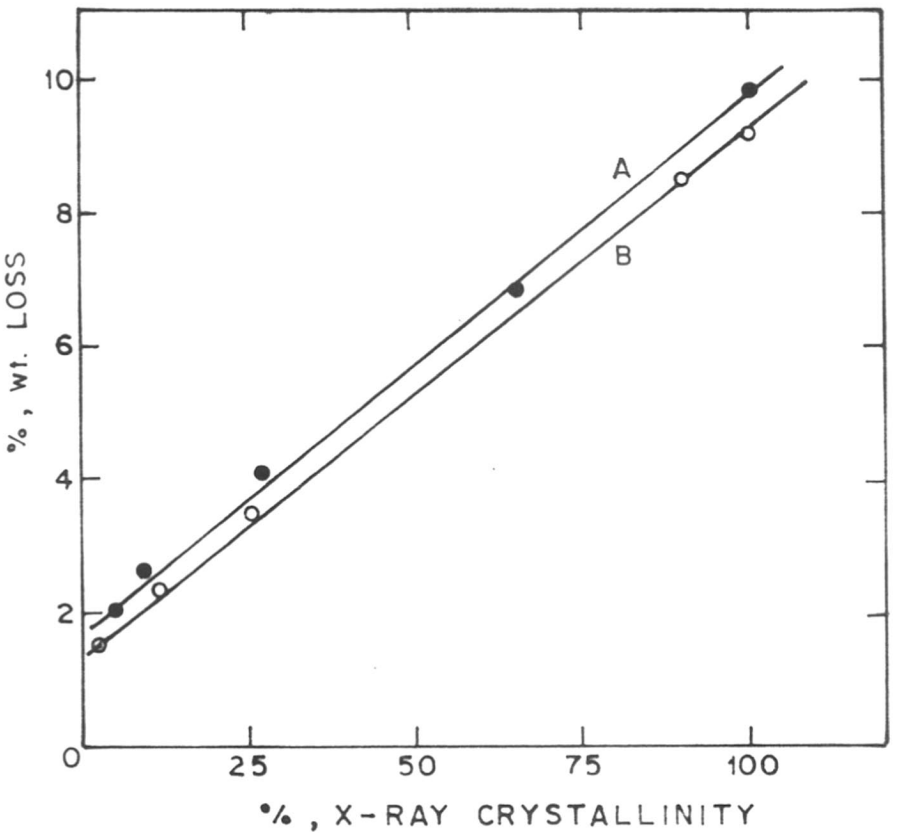

FIG. 2·15. CORRELATION BETWEEN THE WEIGHT LOSS FOR DECOMPOSITION OF TEBA CATIONS AND X-RAY CRYSTALLINITY FOR (A) Al / ZSM-5, SYN. SYS. A. (B) Fe / ZSM-5, SYN. SYS. B.

intersections per unit cell[25], it is concluded that the organic cations are located at the pore intersections.

2.6.7. Scanning Electron Microscopy

The scanning electron micrographs of ZSM-5 pentasil zeolites and representative intermediate phases for TEBA-Br synthesis system (SiO_2/Al_2O_3 = 200, OH^-/H_2O = 5.8 x 10^{-3}, T = 453 K) are illustrated in Fig. 2.16. The crystallization of gel mixture shows the presence of amorphous phase after 2 hours. Figs. 2.16(A) and 2.16(B) indicate that after 8 hours, both amorphous and crystalline phases coexist. The presence of clusters of polycrystalline aggregates at higher crystallization times indicates that crystalline phase must be embedded in the clusters of polycrystalline aggregates as can be seen clearly in the plates marked B and C. Better outlined crystals are observed for 100 per cent crystalline samples [Fig. 2.16(D)] at increased crystallization period with pronounced interlayer-type twinning and developing spherulitic shape. For synthesis system B involving Fe^{3+} substitution using TEBA-Br, the 100 per cent crystalline samples exhibit similar morphology. In both the systems using TEBA-Br, polycrystalline aggregates of about 10-12 μm were obtained.

The morphology of 100 per cent crystalline ZSM-5 zeolite samples prepared by incorporating TEBA-Br as template with different alumina content, keeping the other ingredients the same, is illustrated in Fig. 2.17. The morphology of the

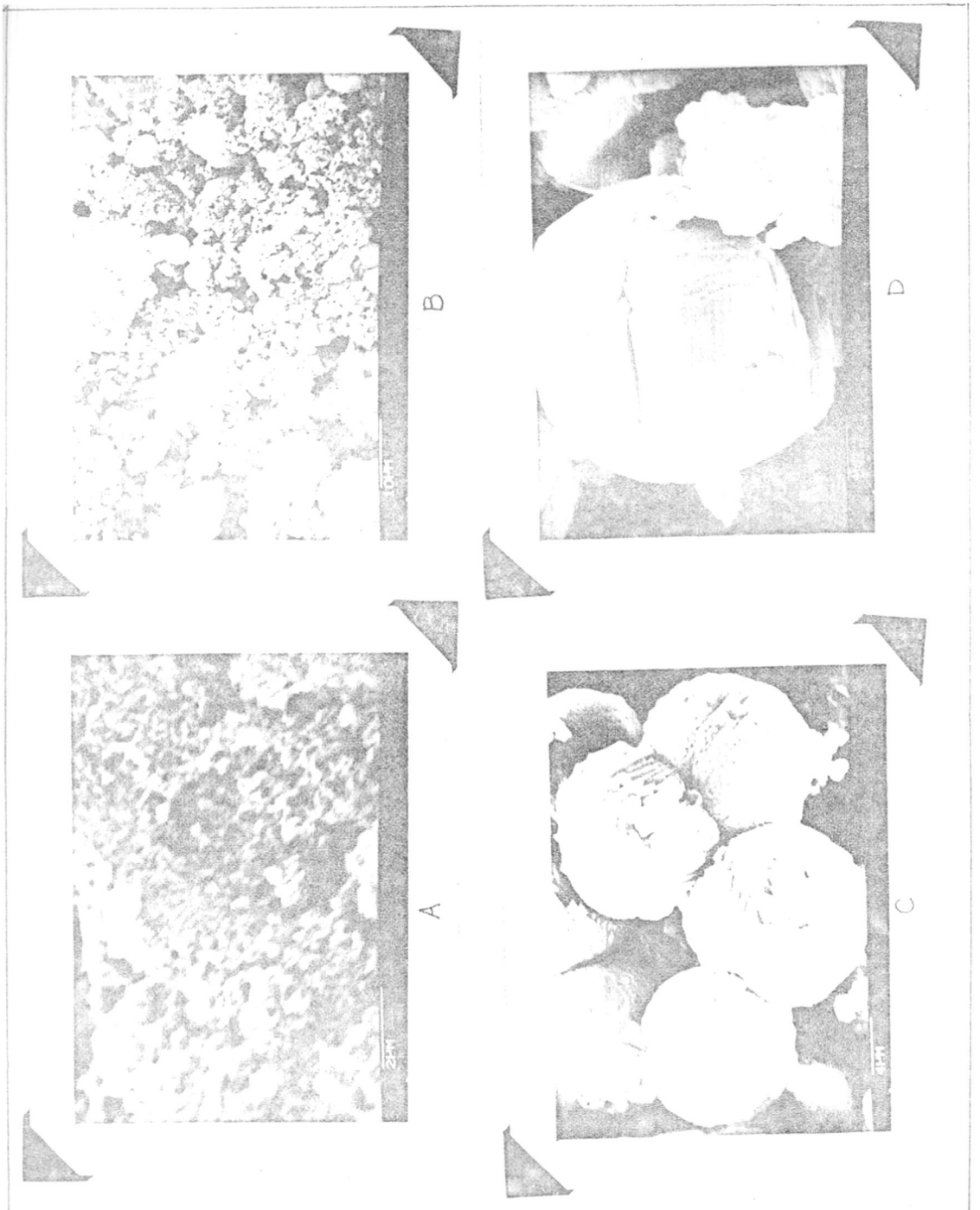

Fig.2.16: SEM photographs of ZSM-5 and intermediate phases, SiO_2/Al_2O_3 = 200
(A) Amorphous, (B) 20% crystalline, (c) 80% crystalline, (D)100% crystalline

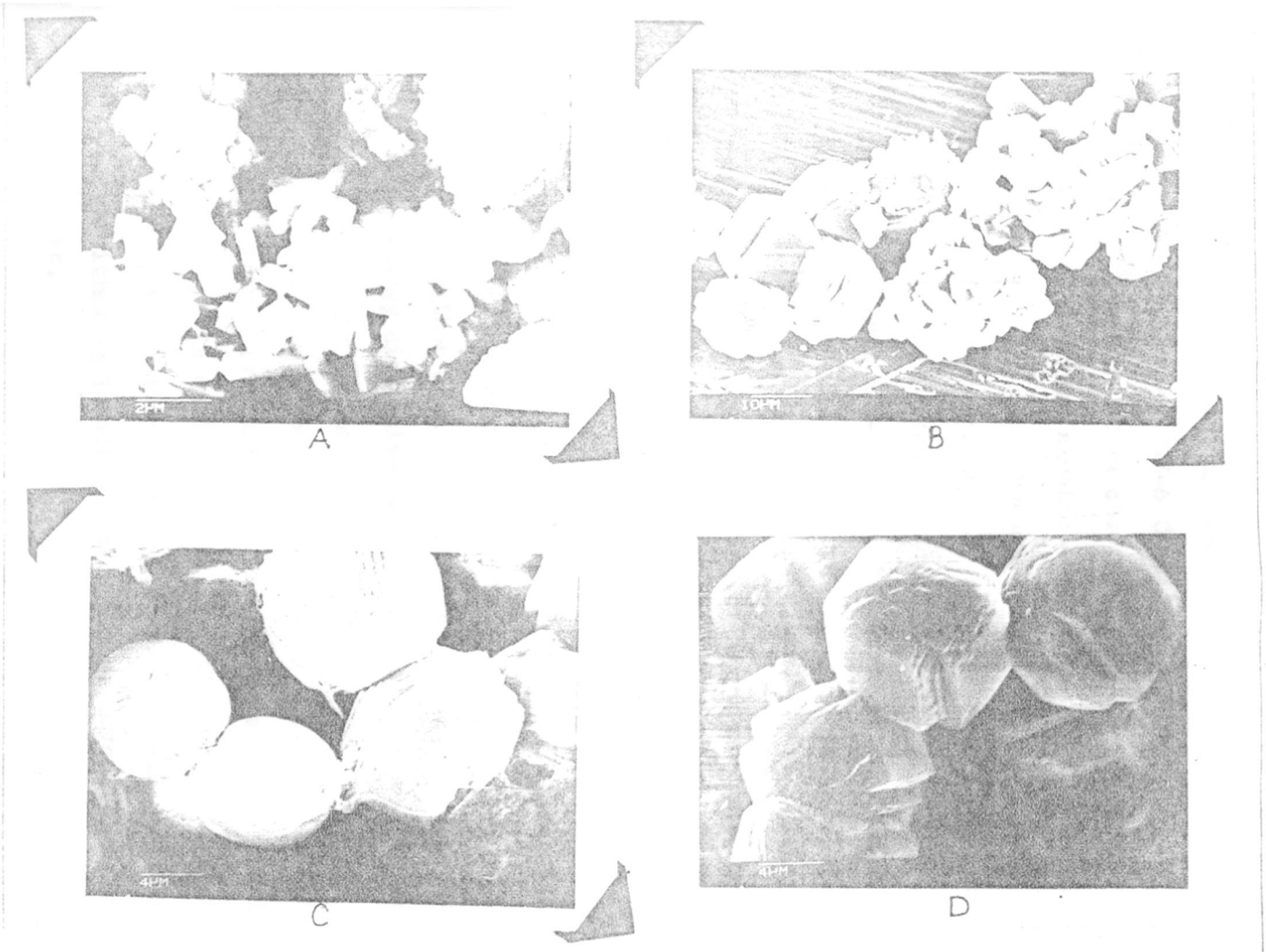

Fig.2.17: Effect of SiO_2/Al_2O_3 ratio on the morphology of ZSM-5 zeolite. SiO_2/Al_2O_3 ratios, (A) 35, (B) 85, (C) 600 and (D) silicalite.

ZSM-5 samples prepared by incorporating TEBA-Br is similar in nature to that of ZSM-5 (SiO_2/Al_2O_3 = 28, 86) previously reported[38a,113b]. It is observed from the SEM plate A (Fig. 2.17) that at higher alumina content in the ZSM-5 zeolite (SiO_2/Al_2O_3 = 35), the product consists of relatively large nets of intergrown rectangular crystals of 2 μm-4μm size. However, aluminium-free (silicalite) zeolite [Fig. 2.17, plate (D)] shows a well defined twinned interlayer cuboid shape crystals composed of 8-10 μm. This is in agreement with the previous observations[126,114,131]. On the other hand, we observed the formation of numerous small ZSM-5 platelets, which were deposited onto the primary large crystals [Fig. 2.17, plate B] on 100 per cent crystallization. Gabelica et al.[132] reported similar behaviour while studying the effect of NH_4^+ ions in ZSM-5 zeolite synthesis; and observed the enrichment of Si in the interior of the crystals rather than the outer rim of the big crystals by using energy dispersive X-ray analysis (EDX). They have explained this on the basis of a secondary nucleation mechanism. Such a morphology suggests that a growth of the nuclei initially starts from the silicate species available. Once the gel is enriched in Al, it will yield, through a secondary nucleation, these small platelet-like crystallites, which either agglomerate separately or cover the primary crystals.

The morphology of crystalline ZSM-5 zeolite samples on the suppression of α-quartz when Et_3N and n-Bu-Br is used during synthesis (SiO_2/Al_2O_3 = 85, $OH^-/H_2O = 3.8 \times 10^{-3}$, OH^-/SiO_2 = 0.149, T = 453 K) is illustrated in Fig. 2.18. The initial crystallization of gel exhibits sphereoidal agglomerates below 4 μm [plate A, Fig. 2.18]. However, on increasing the crystallization time to achieve almost 100 per cent crystallinity, well defined isolated rectangular prismatic crystals with secondary intergrowth are formed [plate B, Fig. 2.18]. A magnified cluster is shown in plate C, Fig. 2.18. At lower OH^-/H_2O and OH^-/SiO_2 ratios (which, in this case, is proportional to pH), the dissolution process would be largely absent and well defined isolated crystals are expected to form[133], probably from more homogeneous Si-rich gel domains, intermixed with aluminosilicate-$Al(OH)_3$ inhomogeneous phases. On the other hand, at higher OH^-/H_2O, and OH^-/SiO_2 ratios, polycrystalline aggregates are formed in high yield producing spherulitic crystals (as shown in Fig. 2.16). Rollmann et al.[133] also reported that at higher OH^-/H_2O and OH^-/SiO_2 ratios, crystal growth and dissolution would be competing and when an equilibrium is reached it may produce such morphology.

2.6.8. Mechanism of Zeolite Crystallization

Two different zeolite synthesis mechanisms have been discussed in the recent literature. McNicol et al.[134] argue in favour of a solid phase transformation mechanism

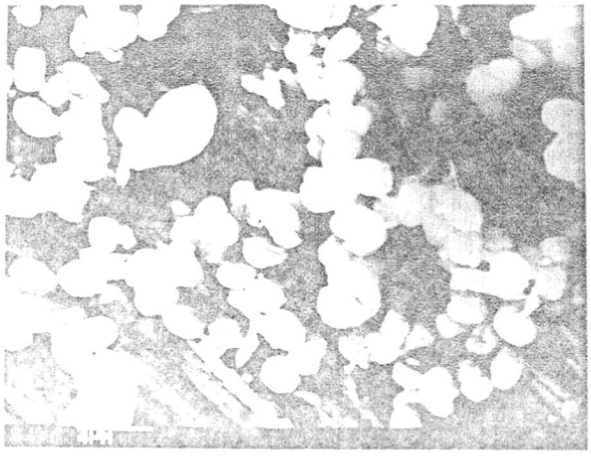

(A)

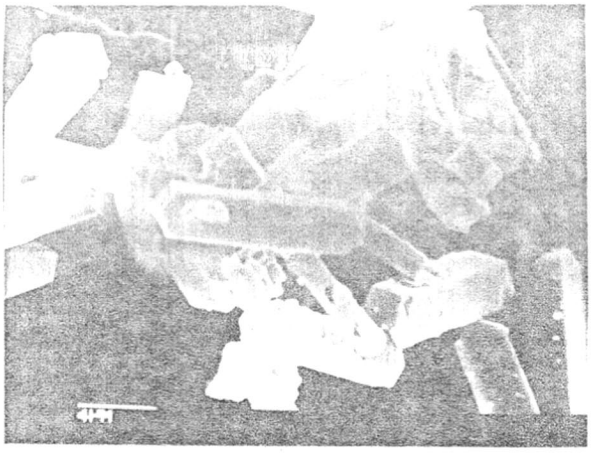

(B)

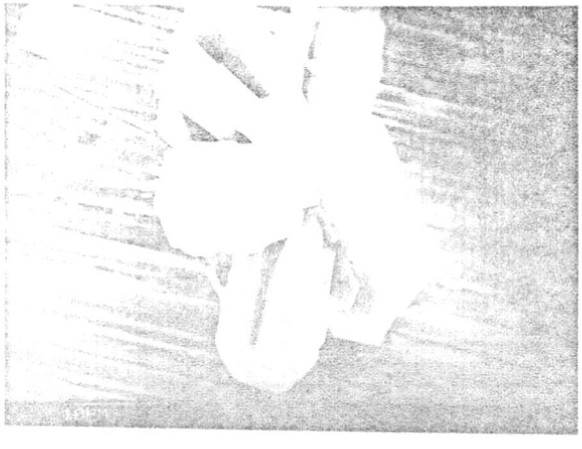

(C)

Fig.2.18: SEM photographs of ZSM-5 zeolite samples after elimination of α-quartz in the system Et_3N^+ n.Bu.Br. (A) initial crystallization, (B) near 100% crystalline, (C) magnified version of B

and Flanigen[29] discusses surface diffusion in the absence of substantial liquid transport, while Sand et al.[52,135], Kacirek and Lechert[136] and Zhdanov[28] present evidence in support of a solution transport mechanism. Recently, Derouaneet al.[117] have described these two mechanisms for the synthesis of ZSM-5 zeolites which depend on the type of reactants, relative concentrations and source of silica.

(i) Crystallization of liquid phase transformation[117]

In the liquid phase mechanism, the nuclei of zeolite crystals are formed in the liquid phase of gel or at the interface of gel phases. The growth of the crystal nuclei proceeds at the expense of aluminosilicate hydrated anion species in the solution. These anions represent different combinations of (Si-O) and(Al-O) tetrahedra[137]. These units can be the structural blocks of the growing crystals. Their composition and structure are given by the composition of the liquid phase. As the silicate species available in the solution are progressively exhausted, to establish equilibrium, continuous dissolution of silica and alumina gel, and of the sol occurs. Therefore, concentration of soluble aluminosilicate species in solution increases.

(ii) Crystallization of solid phase transformation

In the solid phase transformation, a hydrogel is rapidly formed from a solutions composed of monomeric silica and alumina[137] species at higher pH (> 10). A mixture of both

the species yields a hydrous aluminosilicate gel of high sodium content in which organic cations may also be included[117]. The gel composition should not be too different from that of expected reagents ratios. The nucleation of hydrogel occurs rapidly in presence of organic cations, which further interact intimately with the numerous reactive aluminosilicate anions and direct recrystallization process involving the solid-hydrogel transformation or surface nucleation. A rapid and sharp increase in nucleation and growth leading to large number of small polycrystalline zeolite crystallites results. Recent results obtained by Sand and coworkers[111,114] have confirmed the existence of these two different mechanisms. Schematic representation of zeolite ZSM-5 crystallization by (a) liquid phase transformation and (b) solid phase transformation is shown in Fig. 2.19.

Intermediate gel phases were analysed for SiO_2/Al_2O_3, and Na_2O contents in order to ascertain which mechanism is operative. Table 2.8 lists the data for intermediate gel phases for both synthesis systems prepared with the same organic (TEBA) cation that has been used for ZSM-5 pentasil zeolite synthesis. Within the experimental error, it is observed from the data in Table 2.8 that the SiO_2/M_2O_3 and M_2O_3/Na_2O ratios remain nearly constant for amorphous and crystalline zeolite phases. The constancy of Si/Al ratio of the solid phase as well as the absence of apparent crystallites in scanning electron micrographs

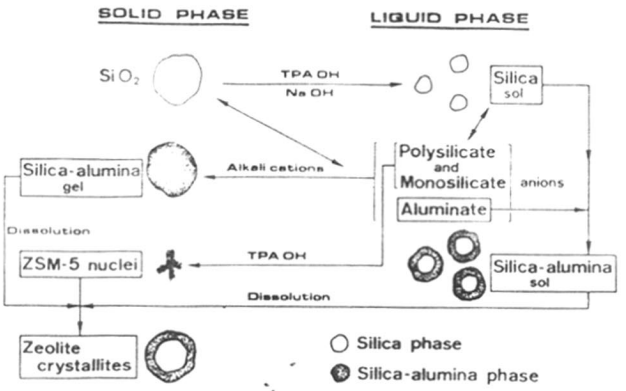

(A)

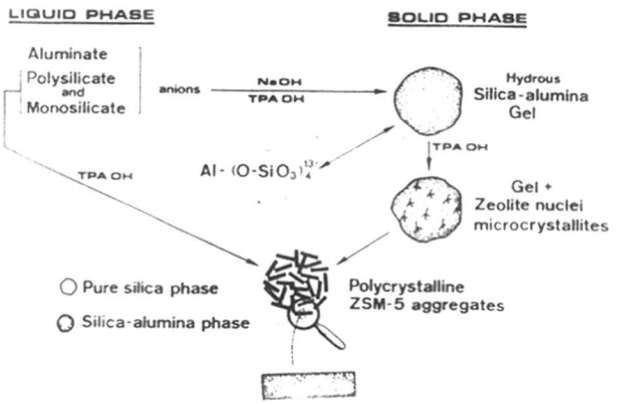

(B)

Fig.2.19: Schematic representation of ZSM-5 crystallization by (A) Liquid phase transformation, and (B) Solid phase transformation.

Adapted from Ref. 132.

TABLE - 2.8

Crystallinity and composition of intermediate phases

System A : Al/ZSM-5			System B : Fe/ZSM-5		
% X-ray crystallinity	SiO_2/ Al_2O_3	Al_2O_3/ Na_2O	% X-ray crystallinity	SiO_2/ Fe_2O_3	Fe_2O_3/ Na_2O
4.5	71.3	1.42	2.2	70.0	1.80
27.0	72.8	1.28	25.0	73.6	1.65
65.5	70.2	1.27	90.0	70.4	1.76
100.0	75.4	1.38	100.0	72.2	1.75

pictures until nearly 100% crystallinity is reached, argue in favour of a crystallization process by solid hydrogel phase transformation[117,138].

2.7. CONCLUSIONS

1. Synthesis of aluminosilicate ZSM-5 zeolite and isomorphous substitution of Fe^{3+} for Al^{3+} in the pentasil zeolite framework, using triethyl-n-butylammonium (TEBA) cation has been demonstrated.

2. The rates of both nucleation and crystal growth of Fe/ZSM-5 crystals are lower when Al^{3+} is replaced by Fe^{3+} in the zeolite framework by using TEBA-Br as the source of organic cation.

3. Suppression of a non-zeolite phase transformation into α-quartz has been achieved by varying OH^-/H_2O ratio in the system when Et_3N + n-Bu-bromide is used as the source of organic cation during the synthesis.

4. The templating or structure-directing role of N^+Et_3-n-Bu cations in the synthesis of pentasil zeolites of the type Al/ZSM-5 and Fe/ZSM-5 is recognized.

C H A P T E R - III

PHYSICO-CHEMICAL CHARACTERIZATION

C O N T E N T S

3.1. INTRODUCTION

During the last decade, the application of zeolite molecular sieves has increased tremendously in the field of adsorption-separation and catalysis. In the synthetic zeolites, the cations are in the sodium/potassium form and the zeolites as-synthesized are not suitable for commercial use. These basic forms can be modified by ion-exchange, thermal treatment, metal impregnation, and fairly wide variations in their physico-chemical properties can be achieved. The variations of the physico-chemical properties of exchanged zeolites are generally determined by the measurements of sorption, thermal and diffusional properties[139,140].

The nitrogen adsorption isotherm for a pure zeolite is quite characteristic and is distinguishable from that of amorphous materials, Johnson[141] used the nitrogen adsorption isotherm of thermally treated zeolite catalyst to estimate the quantity of zeolite in the catalyst. The sorption of nitrogen, not only gives the measure of the surface,accessible to molecules comparable in size with nitrogen, but also the surface area of the samples[142]. From the sorption capacities of water, n-hexane and cyclohexane, the modifications in the pore structure have been determined and the available total void volume has been evaluated. The modifications in the crystal structure are studied by x-ray diffraction[143] and IR spectroscopy[59].

The thermal stability of zeolite structure is determined from DTA curve. The high temperature exotherm is often used to determine the thermal stability of the samples. Thus, the framework distortion caused by ion-exchange and steam treatment has been evaluated from the sorption of nitrogen, water and other suitable hydrocarbons[144], in addition to x-ray and IR data of the samples.

The ZSM-5 pentasil zeolites, in the protonated (H^+) forms are widely used as catalysts in many reactions of industrial importance. A series of novel processes were introduced, based on the unique properties of synthetic ZSM-5 zeolite catalysts[145].

The zeolite ZSM-5 eatalyst exhibits acid activity, an unusual resistance to coking and higher thermal and acid stability as compared to other zeolites. The surface acidity of these zeolites has been studied by classical technique such as thermal desorption of ammonia. In this chapter, we report changes in the structural parameters studied by XRD and IR techniques, alongwith the sorption of nitrogen, water and different hydrocarbons. The acidity of ZSM-5 zeolites with varying SiO_2/M_2O_3 (M= Al^{3+} or Fe^{3+}) ratios is also reported in this chapter.

3.2. EXPERIMENTAL

3.2.1. Preparation of protonated (H^+) ZSM-5 zeolites

The ZSM-5 zeolite samples in as-synthesized form contain occluded and stabilized quaternary ammonium ions and are designated as Al/ZSM-5(C/N) and Fe/ZSM-5(C/N). The organic cations which occupy the channels in the zeolite crystals are removed by heating the sample in a muffle furnace at 823 K for about 10 hours. The final calcination temperature is attained at linear heating rate of 2.5 K min^{-1}. The product is cooled to room temperature and is kept over saturated ammonium chloride solution for a week. The samples are designated as Al/Na-ZSM-5 and Fe/Na-ZSM-5.

In order to obtain NH_4-ZSM-5, the zeolite samples were exchanged under reflux condition with 5M solution of NH_4Cl at a liquid to solid ratio of 15. The samples were filtered, washed with hot water and dried at 393 K overnight. Same procedure was repeated twice to obtain maximum exchange.

The acidic or protonated forms (Al/HZSM-5 and Fe/HZSM-5) were obtained by air calcination of NH_4ZSM-5 samples at 823 K for 10 hours. The heating rate was 2.5 K min^{-1}. Then the samples were cooled to room temperature and kept in a desiccator over saturated ammonium chloride solution for a week.

3.2.2. X-ray Diffraction

The x-ray diffraction patterns were recorded to ascertain the purity in the samples and to detect the structural changes of zeolites after ion-exchange and calcination at different temperatures. The x-ray diffraction patterns of zeolite samples were recorded on Philips PW 1730 x-ray diffractometer using nickel filtered CuK_α radiation $\lambda = (1.5405\text{Å})$.

3.2.3. Thermal Analysis

The thermo-analytical curves were recorded on an automatic Hungarian derivatograph (MOM 102-Budapest) under the following conditions

Sample weight		- 100 mg
Rate of heating		- 10 K min^{-1}
Atmosphere		- Flowing air
Sensitivity :	DTA	- 1/1
	DTG	- 1/5
	TG	- 100

Precalcined and finely powdered α-alumina was used as a reference sample.

3.2.4. Thermal and Steam Stability

The zeolite samples were heated in a muffle furnace to the desired temperature, at heating rate of 2.5 K min^{-1} for 5-6 hours. Then the samples were cooled to room temperature and

kept in the desiccator over saturated ammonium chloride solution.

Steam treatment was carried out by heating the zeolite samples at a heating rate 2.5 K min^{-1} to the desired temperature in the flowing steam, at atmospheric pressure, for about 5-7 hours. After steam treatment, the samples were cooled and kept over saturated ammonium chloride solution in a desiccator for a week. These samples were subjected to x-ray diffraction and thermal analysis.

3.2.5. Nitrogen Adsorption

A conventional all glass BET unit was used for the measurement of nitrogen adsorption and consists of three burettes B_1, B_2 and B_3 (B_3 is not shown in Fig. 3.1), a manometer M and a sample bulb S. High vacuum system consisting of a two stage rotary pump, mercury diffusion pump, McLeod gauge, and a series of cold traps, were used for degassing the sample.

The volume of the burette bulbs was precalibrated with mercury before joining to the adsorption system. The burettes B_1, B_2 were immersed in water jackets, provided with thermowell for temperature measurements. Dead space volume

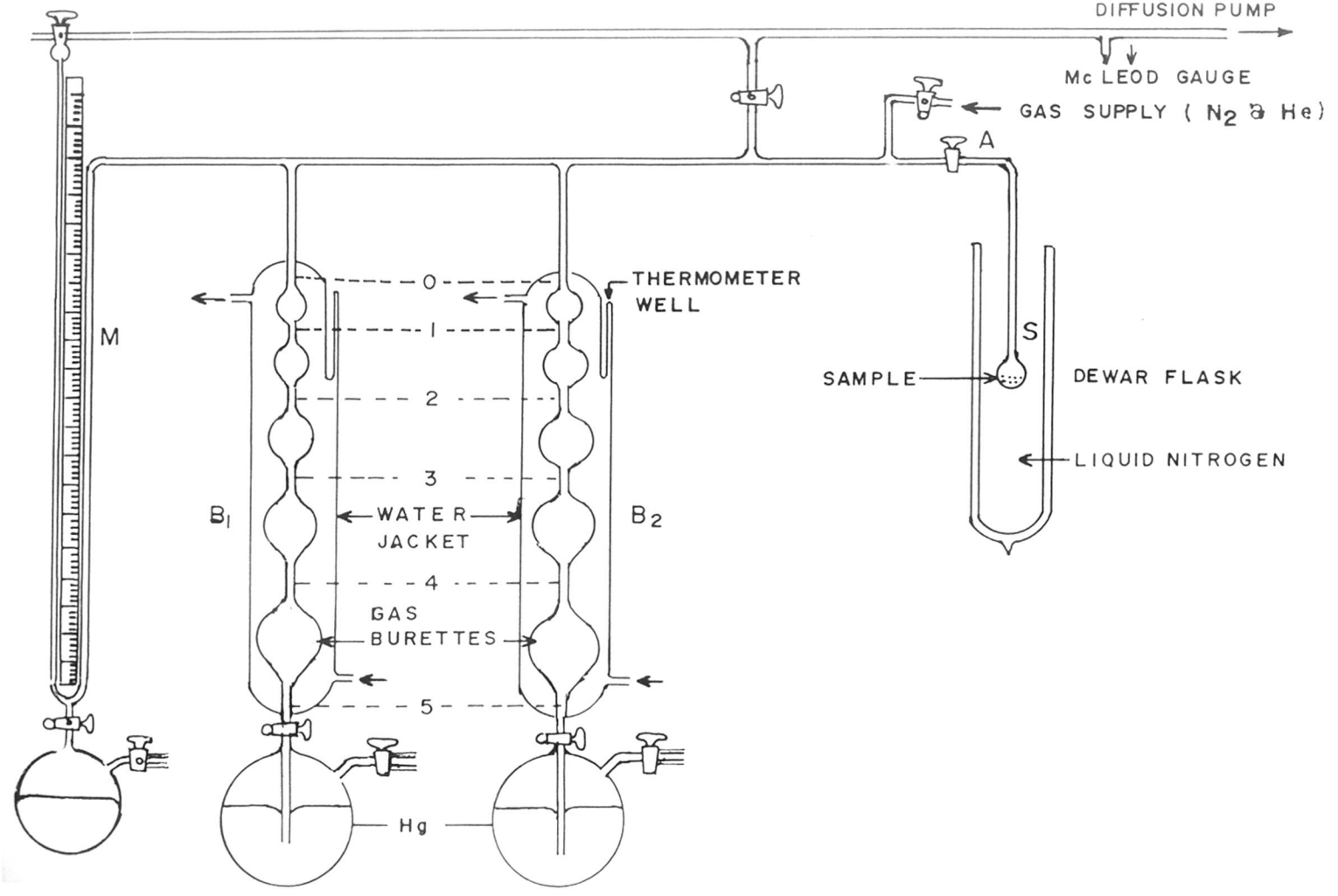

FIG. 3.1. GAS ADSORPTION UNIT FOR THE MEASUREMENTS OF BET SURFACE AREA

in the system was determined by using spectrally pure helium supplied by British Oxygen Co. (UK). About 0.2 to 0.3 g of hydrated sample weighed in the sample bulb was activated by increasing temperature slowly under continuous pumping. The sample was activated at 673 K by evacuation to about 10^{-6} torr for a period of 6 hours. The sample was cooled and dead space volume was determined by using helium at liquid nitrogen temperature. After pumping the helium-gas, a dose of nitrogen was admitted and calibrated. The sample was exposed to N_2 gas at 78 K. The adsorption was measured at different equilibrium pressures. The adsorption measurements were continued by admitting consequent calibrated doses, till a sufficient number of points were obtained. The reversibility was checked by carrying out desorption measurements. The volume of gas adsorbed at STP was estimated as follows

$$V_{ads} = V_1 - V_2 - V_3 \left(1 + \frac{\alpha P}{760} \right) \qquad \ldots 4$$

where V_1, V_2 and V_3 are volumes of gas taken, remaining in the system and in the bulb respectively. The α is the correction for the non-ideality of nitrogen at 78 K. The applicability of the Langmuir or BET isotherms equations for the estimation of surface area was checked by using the following relations

$$\frac{P}{P_o V} = \frac{1}{b.V_m} + \frac{P}{V_m P_o} \qquad \ldots 5$$

$$\frac{P}{V_{ads}(P_o - P)} = \frac{1}{V_m C} + \frac{C-1}{V_m C} \times \frac{P}{P_o} \qquad \ldots 6$$

where $C = e^{(E-E_o)/RT}$ is constant and depends on the sorbate-sorbent system, V_m is the monolayer volume, P_o is the saturation vapour pressure of nitrogen at 78 K, P is the equilibrium pressure, and b is a constant.

The void volume of the zeolite sample was determined from the Dubinin's plots log (a) vs $(\log P_s/P)^2$. The equation used was

$$\log(a) = C - D(\log P_s/P)^2 \qquad \ldots 7$$

where C and D are constants, P is the equilibrium pressure and P_s is saturation pressure.

3.2.6. Sorption and Diffusion Studies

The sorption and diffusion measurements for hydrocarbons in the micropores of ZSM-5 zeolites were conducted on McBain type gravimetric unit (Fig. 3.2). A sensitive silica spring was used for the measurement of weight changes. The zeolite sample, about 90 mgs, was pressed into a pellet and weighed into an aluminium bucket which was

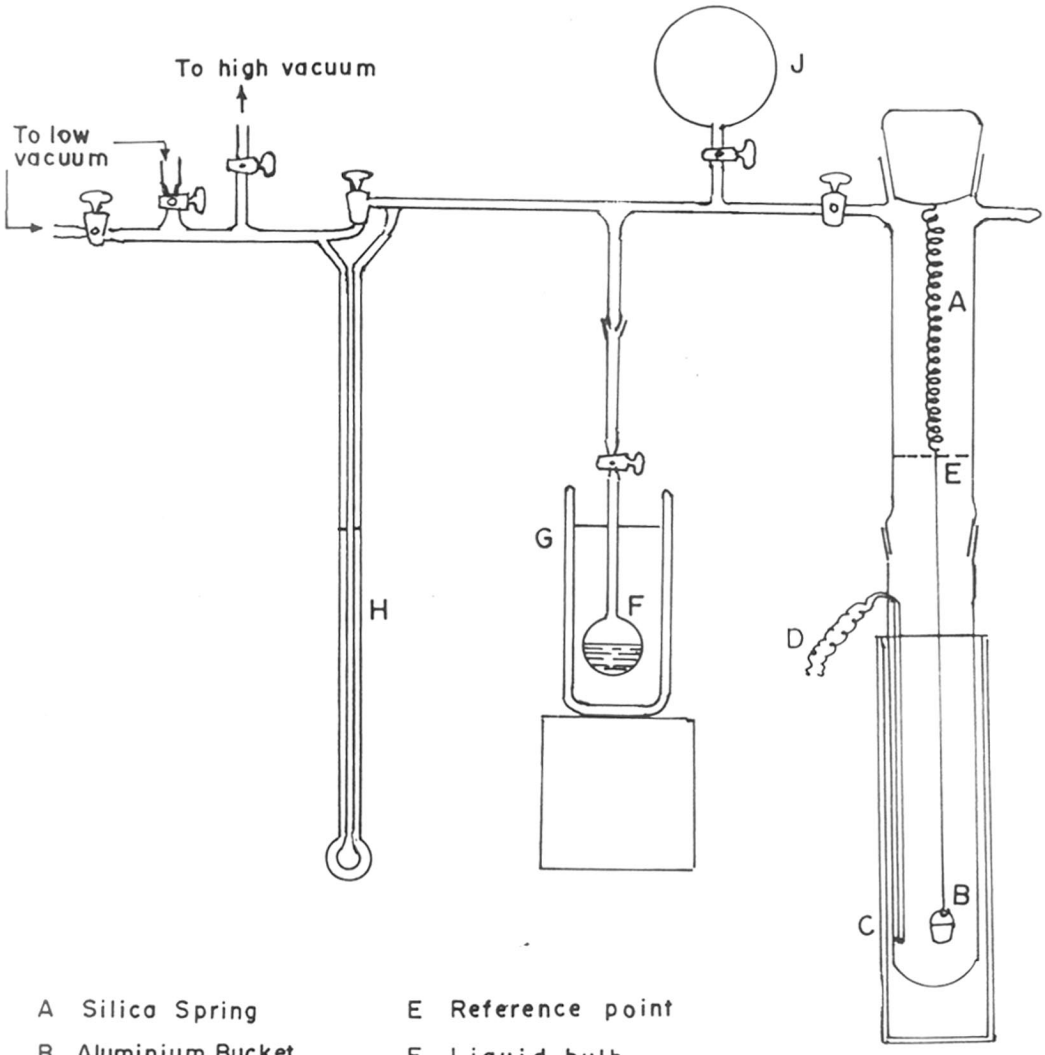

A Silica Spring
B Aluminium Bucket
C Furnace or Thermostat
D Thermocouple
E Reference point
F Liquid bulb
G Thermostat
H Manometer
J Gas Reservoir

FIG.3.2.GRAVIMETRIC ADSORPTION UNIT

attached to silica spring. The assembly was evacuated by means of two-stage rotary pump and mercury diffusion pump to a vacuum of 10^{-6} torr. The sample was activated at 673 K by continuous pumping till a constant weight was obtained. After the zeolite sample had reached a constant weight, the temperature of the sample was lowered to the desired value. To study the equilibrium sorption and rate of adsorption, the sorbate was admitted to the sample at constant temperature and pressure and weight gain was recorded on a cathetometer (accuracy $\pm$ 0.01 mm) as a function of time. After recording the equilibrium sorption, the catalyst was evacuated and heated to 673 K at 10^{-6} torr, and used for the next measurement.

3.2.7. Temperature Programmed Desorption of Ammonia (TPD)

The acidity of catalyst samples was measured by temperature programmed desorption technique. The experimental set up of TPD of NH_3 is shown schematically in Fig. 3.3. 0.4 g of zeolite catalyst sample (10-20 mesh) was taken in a micro-reactor connected to an on-line gas chromatograph (SHIMADZU, GC-R1A Model). Catalyst sample was initially heated to 673 K at a rate of 10 K min^{-1} in the flow of purified and dry N_2 gas, and then coupled to sorptometer for evacuation. It was activated under vacuum at 673 K for 2 hours, cooled down to 523 K and calibrated volume of NH_3 (RCF, 99.5%) was admitted to the sample, and it was further allowed to cool upto 298 K. The

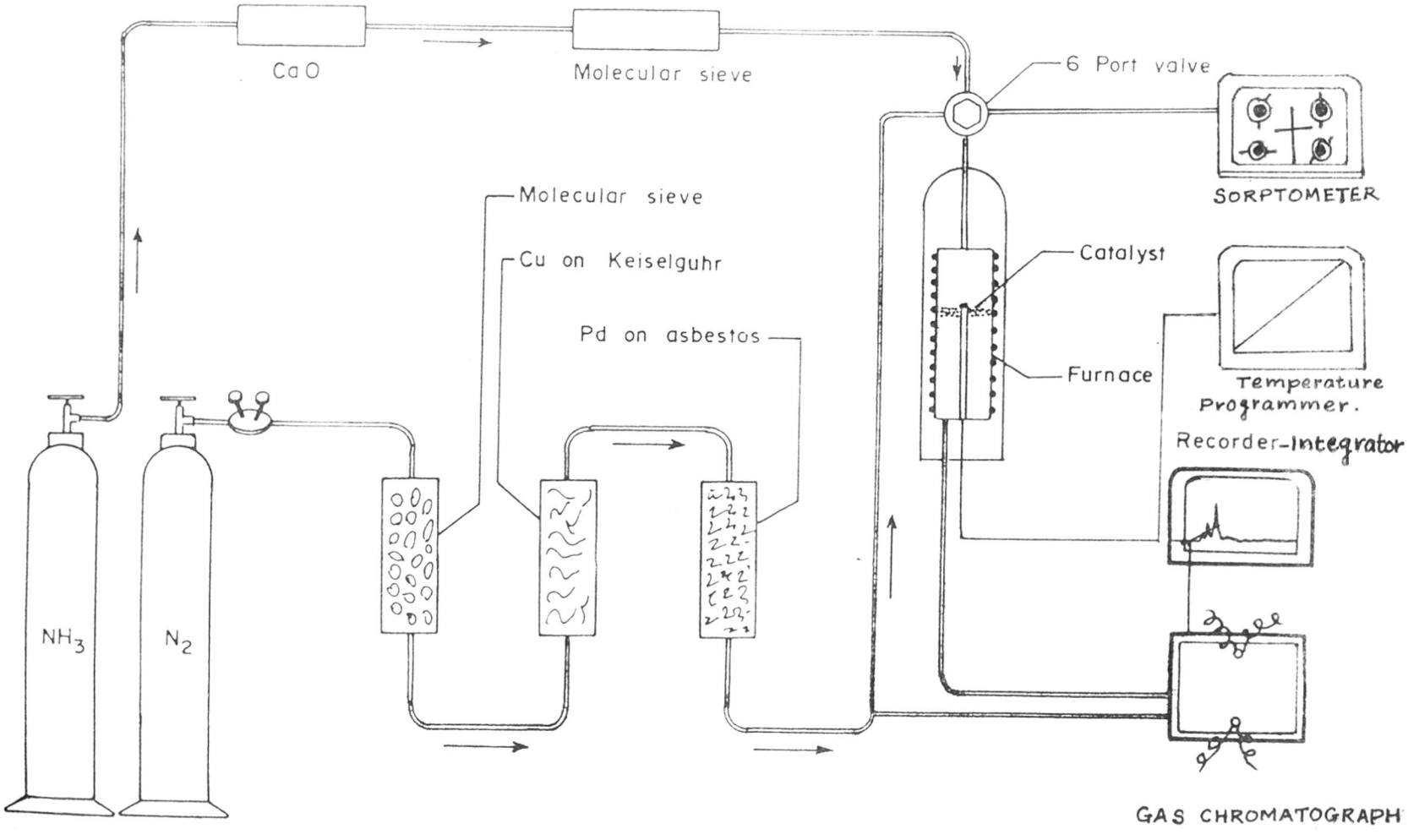

FIG. 3.3. SCHEMATIC DIAGRAM OF TPD UNIT

equilibrium sorption of NH_3 was determined at 298 K, and 200 mm vapour pressure. The loosely adsorbed NH_3 was evacuated at the same temperature. Equilibrium sorption of NH_3 was once again determined at the same temperature and pressure. The difference between the first and second equilibrium sorption was taken as the chemisorbed ammonia.

The sample was then coupled to the on-line G.C. after allowing sufficient time to stabilise the G.C. The sample was heated at a linear rate of 10 K min^{-1} with carrier gas flow rate of 60 ml min^{-1} and the TPD spectrum was obtained on the integrater with per cent area of the peaks. The total volume chemisorbed at 298 K obtained by volumetric measurements and with the subsequent area percentage of thermally desorbed NH_3, acid strength distribution was estimated quantitatively.

3.2.8. Infrared Spectroscopy

The IR spectra of zeolite samples were recorded in the frequency range of 200-1300 cm^{-1} using KBr pellets or nujol/(or H.C.B.) mull technique on PYE UNICAM SP-300 Spectrophotometer.

3.2.9. X-ray Photoelectron Spectroscopy (XPS)

The XPS spectra of zeolite Al/ZSM-5 samples were recorded on an ESCA-3 Vacuum Generator (VG) spectrometer. The exiciting radiation was MgKα with an energy of 1253.6 eV. The spectral resolution of the analyser was 1.0 eV. The spectra were recorded at room temperature under a vacuum of 10^{-8} to 10^{-9} torr. A binding energy of 284.4 eV for C_{1s} level was used as an internal standard for all samples. The accuracy of binding energy as determined with respect to this standard value was within $\pm$ 0.2 eV.

The XPS spectra for zeolite Fe/ZSM-5 samples were also recorded on VG ESCA-3 MgKα, slit width 4 mm, analyser energy 50 eV.

3.2.10. Electron Paramgnetic Resonance Spectroscopy (EPR)

The EPR spectra of polycrystalline Fe/ZSM-5 samples were recorded on Brucker E.R. 100D spectrometer, at room temperature (298 K). The spectrometer was operated at x-band microwave frequency (9.6 GHz) and calibrated with diphenyl picryl hydrazine (DPPH). Spectra were also recorded after various treatments described later. For the comparison, spectra of iron doped aluminium oxide (500-1000 PPM) sintered at 1243 K were recorded.

3.3. RESULTS AND DISCUSSION

3.3.1. X-ray Diffraction(XRD)

The unit cell compositions of Al/ZSM-5 and Fe/ZSM-5 zeolites as determined by chemical analysis are given in Table 3.1.

The x-ray diffraction patterns of Al/ZSM-5 and Fe/ZSM-5 samples is as-synthesized (C/N), Na, NH_4^+ and H^+ form are shown in Fig. 3.4, and 3.5 respectively. In both the systems the first sample was synthesized using TEBA-Br as organic template. The XRD pattern and 'd' values for these samples are in good agreement with reported data[38a].

The most intense peak is observed at 2Θ, 23.0° and 23.1° for (C/N) Al/ZSM-5 and (C/N) Fe/ZSM-5 respectively. The intensity of first two peaks for these respective samples at 2Θ, 7.8°, 8.7° and 8.0, 8.9° were found to increase when the samples are converted to sodium form. The increase in intensity was attributed to the removal of organic cations which are present in the intracrystalline voids[49]. On further conversion to ammonium form, and subsequently to hydrogen form, the intensity of these first two peaks increased, the singlet at 2Θ= 11.8° and 11.95° for the respective forms of these samples was observed, but was not reproduced. The intensity changes and formation of doublets and singlets have been explained[49] as due to the removal of extra framework organic

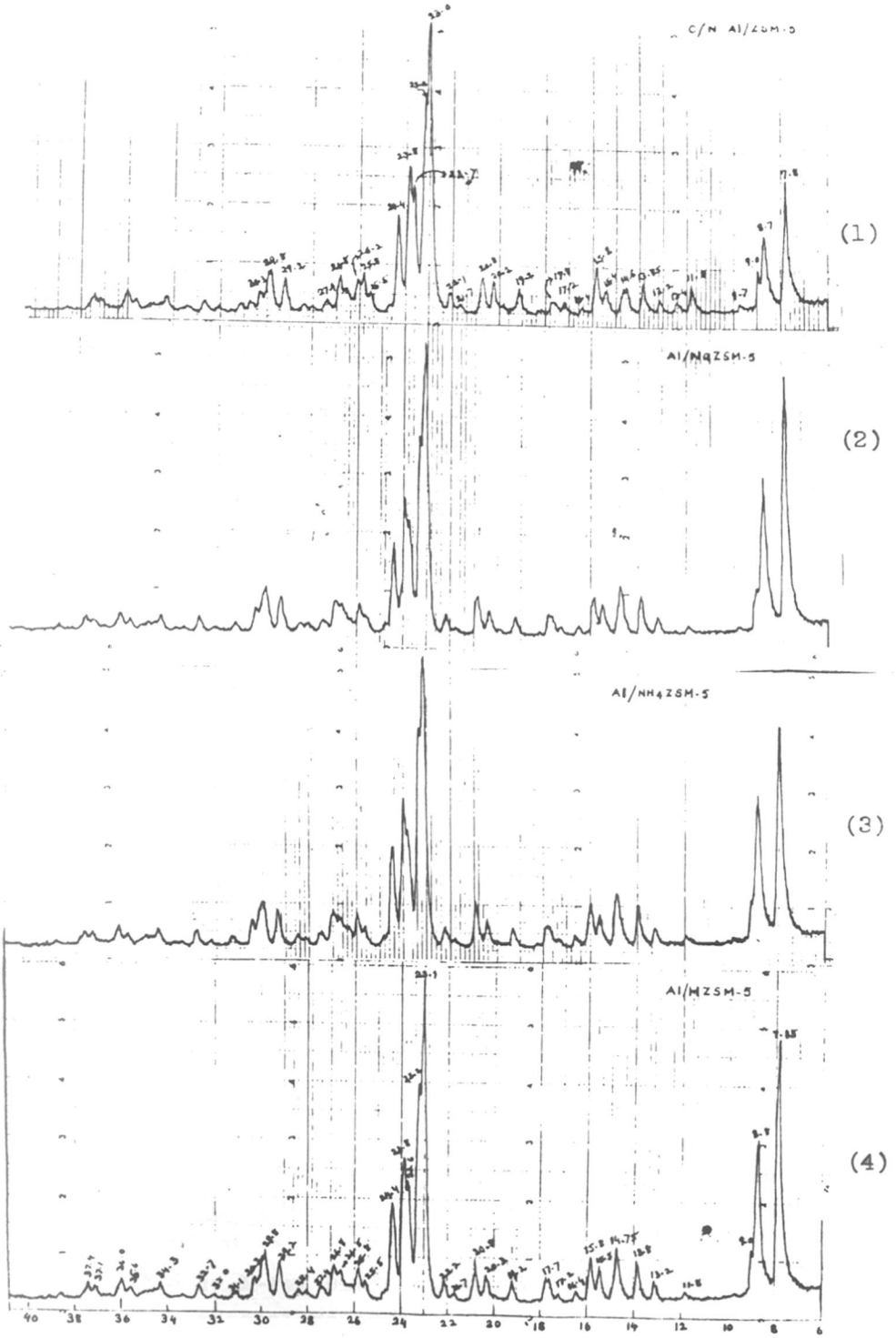

Fig.3.4: X-ray Diffraction Profiles of Al/ZSM-5 Zeolites. (1) as-synthesized (C/N), (2) Na- (3) NH_4- and (4) H- forms

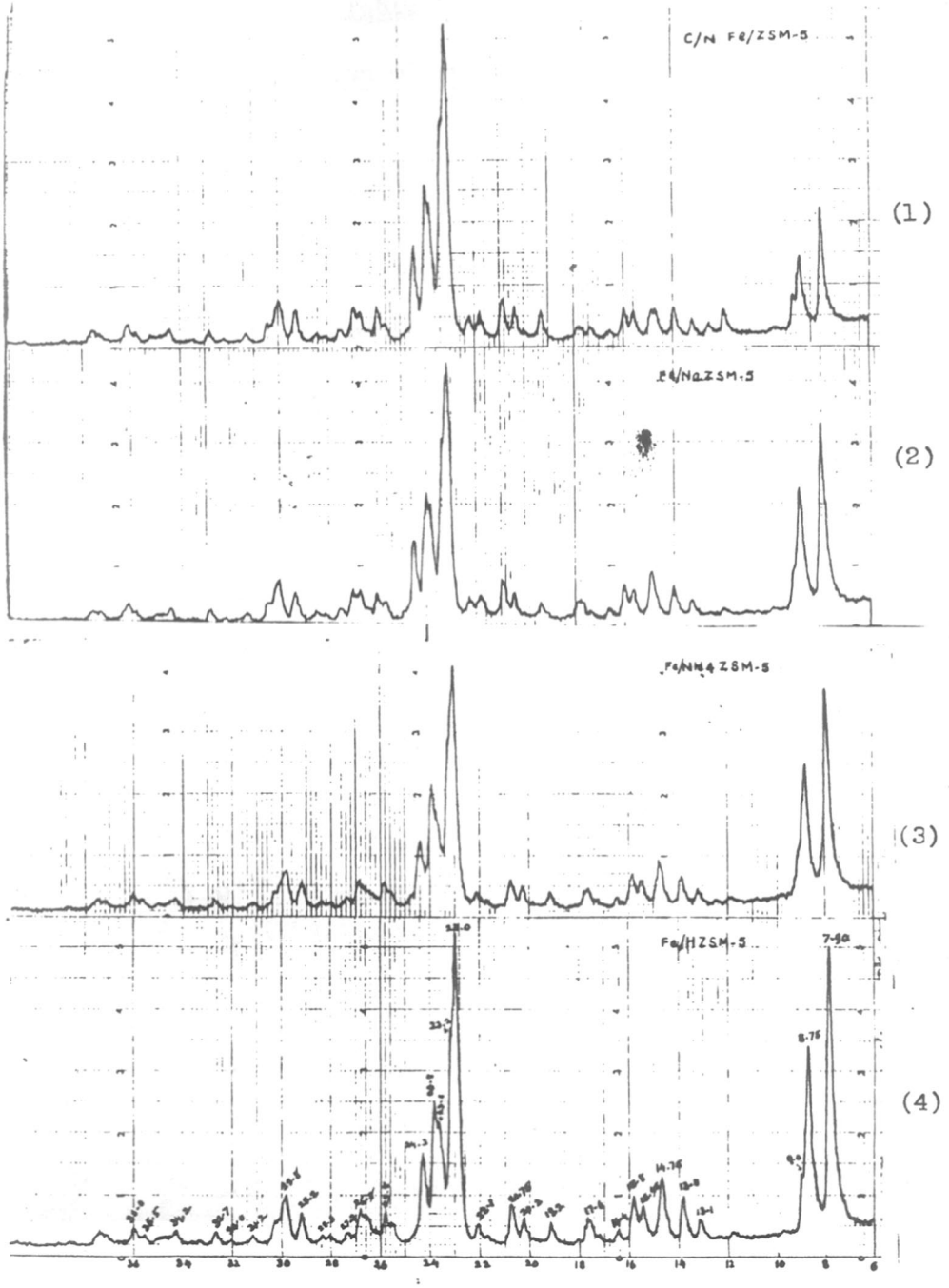

Fig.3.5 : X-ray Diffraction profiles of Fe/ZSM-5 Zeolites. (1) As-synthesized (C/N), (2) Na- (3) NH_4- and (4) H- forms

Table 3.1

The unit cell composition of anhydrous Na/Al/ZSM-5 zeolites

1. $Na_{1.54}[(SiO_2)_{90.90}(AlO_2)_{5.1}]$
2. $Na_{1.74}[(SiO_2)_{93.52}(AlO_2)_{2.48}]$
3. $Na_{1.34}[(SiO_2)_{95.07}(AlO_2)_{0.93}]$
4. $Na_{1.25}[(SiO_2)_{95.67}(AlO_2)_{0.33}]$

For anhydrous H/Al-ZSM-5 Zeolites

1. $Na_{0.05}[(SiO_2)_{90.90}(AlO_2)_{5.1}]$
2. $Na_{0.03}[(SiO_2)_{93.52}(AlO_2)_{2.48}]$
3. $Na_{0.012}[(SiO_2)_{95.07}(AlO_2)_{0.93}]$
4. $Na_{0.03}[(SiO_2)_{95.67}(AlO_2)_{0.33}]$

The unit cell composition of anhydrous Na/FeZSM-5 zeolites

1. $Na_{1.85}[(SiO_2)_{90.55}(FeO_2)_{5.45}]$
2. $Na_{1.45}[(SiO_2)_{93.41}(FeO_2)_{2.59}]$
3. $Na_{1.0}[(SiO_2)_{95.015}(FeO_2)_{0.985}]$
4. $Na_{0.48}[(SiO_2)_{95.67}(FeO_2)_{0.33}]$

For anhydrous H/FeZSM-5 zeolites

1. $Na_{0.07}[(SiO_2)_{90.55}(FeO_2)_{5.45}]$
2. $Na_{0.04}[(SiO_2)_{93.41}(FeO_2)_{2.59}]$
3. $Na_{0.015}[(SiO_2)_{95.95}(FeO_2)_{0.985}]$
4. $Na_{0.03}[(SiO_2)_{95.67}(FeO_2)_{0.33}]$

and inorganic species incorporated into the structural voids during synthesis and changes in the crystal symmetry of the zeolite respectively.

Fig. 3.6 shows the x-ray diffraction patterns of Na/ZSM-5 zeolites with varying SiO_2/Al_2O_3 ratios. The samples of Fe/ZSM-5 system exhibit similar (not shown in figure) x-ray diffraction pattern except some minor variations in the relative intensity of peaks at 2θ, 7.8, 8.7. With increase in SiO_2/Al_2O_3 ratio, the increase in intensity of two peaks at 2θ, 7.8, 8.7 is observed. This may be attributed to the decrease in alumina and or iron and sodium content in the zeolite framework. For example, comparison of XRD pattern of zeolite ZSM-5[49] (SiO_2/Al_2O_3 = 70) and silicalite[25] with respect to above mentioned peaks reveals that the intensity is higher in case of silicalite where alumina and sodium content is almost negligible in the zeolite framework.

In addition, with decrease in alumina and/or iron content, the separation of the peaks at 2θ, 45.1° and 45.5° increases. In order to correlate the separation or the spacing (Δ) between the two peaks with alumina content, the XRD spectra of various samples of Na/ZSM-5 having different SiO_2/M_2O_3 ($M = Al^{3+}$ or Fe^{3+}) ratios were scanned in the range 2θ, 44° to 46°, with a chart speed of 1/8° min^{-1} and 1000 counts $second^{-1}$. Fig. 3.7 represents the plot of per cent

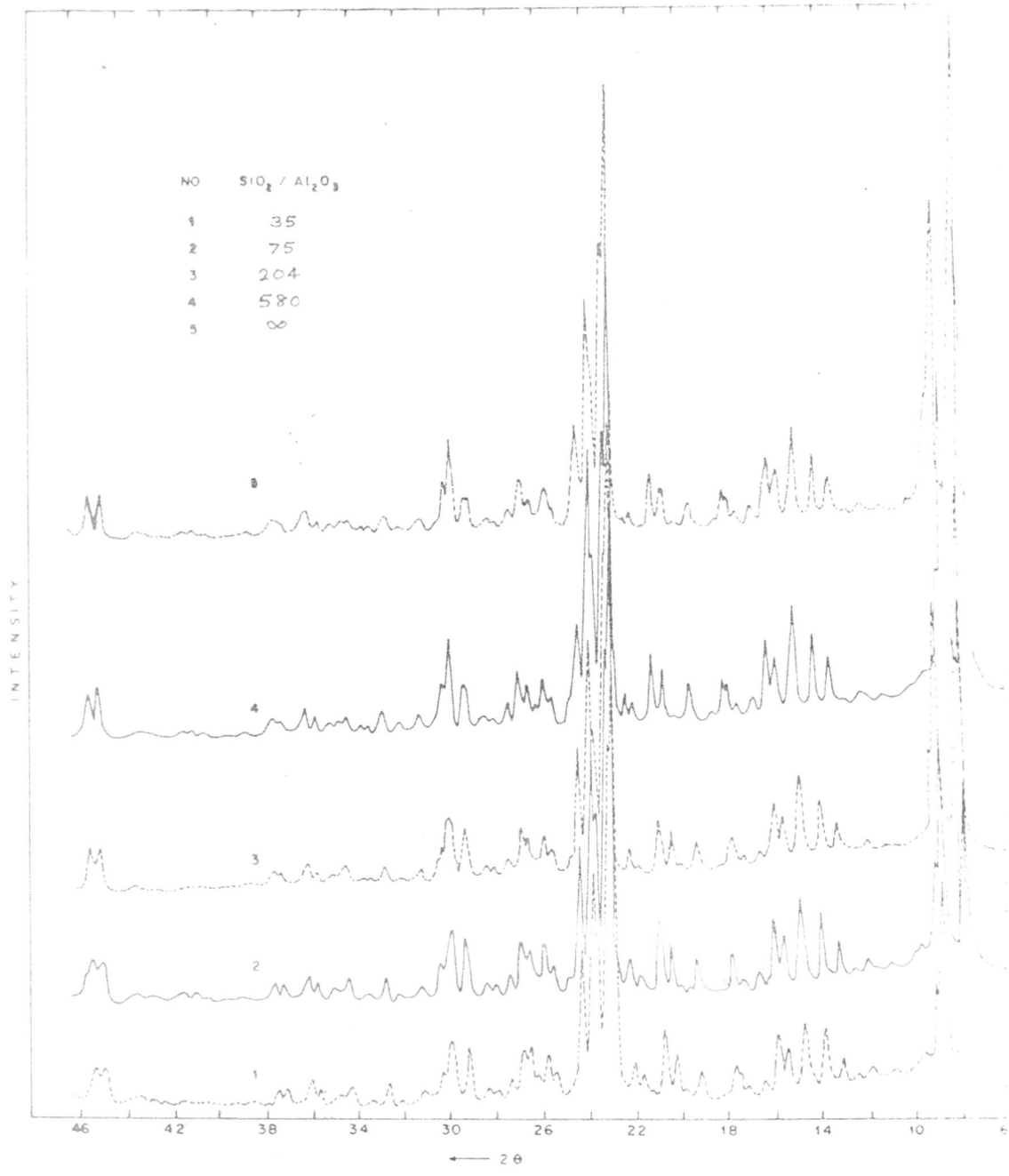

FIG 3.6. X-RAY DIFFRACTION PROFILES OF Na ZSM-5 ZEOLITES

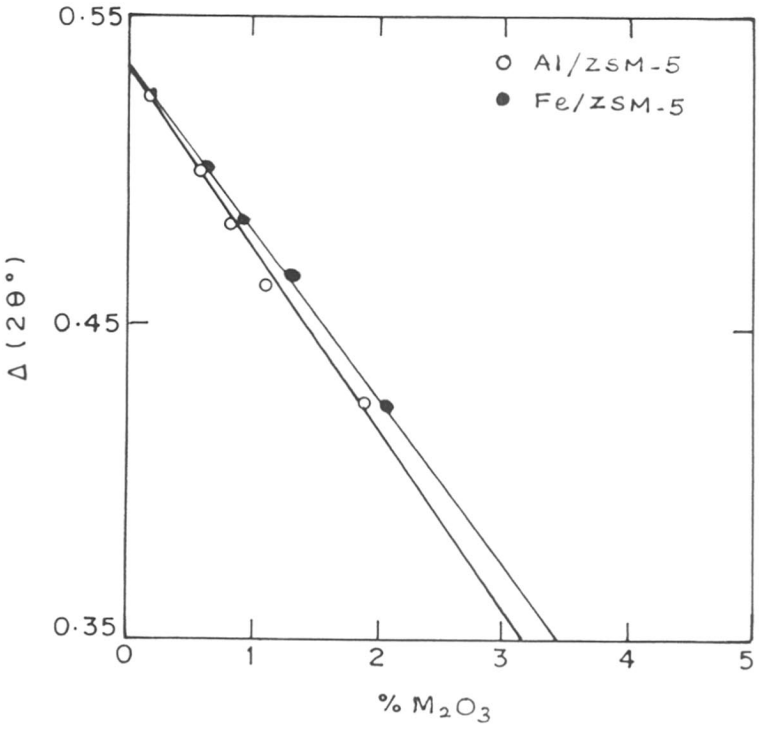

FIG. 3.7. EFFECT OF SiO_2/M_2O_3 RATIO ON SPACING 'Δ' BETWEEN THE PEAKS AT 45·0° AND 45·4°, 2θ IN XRD PATTERNS

M_2O_3 (M = Al^{3+} or Fe^{3+}) vs Δ spacing. The straight line plot with slope 0.051 and 0.049 for Al/ZSM-5 and Fe/ZSM is obtained respectively. The precise determination of Δ can thus be used as non-destructive method for the determination of Al or Fe content of pentasil ZSM-5 zeolite.

Breck[146] reported that the lattice parameters of the crystals vary as the impurities are incorporated which produce changes in peak positions and intensities in the XRD pattern. In case of zeolites, lattice parameters vary with the degree of Al^{3+} substitution for Si^{4+}. Although no considerable shift is observed at peak positions, when Fe^{3+} is replaced for Al^{3+} in the zeolite framework, but a noticeable broadening of peaks in Fe/ZSM-5 XRD pattern is observed in comparison with that of Al/ZSM-5 pattern, which probably results from the inhomogeneous distribution of Fe within individual crystals. Similar observations have been reported by Bibby et al[54] for aluminosilicate zeolites.

The loss in crystallinity, on calcination, estimated from the decrease in x-ray diffraction peak area in the range $2\theta = 22^{\circ}$ to 25° for Al/ZSM-5 and Fe/ZSM-5 samples calcined at different temperatures for fixed period of time (5 hours), is shown in Fig. 3.8.

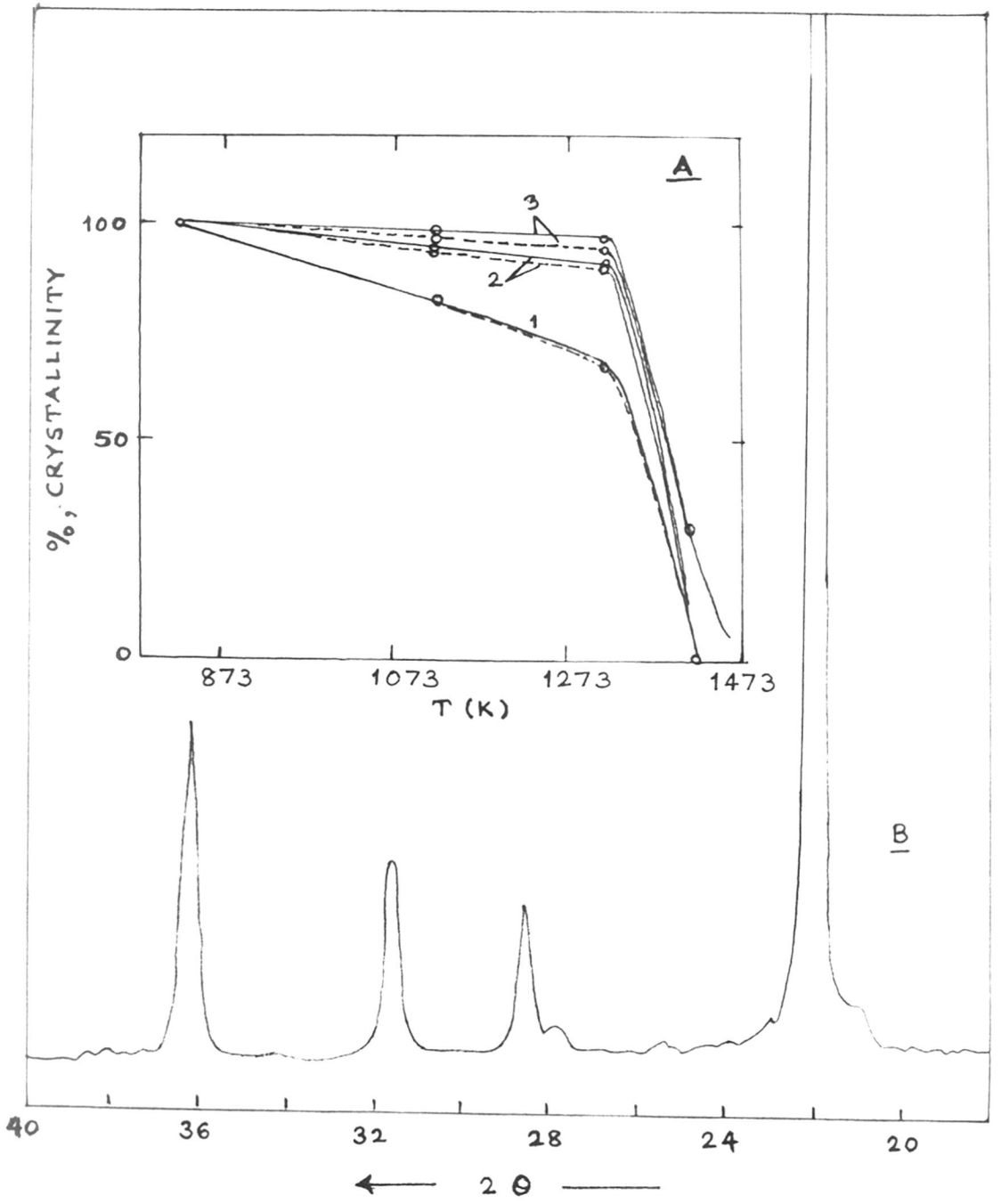

FIG. 3.8. A. THERMAL STABILITY OF Na/ZSM-5 ZEOLITES
B. XRD PATTERN OF α-CRISTOBALITE

The samples calcined at 823 K are considered as 100% crystalline, It is observed that sample Na/Al-ZSM-5 (204), Na/Fe-ZSM-5 (193) and Na/Al-ZSM-5 (580), Na/Fe-ZSM-5 (579) [numbers in the bracket refer to SiO_2/M_2O_3 ratios] calcined at 1323 K for 5 hours did not show any considerable loss in crystallinity; however, the zeolite sample Na/AlZSM-5 (75.4) and Na/FeZSM-5 (72) showed (Fig. 3.8A, curve 1) depression in crystallinity of about 30 to 35%. It reveals from this that higher the silica content in zeolite framework, more stable the crystalline structure. Further, the thermal stability of Na/AlZSM-5 and Na/FeZSM-5 zeolites with SiO_2/M_2O_3 ratios of 75.4, 204, 580 and 72, 193, 579 respectively was examined by calcining the samples at 1423 and 1523 K for 5 hours. The first two samples of respective zeolites were converted to α-cristobalite at 1423 (Fig. 3.8A, curves 1,2) while last samples (SiO_2/M_2O_3 = 580, 572) (Fig. 3.8A, curve 3) showed no structural transformation upto 1423 K. This is in good agreement with the earlier reported observations[113a]. This further confirms the dependence of the structural stability on the SiO_2/M_2O_3 ratios in the pentasil type ZSM-5 zeolites (Fig. 3.8 B).

The x-ray diffraction patterns of H/AlZSM-5 (75.4) and H/FeZSM-5 (72) zeolite calcined in temperature range of 773 to 973 K in presence of steam are shown in

Fig. 3.9. The steam treated samples exhibit the crystallinity within ± 10% of that of the original zeolite samples. It also reveals that with the increase in temperature of the steam treatment the increase in intensity of the peaks at 2 Θ, 7.9° and 8.8° has occurred. On the other hand, the formation of doublet or singlet was not observed. The relative intensity values of the peaks at 2 Θ, 7.9° and 8.8° with respect to the peak at 2 Θ, 23.1° for both H/AlZSM-5 and H/FeZSM-5 samples are given in Table 3.2.

TABLE - 3.2

Effect of steam treatment temperature on XRD peak intensity of H/ZSM-5 zeolites

Steam treatment temp.K	Relative intensity at 2 Θ			
	H/AlZSM-5		H/FeZSM-5	
	7.9°	8.8°	7.9°	8.8°
-	0.86	0.62	0.68	0.52
773	0.89	0.66	0.85	0.55
973	0.93	0.68	0.91	0.63

An increase in intensity has been attributed to the dealumination of zeolite at elevated temperatures. Vedrine et al.[65] also reported that the silica to alumina ratio of the sample was increased due to dealumination, when zeolite ZSM-5 was heated upto 1200 K for 6 hours under vacuum, and was confirmed by XPS data.

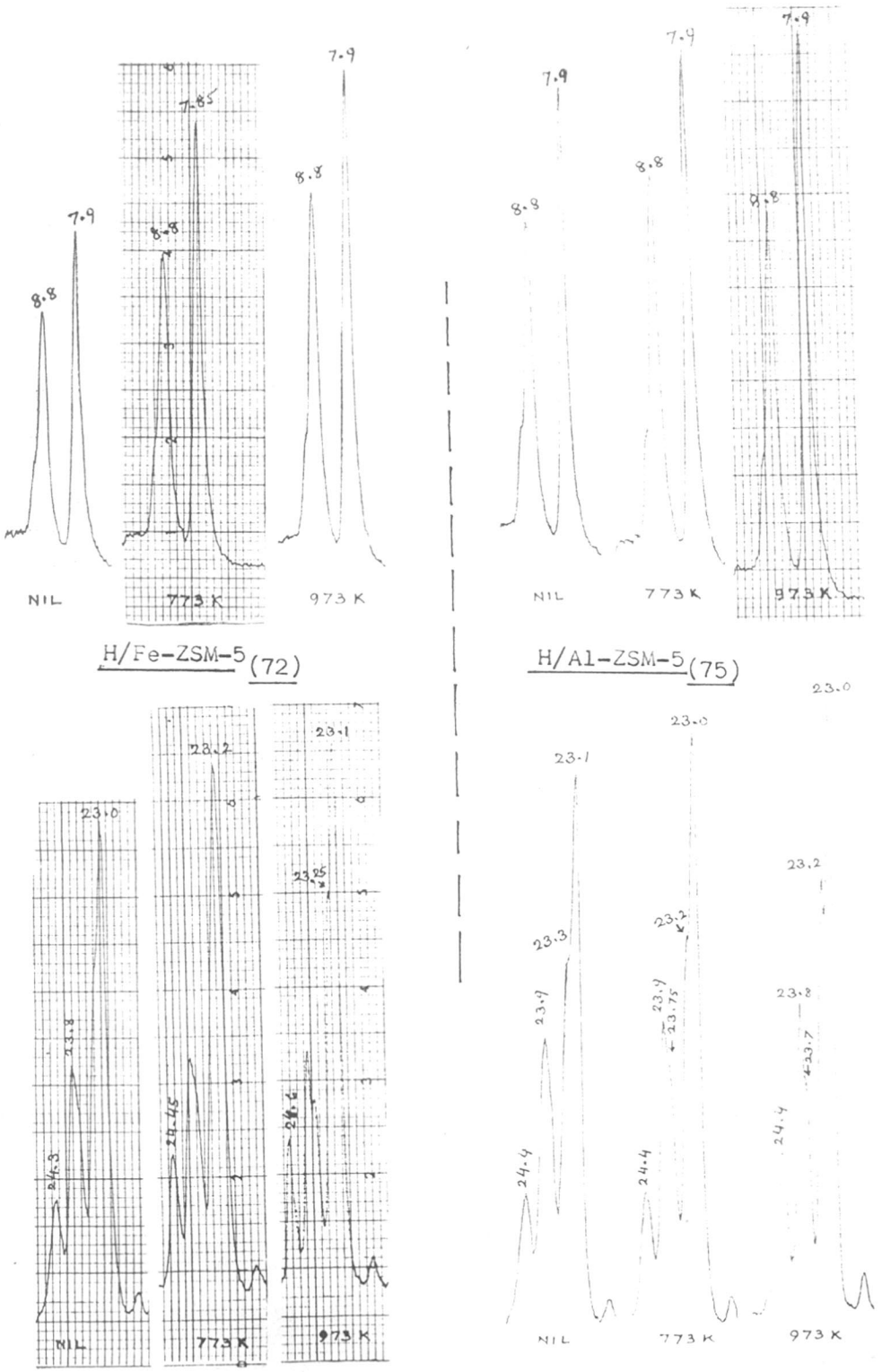

FIG. 3.9. XRD Patterns for Steam treated zeolite samples.

3.3.2. Thermal Analysis

DTA and TG curves for as-synthesized (C/N), Na^+, NH_4^+ and H^+ forms of Al/ZSM-5 and Fe/ZSM-5 zeolites are illustrated in Fig. 3.10. The structural collapse of the zeolite crystals is accompanied by liberation of heat. Obviously, the position of this exothermic peak has often been considered as measure of thermal stability. Fig.3.10 shows that both the zeolite samples in C/N, Na^+, NH_4^+ and H^+ forms do not exhibit such exothermic effect upto 1273 K indicating the high thermal stability of these ZSM-5 pentasil zeolites.

As described earlier, all the above mentioned forms of ZSM-5 zeolites show small endothermic effect in the temperature range 298 to 473 K, due to dehydration of physically adsorbed water. On the other hand, the C/N and NH_4^+ forms show exothermic effect in the temperature range 523 to 873 K due to oxidative decomposition of organic cations and NH_4^+ ions, respectively.

Both, the Brönsted and Lewis acid sites, are existing in zeolites. The former are protons attached to the lattice oxygen atoms, while the latter can be the charge compensating cations or trigonal aluminium atoms at the oxygen deficient sites or cations positions. The protons can be introduced into the zeolite structure by ammonium exchange and subsequently deammoniation, as well as by hydrolysis of cations or reduction of cations to a lower valency state. The

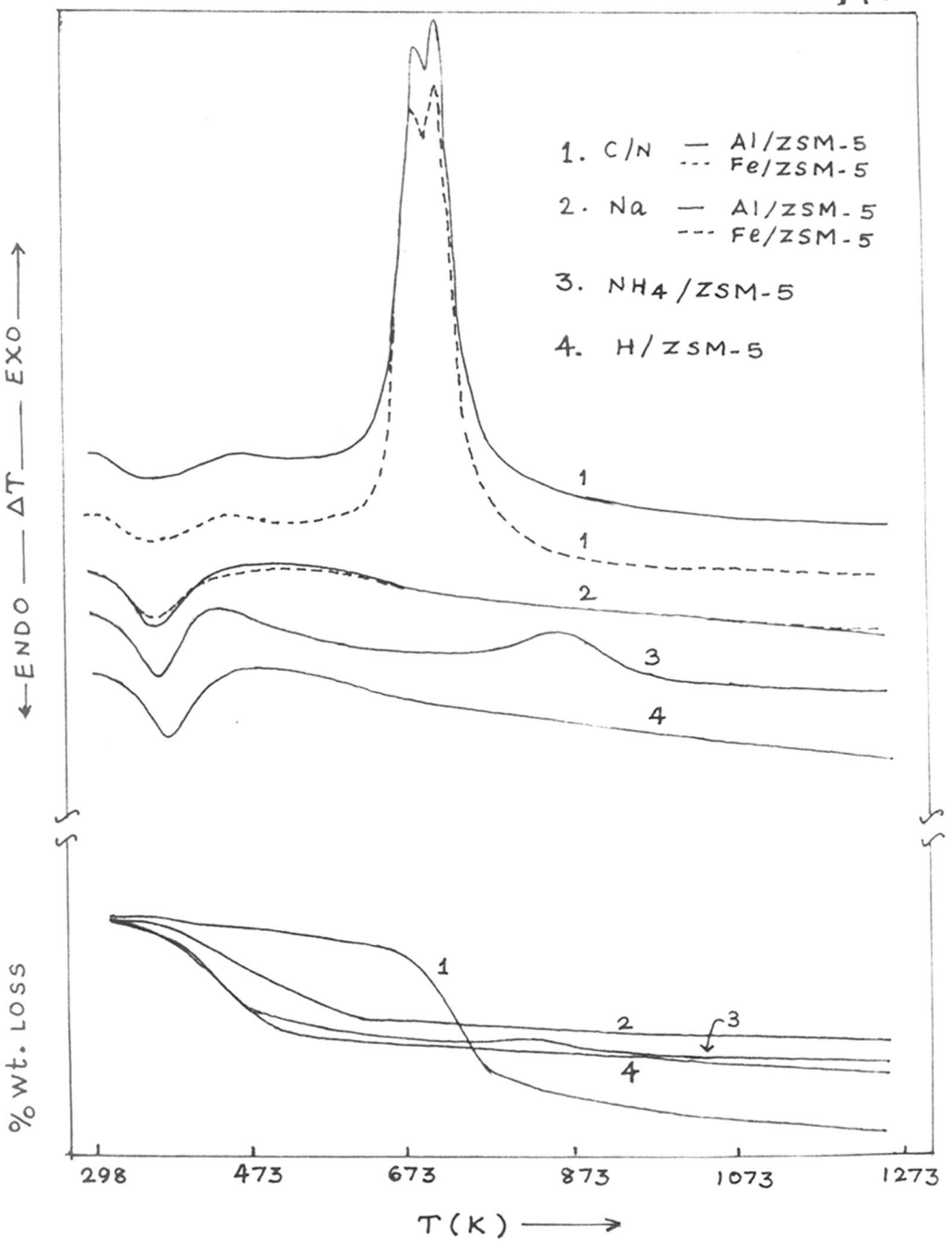

FIG. 3.10. DTA AND TG CURVES FOR DIFFERENT FORMS OF ZSM-5 ZEOLITES.

mechanism of deammoniation of the zeolite framework can be expressed as

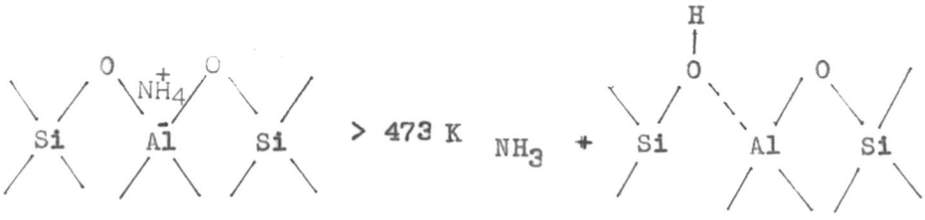

On further heating dehydroxylation of zeolite takes place. During the dehydroxylation process, the Brönsted acid sites are converted to Lewis acid sites. The dehydroxylation process for zeolite is generally assumed to occur according to the following scheme

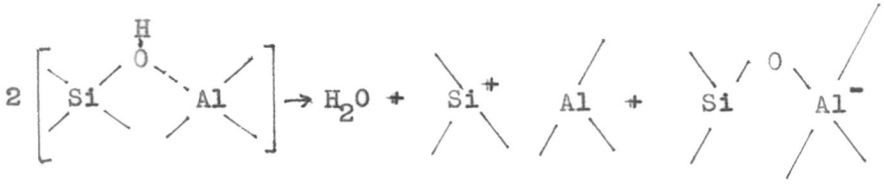

The TG curves for H/ZSM-5 zeolites with different SiO_2/M_2O_3 ratio are shown in Fig. 3.11A. Similarly, TG curves for H/ZSM-5 (75) zeolite samples obtained by steam treatment at different temperatures are also illustrated in Fig. 3.11B. It is observed that a continuous loss of adsorbed water occurs at temperatures upto about 550°K, then there is a region of constant weight, followed by a low but significant loss of weight above 700 K. The weight loss observed upto about 550 K reveals the dehydration of hydrated zeolite, resulting in a completely anhydrous form. Above 700 K a significant continuous

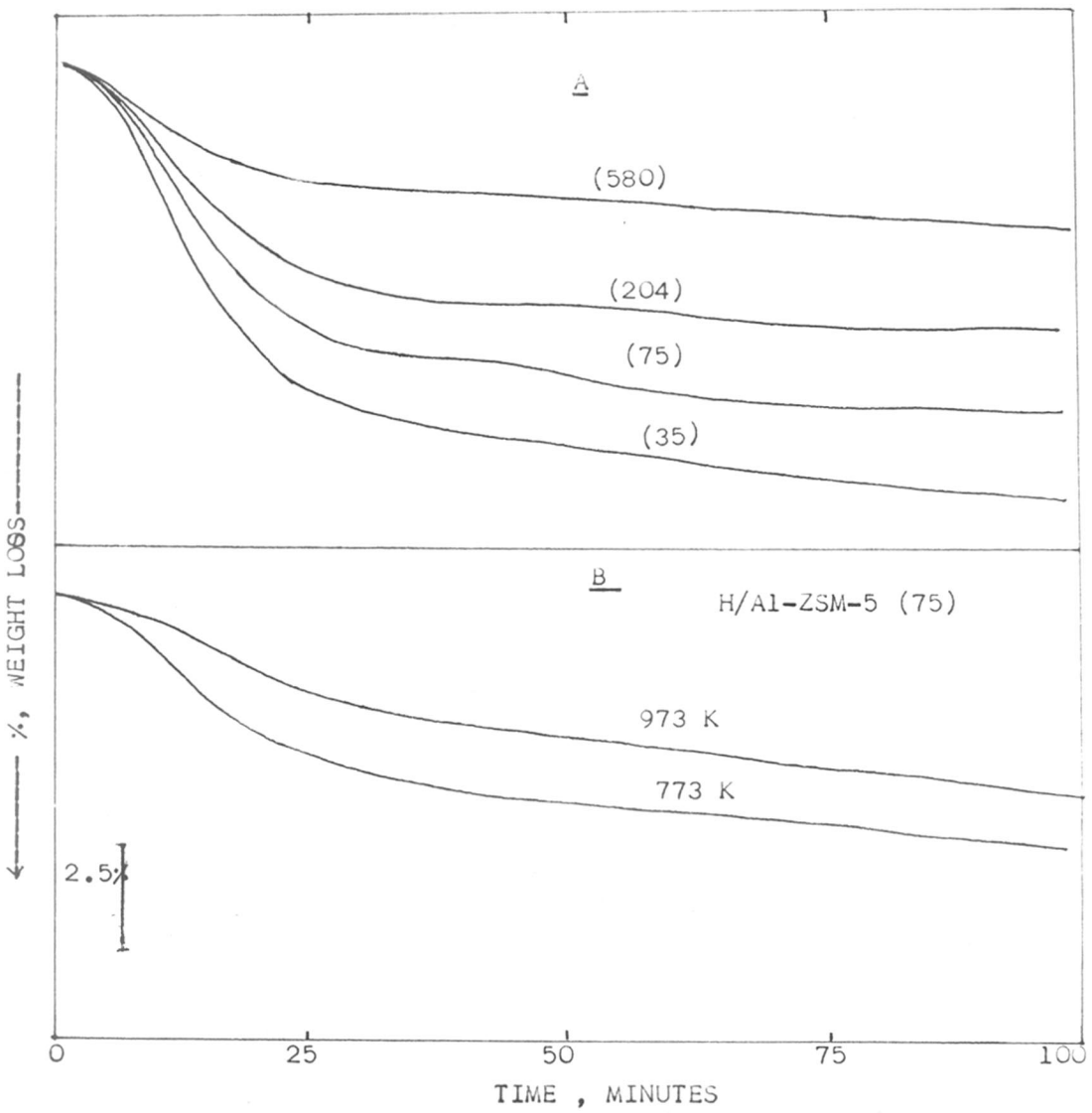

FIG.3.11. TG CURVES FOR H/Al-ZSM-5 ZEOLITES.
A. OF DIFFERENT RATIO(SiO_2/Al_2O_3) INDICATED IN BRACKETS
B. OF STEAM TREATMENT TEMPERATURE AS INDICATED

weight loss due to dehydroxylation of Brönsted acid sites generating Lewis acid sites is observed. The number of hydroxyl groups per unit cell calculated from the observed weight loss between 700 and 1273 K is summarised in Table 3.3.

Table 3.3

Thermal analysis of H/ZSM-5 Zeolites*

Sample	Temp. of steam treatment (K)	% Wt. loss			No. of OH group per unit cell
		Total	Dehydration upto 773 K	Dehydroxylation between 773-1273 K	
H/AlZSM-5(35)	-	10.50	10.00	0.50	3.2
H/AlZSM-5(75)		10.00	9.66	0.35	2.3
H/AlZSM-5(204)	-	5.40	5.12	0.28	1.8
H/AlZSM-5(580)	-	4.80	4.60	0.20	1.3
H/AlZSM-5(75)	773	5.50	5.28	0.22	1.32
H/AlZSM-5(75)	973	4.25	4.16	0.11	0.70

* Similar trend has been exhibited by H/Fe-ZSM-5 zeolites also.

Figures in brackets indicate SiO_2/Al_2O_3 ratio.

The gradual decrease in number of hydroxyl groups with increase in SiO_2/M_2O_3 ratio and steam treatment samples at various temperatures is expected. Vedrine et al[65] studied the adsorption of pyridine on H/ZSM-5 zeolite by IR spectroscopy and reported that the intensity of the adsorption band at 1540 cm^{-1} due to pyridinium ion decreased as the activation temperature was increased from 773 to 1273 K.

3.3.3. Nitrogen Adsorption

Nitrogen adsorption isotherms for Na/Al-ZSM-5 and Na/FeZSM-5 zeolites with varying crystallinity (estimated from XRD data) are shown in Figs. 3.12, 3.13. The isotherms exhibit different behaviour for samples with low and high crystallinity. For highly crystalline samples, a very rapid uptake at low relative pressure followed by a flat region at increased relative pressure was observed, while for low crystalline zeolites slow and sluggish uptake with increase of relative pressure was observed. Fig. 3.14A shows a plot of the amount of nitrogen sorbed at $P/P_o = 0.5$ (in cc per gm of zeolite) vs X-ray crystallinity. A straight line plot with positive intercept is obtained.

Two isotherm equations are commonly used to determine the surface area of solids. These are Langmuir and Brunauer Emmett and Teller (BET) equations. The Langmuir equation is based on monolayer approach while BET on multilayer approach.

The graphical representation of BET surface area and void volume vs synthesis time for the reaction gel composition $SiO_2/M_2O_3 = 85$, $OH^-/H_2O = 6.0 \times 10^{-3}$, at 453 K is given in Fig. 3.14 B. The maxima occurs at synthesis time 32 and 36 hours, for Al/ZSM-5 and Fe/ZSM-5 corresponding to BET surface area 436 m^2/g, 419 m^2/g and Dubinin void volume of 0.19 cc/g 0.184 cc/g respectively.

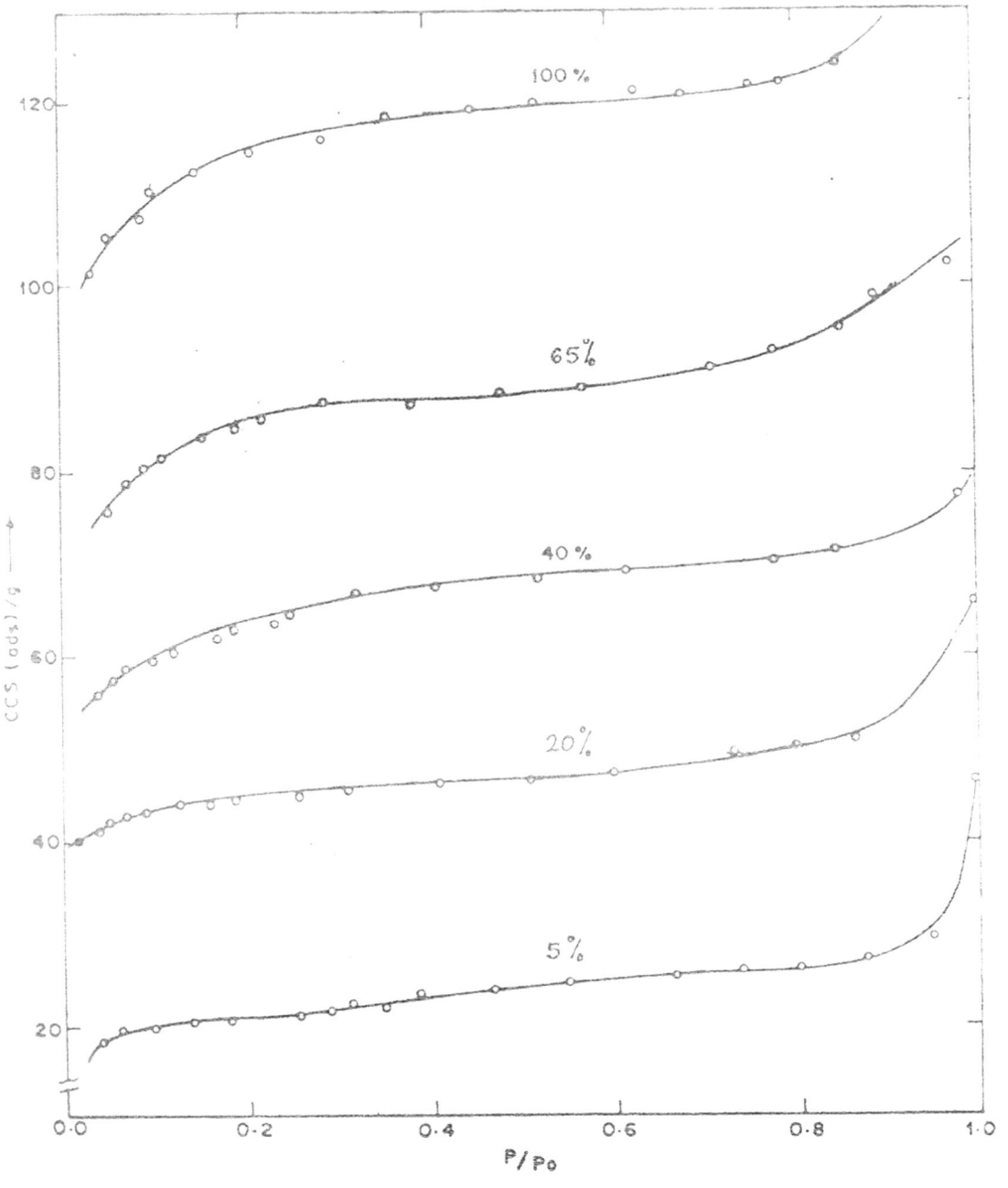

FIG. 3.12. NITROGEN ADSORPTION ISOTHERMS OF Na/ZSM-5 SAMPLES OF DIFFERENT CRYSTALLINITY.

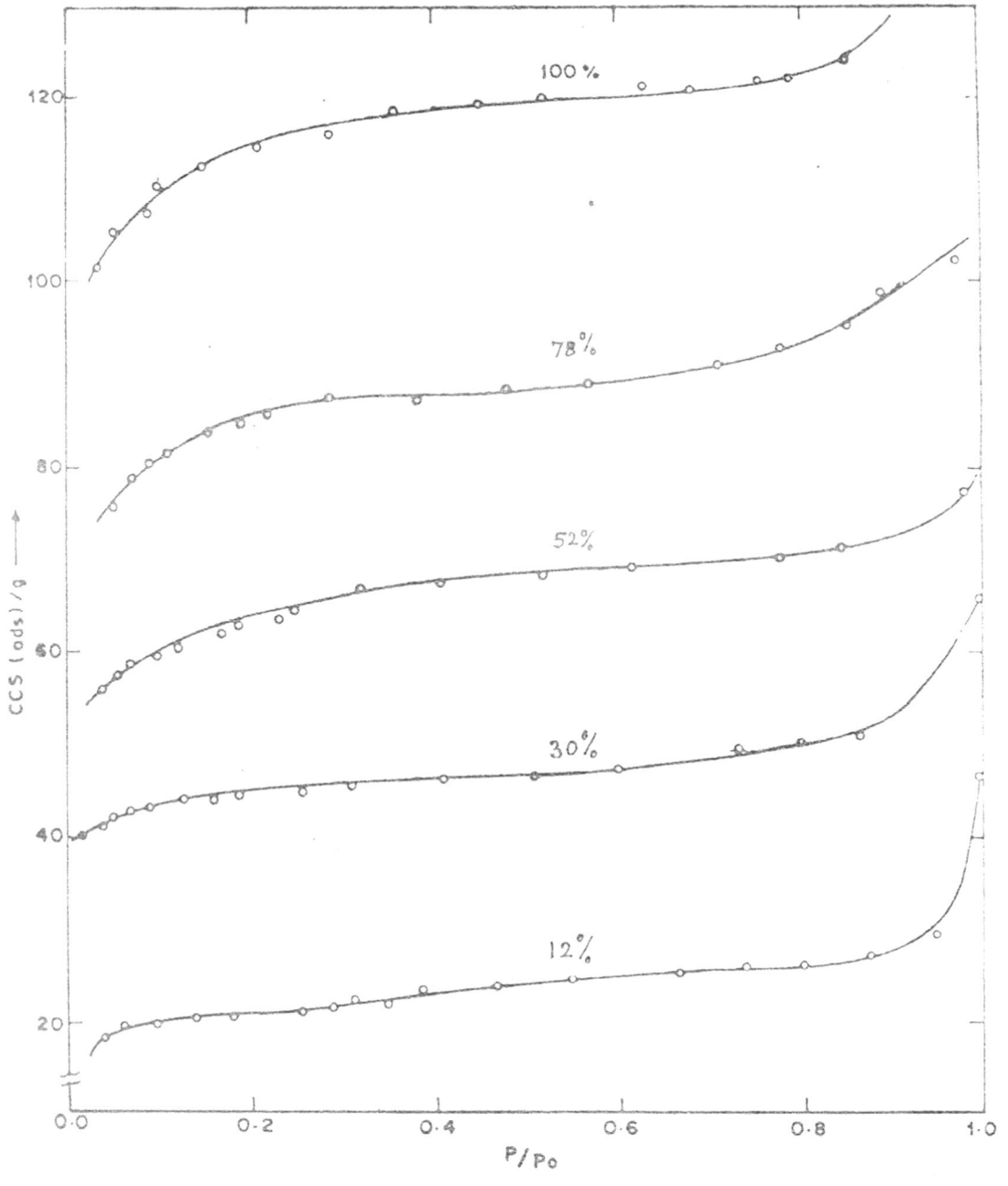

FIG. 3.13 . NITROGEN ADSORPTION ISOTHERMS OF Na/FeZSM-5 SAMPLES OF DIFFERENT CRYSTALLINITY.

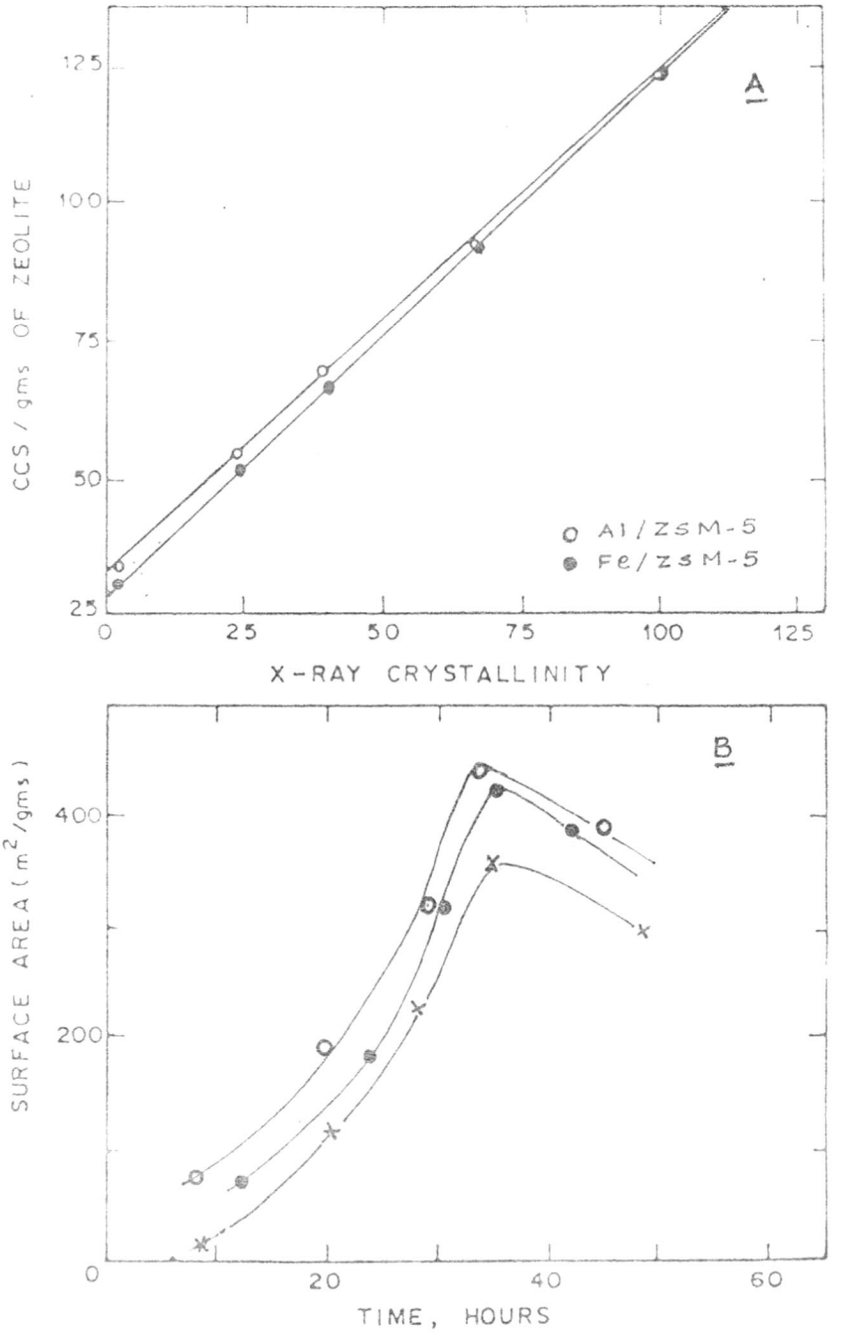

FIG. 3.14 . A) RELATION BETWEEN AMOUNT OF NITROGEN ADSORBED VS X-RAY CRYSTALLINITY, ($P/P_o = 0.5$)

B) SURFACE AREA AND VOID VOLUME VS SYNTHESIS TIME. $SiO_2 / Al_2O_3 = 85$, $OH^- / H_2O = 6.0 \times 10^{-3}$, $T = 453\,K$

The values of surface area for various Na/ZSM-5 for both Al and Fe zeolites synthesized at different synthesis time and the 100% crystalline samples with different SiO_2/M_2O_3 ratios are given in Table 3.4, and 3.5.

Table 3.4

Effect of crystallization time on surface area and void volume of ZSM-5 Zeolites

Synthesis time (hr)	Surface area m^2/gm		Void volume cc/gm
	BET	Langmuir	
8(12)	71(68)	96(94)	0.034(0.033)
20(24)	180(171)	250(243)	0.090(0.087)
28(30)	305(296)	366(359)	0.130(0.128)
32(36)	436(419)	537(517)	0.191(0.184)

Bracketed figures indicate data for Fe/ZSM-5 zeolite

Table 3.5

Surface area and void volume for 100% crystalline Na/ZSM-5 Zeolites*

Sample	Surface area m^2/g		Void volume cc/g
	BET	Langmuir	
Na/ZSM-5(35)(33)	431,414	530,505	0.189,0.180
Na/ZSM-5(75)(72)	436,419	537,517	0.191,0.184
Na/ZSM-5(204)(193)	434,415	532,510	0.190,0.182
Na/ZSM-5(580)(579)	425,412	525,500	0.187,0.179

* Underlined numbers indicate data for Fe/ZSM-5.

* Bracketed numbers indicate SiO_2/M_2O_3 ratio.

From sorption data one can conclude that nitrogen adsorption measurements give data complimentary to the XRD for the determination of the purity and/or crystallinity of ZSM-5 zeolites.

3.3.4. Sorption and Diffusion in ZSM-5 zeolites

The sorption of water, n-hexane and cyclohexane in ZSM-5 zeolites of different SiO_2/M_2O_3 ratios synthesized using TEBA-Br, are given in Table 3.6.

The uptake of n-hexane, $\backsim 1.28 \times 10^{-3}$ m mole g^{-1} agrees with that reported by Anderson et al[65], confirming identity of the sample. While decrease in water and nearly constant uptake of n-hexane corresponds to general expectation, the decrease in cyclohexane sorption with increase in SiO_2/M_2O_3 ratio is surprising. It may be possible that while adsorption of n-hexane occurs in both the pores and channel intersections, cyclohexane having larger cross-sectional area is adsorbed preferentially at channel intersections only. In partial support of this result, it has been observed that the catalytic activity for the isomerisation of xylenes where locus of the activity is mainly at the channel intersections, correlates with the amount of cyclohexane adsorbed[147]. No such correlation was, however, found for n-hexane adsorption.

In order to understand the sorption capacity in terms of various organic sorbate molecules of varying length and critical diameters, sorption kinetics have been carried out with n-pentane, n-hexane, n-heptane, 2-methylpentane, 2,3-dimethylbutane, benzene, toluene and TMB, with three xylenes. Table 3.7 summarises equilibrium sorption capacities for both H/Al-ZSM-5 (75) and H/FeZSM-5(72) at $P/P_o = 0.8$ at temperature 298 K and at a sorption time of 120 minutes.

Table - 3.6

Influence of SiO_2/M_2O_3 ratio on the sorption properties of ZSM-5 zeolites

Sample	a	Na/AlZSM-5 Amt. adsorbed m mole g^{-1}			Sample	a	Na/FeZSM-5 Amt. adsorbed m mole g^{-1}		
		H_2O	n-C_6H_{14}	C_6H_{12}			H_2O	n-C_6H_{14}	C_6H_{12}
Na/ZSM-5(35)	6.7	1.29	0.63	Na/ZSM-5(33)	6.65	1.28	0.61		
Na/ZSM-5(75)	5.5	1.28	0.57	Na/ZSM-5(72)	5.47	1.28	0.54		
Na/ZSM-5(204)	3.8	1.28	0.39	Na/ZSM-5(193)	3.62	1.27	0.36		
Na/ZSM-5(580)	3.0	1.27	0.36	Na/ZSM-5(579)	2.98	1.26	0.33		

a - SiO_2/M_2O_3 ratio (M = Al^{3+} or Fe^{3+})

Table 3.7

Sorption data for various hydrocarbons in H/AlZSM-5(75) and H/FeZSM-5(72) zeolites

Sorbate	Uptake g g^{-1} of zeolite	
	H/AlZSM-5(75)	H/FeZSM-5(72)
n-Pentane	0.01	0.098
n-Hexane	0.116	0.112
n-Heptane	0.134	0.132
2-Methylpentane	0.082	0.080
2,3-Dimethylbutane	0.051	0.048
Cyclohexane	0.056	0.052
Benzene	0.12	0.115
Toluene	0.11	0.11
p-Xylene	0.15	0.14
m-Xylene	0.032	0.029
o-Xylene	0.028	0.026
TMB(1,2,3-trimethyl-benzene)	0.014	0.012

The kinetic study revealed that the sorption of linear paraffins, isoparaffins, toluene and p-xylene occurs more readily than that of dimethyl paraffins and of ortho and meta xylenes indicating steric restrictions. The difference between adsorption of benzene and p-xylene is due to the additional interaction forces of methyl hydrogen atoms as well as entropy contribution resulting from more favourable packing of p-xylene[148].

Relative sorption rates with 6 carbon atoms suggest that the rate of mass transport of hydrocarbon into zeolite crystallites follows the order

n-paraffins > monomethyl paraffins,

aromatics > dimethyl paraffins.

On the basis of available sorption data, it appears that molecules having a cross-section greater than 6.4 x 6.9Å would be excluded from the interior of the zeolite. From the knowledge of adsorbed amounts and assuming end to end configuration of sorbed molecules, Derouane et al.[91] evaluated the channel length occupied per unit cell by the adsorbates, which amounts to a total value of 88Å for both the types of channels and 59Å for linear elliptical channels. From these observations it can be concluded that

(i) Linear aliphatics have an aceess to both the channel systems,

(ii) Isoaliphatic compounds experience steric hindrance which may restrict their adsorption and diffusion in the sinusoidal channel system,

(iii) Aromatic compounds and other methyl substituted aliphaticshave strong preference for diffusion and/or adsorption in the linear and elliptical channels.

3.3.5. X-ray Photoelectron Spectroscopy (XPS)

XPS has been extensively used to study the external layer of zeolite surfaces[149-151]. Temper et al[150] studied zeolites by XPS and concluded that the silicon to aluminium ratio of the zeolite surface is about twice that of the bulk. Further studies on the same zeolite showed that a partial dealumination of the surface occurs. When ferric exchanged Y zeolite was heated at 823 K for 5 hours in air, the surface silicon to aluminium ratio was found[152] to decrease from 4.48 to 2.51. Recently, Van Ballmos and Meiev[153] found by microprobe analysis that the Al concentration at the surface of HZSM-5 crystals is invariably higher than that in the core.

It has been well established that the presence of aluminium in the zeolite framework is related to the existence of acidic (active) sites. Therefore, increasing attention should be given to the study of the actual distribution of Al

at the surface of ZSM-5 zeolites. A systematic XPS study was therefore made to investigate the surface composition of HZSM-5 catalyst when it was calcined in presence of steam at different temperatures. The XPS measurements for steam treated H/AlZSM-5 zeolites were performed as described earlier using MgKα as the source ($h\nu$ = 1253.6 eV). The spectra are presented in Fig. 3.15. The surface silicon to aluminium ratio designated as (Si/Al)s, was calculated from the intensity of Si_{2p} and Al_{2p} peaks in the XPS, corrected by Wagner's intensity factors[154]. The bulk silicon to aluminium ratio designated as $(Si/Al)_B$, was calculated from conventional chemical analysis. The data is summarized in Table 3.8.

Table 3.8

Effect of steam treatment temperature on the surface composition of H/AlZSM-5(75) zeolite

Steaming temp.(K)	Binding energy eV		Intensity		Si/Al ratio
	Si_{2p}	Al_{2p}	ISi_{2p}	IAl_{2p}	
-	106.2	75.0	3.6	0.10	36.0
773	106.6	75.0	3.3	0.12	27.5
973	103.0	74.5	3.4	0.17	20.0

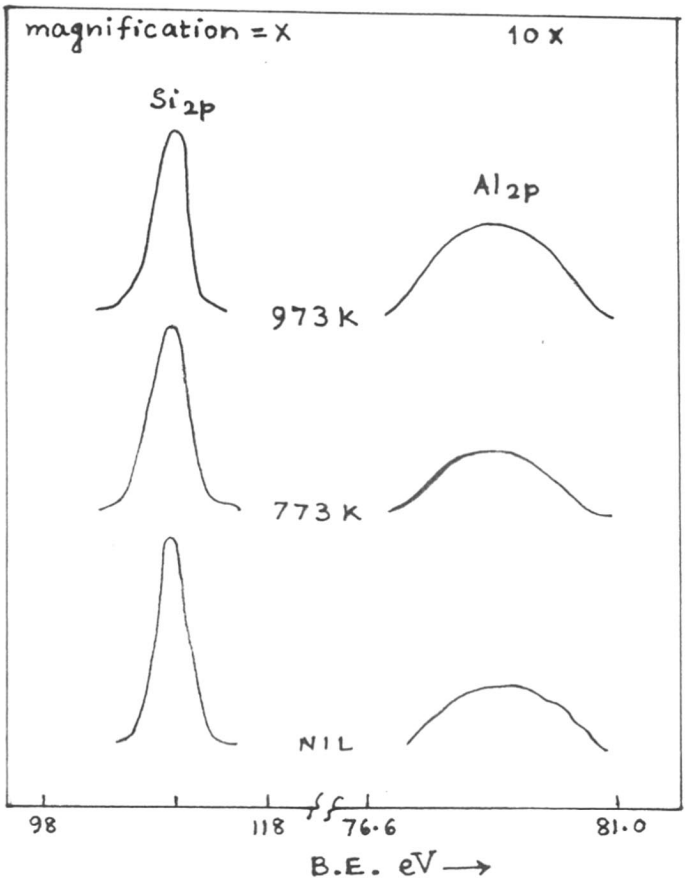

FIG. 3.15. XPS SPECTRA OF H/AlZSM-5(75) ZEOLITE. NUMBERS INDICATE TREATMENT TEMPERATURE.

The results obtained show that

(i) the surface (Si/Al)s ratio is nearly similar to that of bulk (Si/Al)B for untreated H/AlZSM-5 zeolite,

(ii) the surface (Si/Al)s ratio decreases as steam treatment temperature is increased,

(iii) with increasing steam treatment temperature a significant shift in the binding energy value for Al_{2p} peak is observed.

It can be concluded from the above results that the surface of H/AlZSM-5 zeolite is enriched with aluminium at increased steam treatment temperature. This may be attributed to the migration of framework aluminium ions from bulk to the external surface of zeolite.

The fact that the ferric ions in Fe/ZSM-5 type pentasil zeolite are in trivalent state and are indeed situated in the lattice site of the framework is confirmed by XPS data (VG, ESCA 3 MgKα, slit width 4 mm, analyser energy 50 eV). Fig. 3.15(a) illustrates the XPS spectra iron and oxygen in Fe/ZSM-5 and in the sample of silicalite containing Fe_2O_3.

The binding energy of the $Fe_{2p_{3/2}}$ level in both the samples (value of 103.3 eV for Si_{2p} level as the internal standard) were 711.6 eV for Fe/ZSM-5 and 711.0 eV for Fe_2O_3

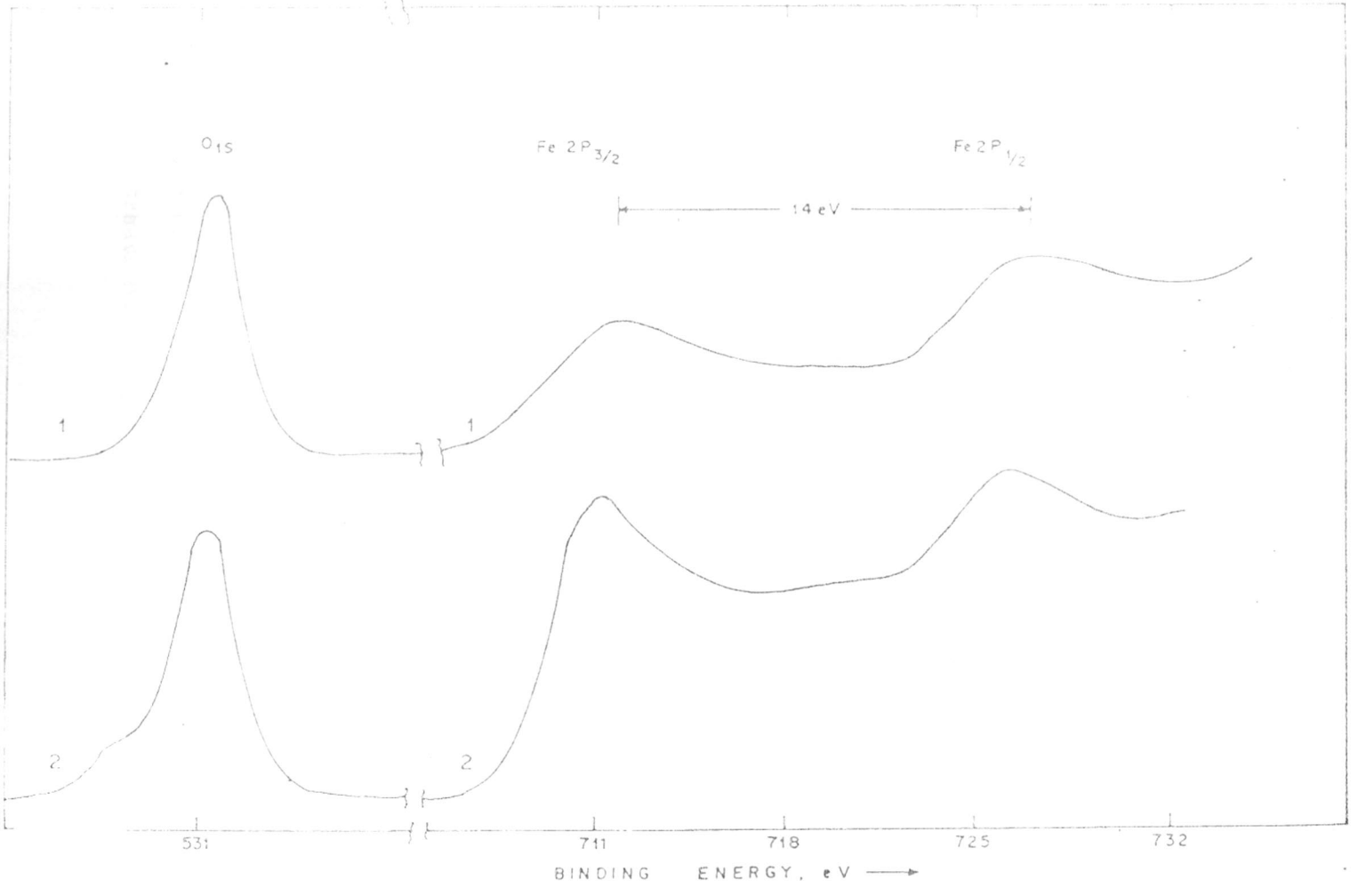

FIG. 3.15(a) XPS SPECTRA OF 1) Fe/ZSM-5 2) Fe_2O_3 + SILICALITE

impregnated silicalite indicating that Fe ions are in the trivalent oxidation state in both the materials. A $2P_{3/2}$-$2P_{1/2}$ splitting of 14.0 eV was observed for both these samples. However, only one O_{1s} peak (for zeolite lattice oxygen) is observed for Fe/ZSM-5 pentasil zeolite, while two peaks at 531.5 eV and 529.1 eV are exhibited by 3.5% Fe_2O_3 impregnated silicalite sample. The peak at 531.5 eV corresponds to the zeolite lattice oxygen, the other peak is due to the oxygen associated with the occluded Fe_2O_3 phase. Stencel et al[154a] for a sample of ZSM-5 containing occluded Fe_2O_3 have also observed two O_{1s} peaks at 532 eV and 529 eV corresponding to oxygen ions in the zeolite lattice and Fe_2O_3 respectively.

3.3.6. Electron Paramagnetic Resonance Spectroscopy (EPR)

The EPR spectroscopic study showed that the traces of Fe^{3+} which are incorporated into the zeolite during the synthesis are usually located[155,156] in

(i) the exchangeable sites of zeolite framework, or

(ii) randomly oriented in hydroxy oxide form, or

(iii) in the aluminosilicate framework where they replace Al.

To identify the position of Fe^{3+} ions in Fe/ZSM-5, the EPR spectra of Fe/ZSM-5 samples were recorded after various treatments (Fig. 3.16). For the comparison purpose,

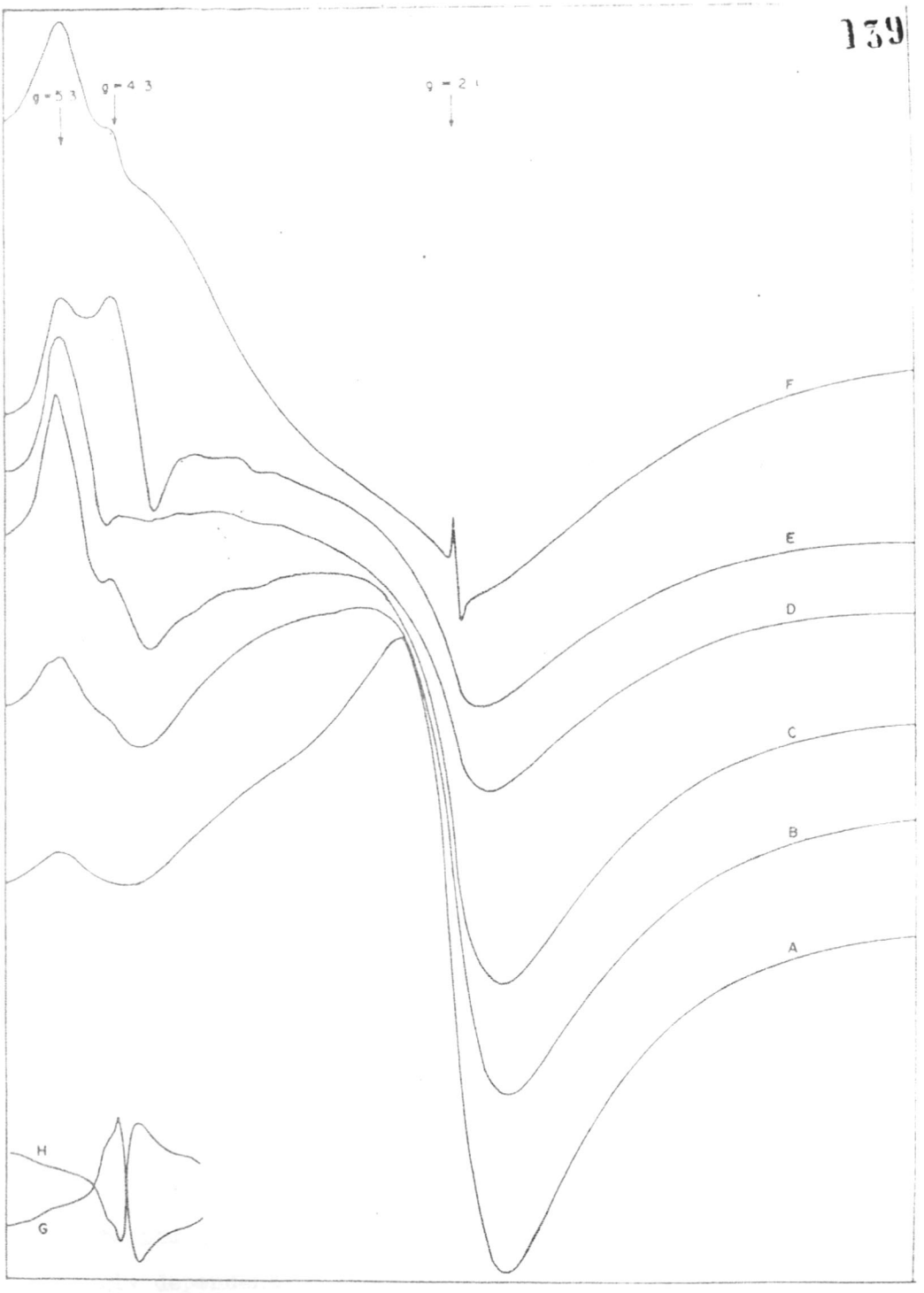

FIG. 3.16 . E.p.r. SPECTRA OF Fe^{3+} IN Fe/ZSM-5
A) H-Fe/ZSM-5, AND SAMPLES TREATED IN VACUUM AT
B) 295 K C) 373 K D) 473 K E) 573 K F) 773 K
G & H) Al_2O_3 CONTAINING Fe^{3+} IN LATTICE POSITION

EPR spectra for Al_2O_3 sintered at 1243 K and containing iron impurity in the lattice position were also recorded.

The thermal treatment of Fe/ZSM-5, in vacuum, considerably increases the intensity of the signals at g = 4.3 and 5.3, while intensity of the signal at g = 2.0 decreases with the change in shape (Fig. 3.16). When the sample is oxidised in O_2 and exposed to water for rehydration, new broad signals, designated at P, Q, R are developed (Fig. 3.17).

g = 2.0 - The signal at g = 2.0 has been assigned[155] to the Fe^{3+} hexacoordinated complexes located at the cationic sites of the original hydrated zeolites. The thermal treatment of Fe/ZSM-5 in vacuum, caused decrease in intensity and simultaneously g factor was shifted to lower values. The sharp peak obtained at g = 2.0, when sample was heated in vacuum at 473 K, may be due to presence of O_2^- species. Since the ion exchange does not show any change in Fe_2O_3 content, the further discussion obviously, is limited to last two points only.

g = 2.3 - The signal at g = 2.3 was assigned[155,157] to randomly oriented Fe^{3+} ions with the character of oxides and hydroxides, which did not belong to the structure of zeolite itself. The shape and intensity of this signal is strongly dependent on reduction condition. The weak signals at P, Q and R may be arising due to the traces of Fe^{3+} species formed from occluded salts and these salts might have been responsible for the broad peak exhibited by the origianal sample.

g = 4.3 From the EPR spectra and on the basis of signal assignment[155,157-159], the signal at g = 4.3 is attributed to the Fe^{3+} tetrahedrally coordinated in the zeolite framework. The existence of further signals of g > 5.3, can be explained by the presence of Fe^{3+} complexes with respect to the ligands and/or, distortion of the symmetry[159,160]. The intensity of the signal at g = 4.3 increases by the vacuum treatment upto 573 K and the decreases. When Fe^{3+} is present at exchangeable sites, the intensity of the signal at g = 4.3 is not affected by vacuum treatment[157]. After rehydration, the intensity and shape of the signals correspond to that of the original zeolite (Fig.3.17). The reduction of Fe^{3+} in Fe/ZSM-5 skeleton did not occur during vacuum treatment. Further treatment in air and in O_2 caused decrease in intensity at g = 4.3 and 5.3. It reveals from these observations that Fe^{3+} ions present in Fe/ZSM-5 zeolite are mainly in the tetrahedral positions.

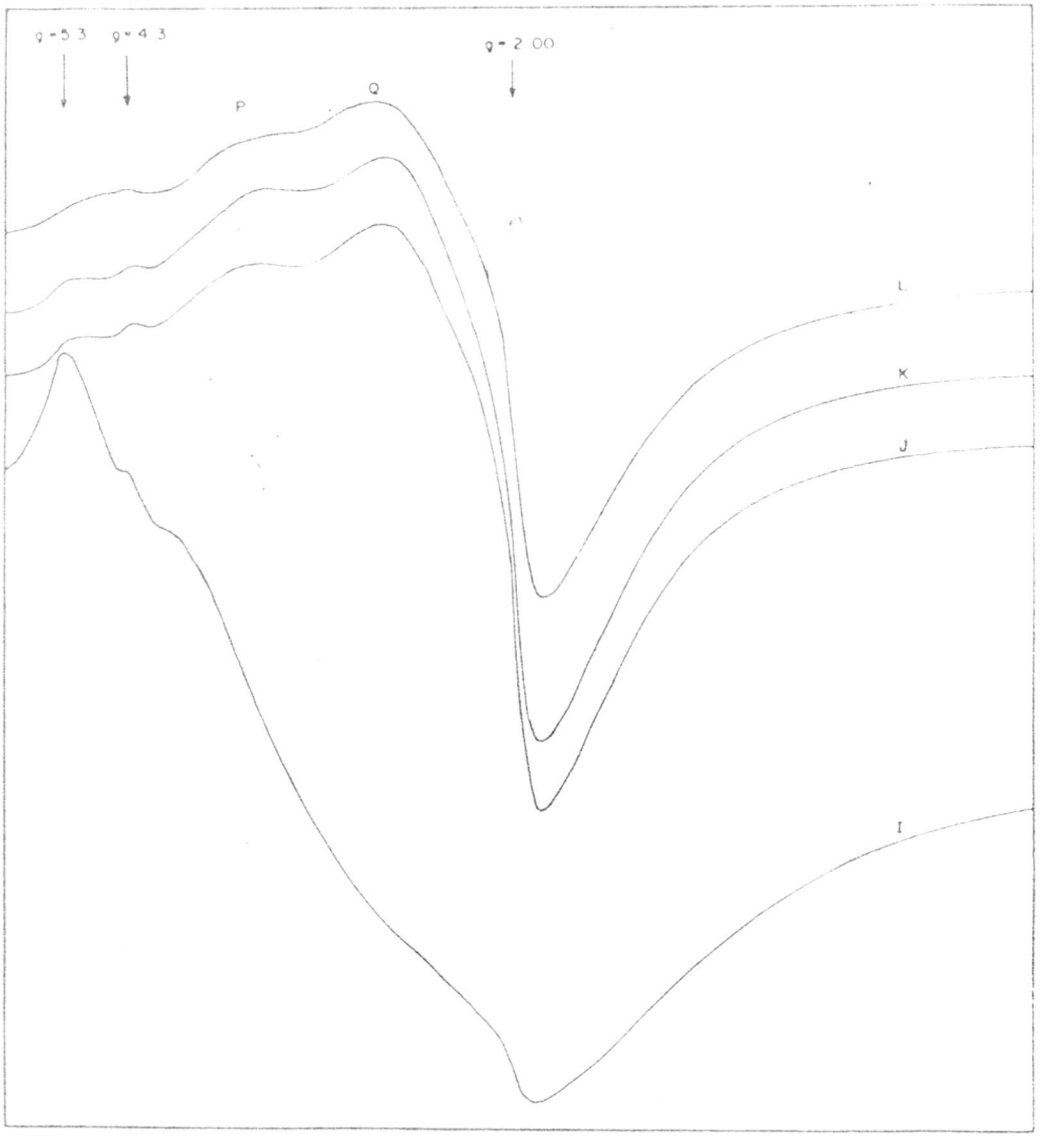

FIG. 3.17. E.p.r. SPECTRUM OF Fe^{3+} IN Fe/ZSM-5

I) AT 297 K (SAMPLE OPENED TO AIR)

J) OXIDISED IN O_2 AT 773 K

K) DEGASSED AT 573 K

L) REHYDRATED

3.3.7. Infrared Spectroscopy

The IR spectra of H/AlZSM-5 zeolites shown in Fig. 3.18 have been found to be practically identical with that of Na/AlZSM-5 spectra in the 300-1200 cm^{-1} region. This reveals that replacement of sodium by H^+ ions has no effect on the vibrations in the zeolite framework. The assignment of IR lattice vibrations in the frequency range 300-1200 cm^{-1} for ZSM-5 zeolite is given in Table 3.9.

Table 3.9

Framework vibration frequencies for Na/Al-ZSM-5 Zeolite

Wave number (cm^{-1})	Assignment
450	Si-O bending
550	Distorted double 5 rings
590	ELC5
620	ELC5
680	-
720	ITSS
790	ELSS
840	ELSS
1075	ITAS
1220	Si-O asymmetric

ELC5 - external link complex five membered ring.
ELSS - external link symmetric stretch.
ITSS - internal tetrahedral symmetric stretch.
ITAS - internal tetrahedral asymmetric stretch.

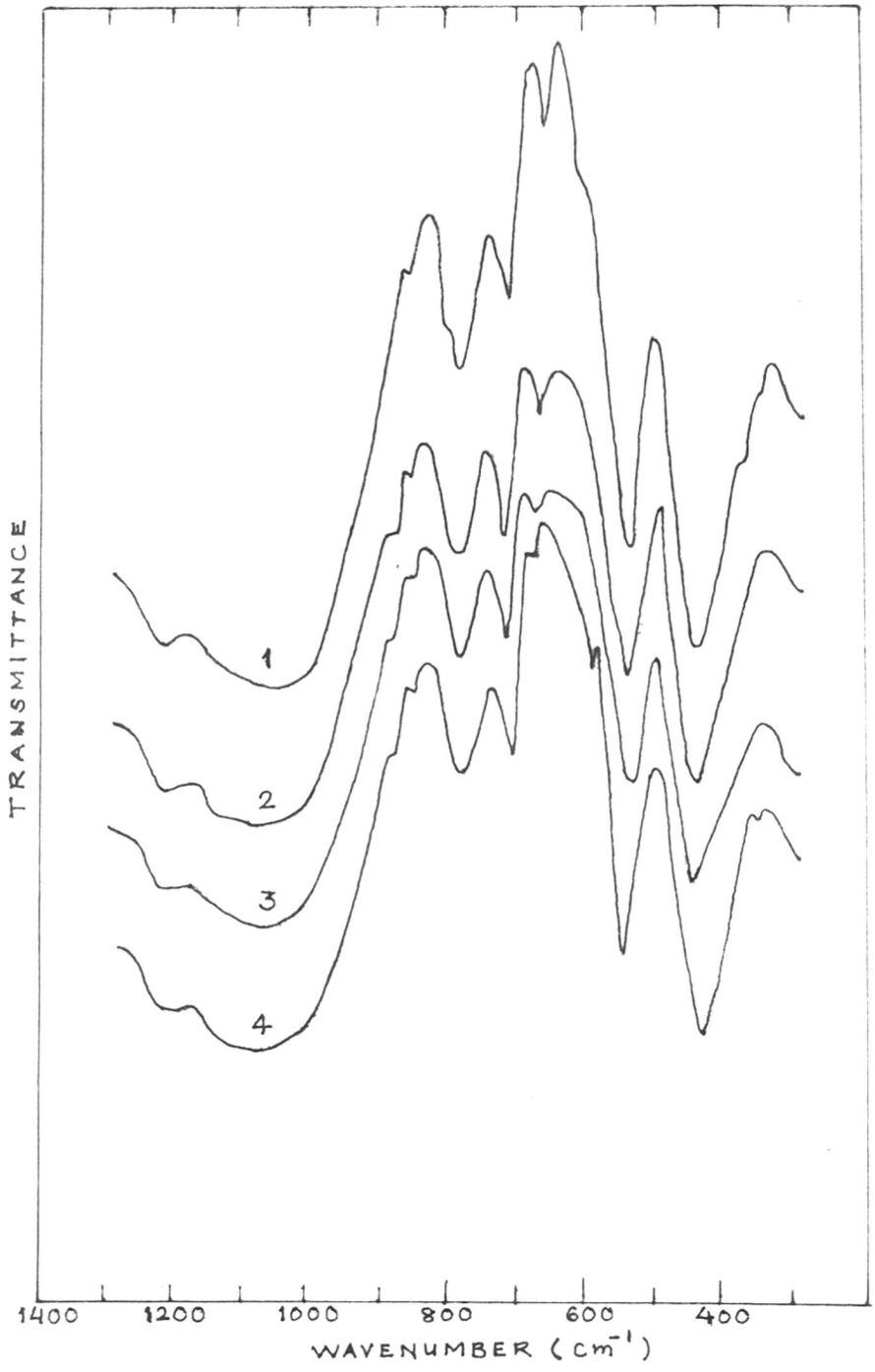

FIG. 3.18 IR SPCTRA OF Al/HZSM-5 ZEOLITES 1-4 REFER SiO_2/Al_2O_3 RATIOS, 35, 75, 204 AND 580 RESPECTIVELY.

The most intense absorption band occurs in the 950 to 1100 cm^{-1} region and is related to the T-O asymmetric stretching vibration (T = Si or Al). This vibration is sensitive to the Si/Al ratio, and is shifted to higher frequency with increasing content of silica[161]. Since mass of Si and Al are nearly same, the increase in frequency with increase of Si content is related to the vibration in the bond length of Al-O and lower electronegativity of Al results in the decrease in the force constant[162]. To obtain exact value of shift in IR frequency for asymmetric stretching vibration band occurring at around 1100 cm^{-1}, the IR spectra of H/AlZSM-5 zeolites with varying SiO_2/Al_2O_3 were scanned in the frequency region 1100-1300 cm^{-1} with reduced chart speed. The frequency maxima of this asymmetric stretch band is plotted against the atom fraction of Al in the framework tetrahedral site (see Fig. 3.19). A quantitative relationship is obtained. Similar shift for varying SiO_2/Al_2O_3 ratio in the zeolite was reported by many authors[161-163]. The position of asymmetric T-O stretch bend for silicalite at 1200 cm^{-1} is very close to that for pure silica in the 1000cm^{-1} region.

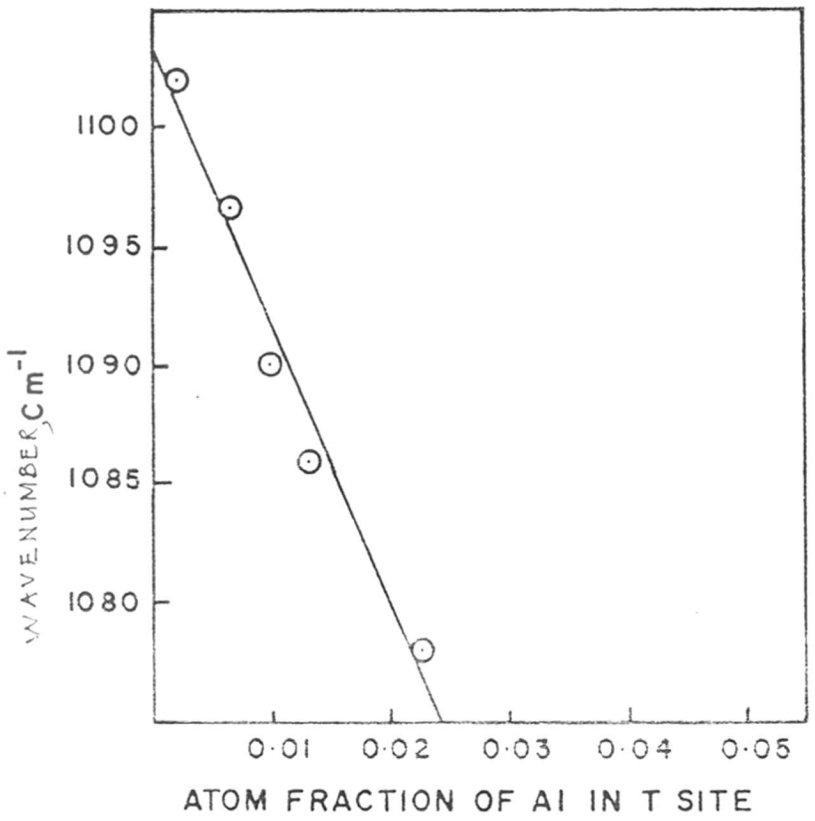

FIG. 3.19. SHIFT IN IR FREQUENCY Vs ATOM FRACTION OF Al IN T SITE OF Na/Al.ZSM-5 ZEOLITES.

3.3.8. Temperature Programmed Desorption of Ammonia (TPD)

Al/ZSM-5 series : Acid strength distribution can be derived from the rate of desorption of chemisorbed ammonia at increasing temperatures. The zeolites release the NH_3 over a wide temperature range. The experimental technique adopted for TPD has been explained previously. The ammonia TPD profiles for Na/AlZSM-5, H/AlZSM-5 and H/FeZSM-5 are shown in Fig. 3.20 and acid strength distribution is tabulated in Table 3.10.

Three distinct stages for desorption of ammonia at about 298-350, 350-600, 600-775 K were observed corresponding to weak, medium and strong acid sites, similar to Topsøe et al[64]. Anderson et al[75] have observed four TPD peaks around 400-430, 470-490, 550-600 and 780-800 K. The assignment of TPD peak has been made[64] as follows:

(1) The first peak (α - chemisorption state) is due to the sites located on the external surface onto some type of extraneous material, or due to interaction of ammonia molecules with surface oxide or hydroxide groups by non-specific hydrogen bonds.

(2) The second peak (β-chemisorption state) is associated with the crystallites and Na ions which are known to act as adsorption centres for NH_3 and also on weak Brönsted sites.

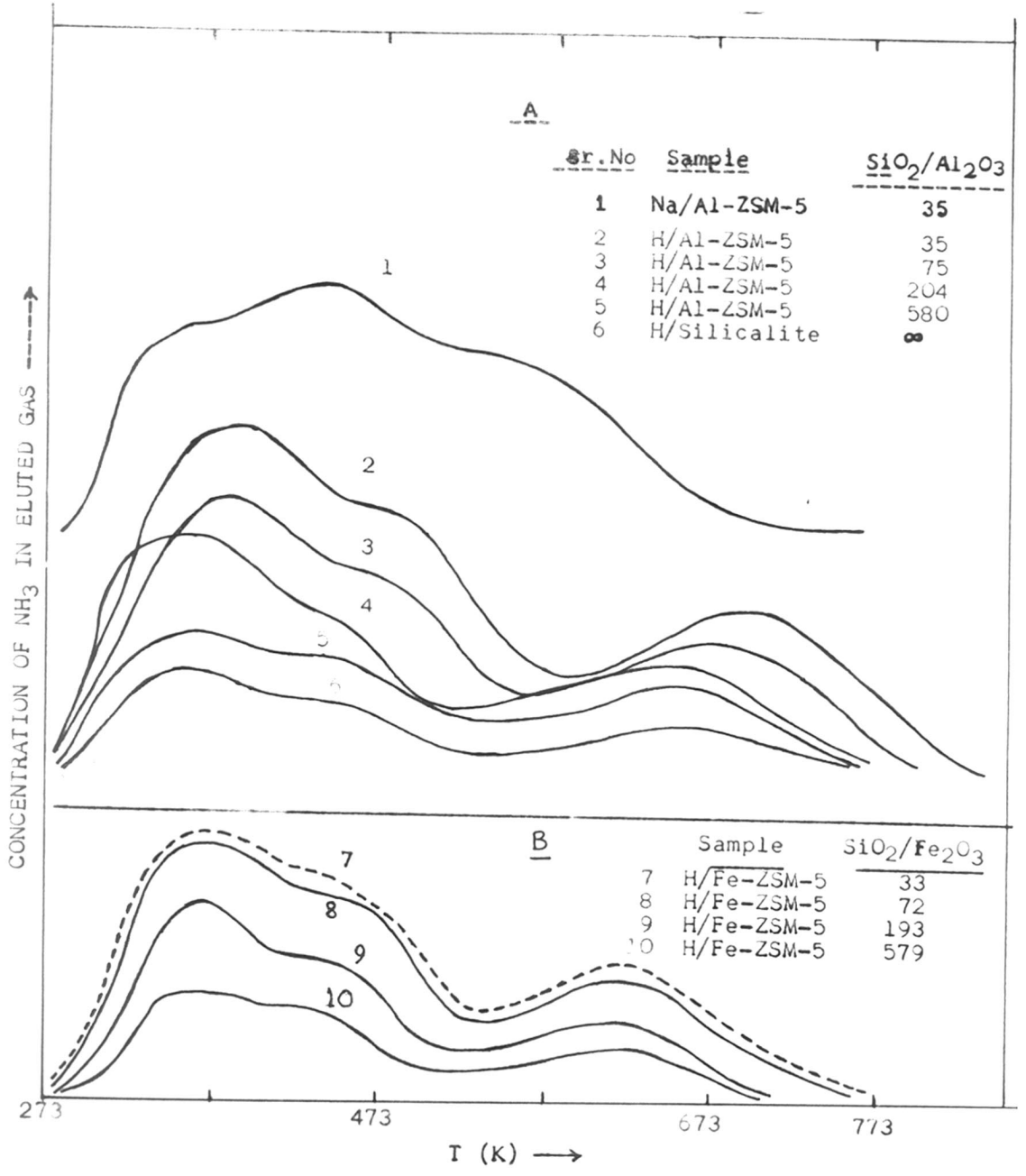

FIG. 3.20. A. TPD SPECRA OF NH_3 FROM Na-AND H/Al ZSM-5 ZEOLITES
B. TPD SPECRA OF NH_3 FROM H/Fe-ZSM-5 ZEOLITES.

(3) The third peak (γ-chemisorption state) which occurs at 573-773 K is associated with the sorption of ammonia on strong structural Brönsted acid sites.

The area of first + second TPD peaks (α,+ β chemisorption states) does not vary significantly with the replacement of Na^+ ions by H^+ ions, while the area of the third (γ-) peak increased to some extent. When Na-TEBA-ZSM-5 (C/N) containing Na^+ and $TEBA^+[(Et_3N\text{-}nBu)^+$, in channel intersections] was calcined, Na^+ ions might migrate to sites in channel intersections occupied by $TEBA^+$ earlier, hence γ-state of Na/Al-ZSM-5 has lower T_{max} than H/Al-ZSM-5. On increased SiO_2/Al_2O_3 ratio, it is observed that the total acidity decreases, this is because of reduced framework charge density. There is a remarkable deviation from 1:1 ratio of Al atoms : number of NH_3 molecules to lower side, as the framework Al increases. It is expected that increase in AlO_4 concentration in framework also increases the tendency of framework hydrolysis resulting in extralattice $Al(OH)_x^{3-x}$ cationic species, if the intermediate thermal treatment conditions are not carefully controlled to avoid hot-spots[164]. Then the structure of strong acid sites cannot be assumed to be a Brönsted or Lewis site, but a combination of them to form a super acid site like

$$Si[(OAl)_{n-1}]^{n-1} \text{ --- } M^{3+}.(n-1)/3$$

where n is the valency of M (M = Al or Fe) such a possibility has already been advanced by many authors[165,166]. It is observed that the T_{max} for strongest acid sites increases from 653 to 722 K as SiO_2/Al_2O_3 ratio decreases from 580 to 35. This can be attributed to the formation of super acid sites. The nature of such acid strength distribution over these ZSM-5 zeolite catalysts is also manifested in the characteristic product distribution in isofeed, and methanol reactions (Chapter IV). Auroux et al.[74] have also reported an increase in the initial heat of adsorption of NH_3 with decrease in SiO_2/Al_2O_3 ratio.

Fe/ZSM-5 series : The nature of TPD spectra for Fe/ZSM-5 samples (Fig. 3.20 B) also suggests that Fe^{3+} is isomorphously substituted in SiO_4 framework. Although, there is no report of any TPD data for Fe/ZSM-5 in the literature to our knowledge, the α, β and γ peaks in it can be ascribed to desorption of NH_3 in comparison with that of H/Al-ZSM-5 possessing three different energitic acid sites. The major difference in the TPD spectra and acid sites of H/Fe-ZSM-5 and H/Al-ZSM-5 is that, all the sites in H/Fe=ZSM-5 are weaker than that in H/AlZSM-5. The strongest peak may be attributed to the desorption of NH_3 chemisorbed on super acid sites as already explained for H/Al-ZSM-5 zeolites. There is also a significant increase in T_{max} for -γ peak on decreasing SiO_2/Fe_2O_3 ratio.

By applying simple electrostatic model with the help of NMR and TPD studies, Scholle et al.[167] have concluded that the acidity of framework hydroxyl groups in H/B-ZSM-5 is weaker than that of H/Al-ZSM-5. The framework hydroxyl groups in H/Al-ZSM-5, H/Fe-ZSM-5 and H/Silicalite can be represented as

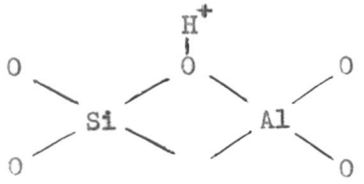

H/AlZSM-5

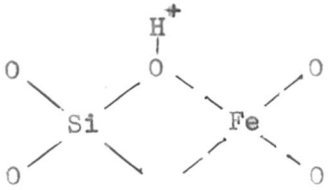

H/Fe-ZSM-5

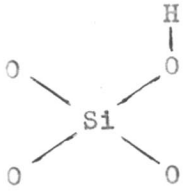

H/Silicalite

By applying qualitative electrostatic valence bond model of Pauling[168] the bond strength of Si-OH-Al, Si-OH-Fe and Si-OH can be compared. Accordingly, the bond strength S, on the cation is defined as

$$S = Z_e/V$$

where Z_e is the charge on cation and V the coordination number of cations.

The bond strength S_{Si-O} is then equal to 1. The charge on an anion -eZa is defined as

$$-eZa = \quad Si$$

where Si is the bond strength of all bonds of anion. Hence charge on O^{2-} anion on Si-OH group is

$$Z_o = 2 = S_{(Si-O)} + S_{(O-H)}$$

Therefore bond strength Si-O in Si-OH is equal to 1.

Similarly, bond strength of Al-O bond in Si-OH-Al is 3/4, and the charge on the shared oxygen is calculated as

$$Z_o = 2 = Si_{(Si-O)} + S_{(Al-O)} + S_{(O-H)}$$

Hence, bond strength of the O-H bond in Si-OH-Al is equal to 1/4.

The Pauling electronegativity difference between oxygen (EN = 3.5) and Iron (EN = 1.9) is less than the difference between oxygen and aluminium (EN = 1.5), hence it is expected that the bond strength $S_{(Fe-O)}$ is also less than $S_{(Al-O)}$. According to the above equation the bond strength of the O-H bond in Brönsted acid site of H/FeZSM-5 will be greater than that in H/Al-ZSM-5, hence Brönsted acid sites on H/Fe-ZSM-5 should be weaker than that of H/Al-ZSM-5 zeolites. Consequently, the T_{max} of NH_3 desorption from strongest acidic sites of H/Fe-ZSM-5 should be less than

that of H/Al-ZSM-5. It can be seen from the Table 3.10 that T_{max} of γ-peak for H/Fe-ZSM-5 series varies from 623 to 608.K. As the small γ-peak in TPD of [Fig.3.20(6)] H/Silicalite has its origin in impurity, Al atoms present during synthesis, it has T_{max} greater than that of H/Fe-ZSM-5.

In the light of the above observations we can conclude from the TPD results that acid strength of framework hydroxyl groups is in the order

H/Al-ZSM-5 > H/Fe-ZSM-5 > H/Silicalite.

The product distribution in the isofeed and methanol reactions over these zeolites again supports the same trend.

Table 3.10

Acid strength distribution over H/ZSM-5 pentasil zeolites

Sr. No.	Sample[a]	Chemisorption of NH_3 in ∝ and β peak		Chemisorption of NH_3 in γ-peak	
		Peak max. temp.(T_{max})K	NH_3 mole/u.c.	Peak max. temp.(T_{max}) K	NH_3 mole/u.c.
1.	Na/Al-ZSM-5(35)	448	6.88	573	1.63
2.	H/Al-ZSM-5(35)	398	7.12	718	2.46
3.	H/Al-ZSM-5(75)	398	4.60	693	2.30
4.	H/Al-ZSM-5(204)	379	3.34	673	1.00
5.	H/Al-ZSM-5(580)	363	1.12	653	0.48
6.	H/Silicalite(00)	358	1.36	653	0.38
7.	H/Fe-ZSM-5(33)	393	4.04	623	2.13
8.	H/Fe-ZSM-5(72)	388	4.60	618	1.80
9.	H/Fe-ZSM-5(193)	378	3.07	613	1.21
10.	H/Fe-ZSM-5(579)	373	1.73	608	0.78

a = Bracketed figures indicate SiO_2/M_2O_3 ratio; M = Al^{3+} or Fe^{3+}.

3.4. CONCLUSIONS

(1) The XRD data reveal that the structure of ZSM-5 pentasil zeolites of the type Al/ZSM-5 and Fe/ZSM-5 is stable upto 1273 K.

(2) The nitrogen adsorption measurements can be used to determine the crystallinity and/or purity of ZSM-5 pentasil zeolites.

(3) The amount of cyclohexane (but not n-hexane) adsorbed on both Al/ZSM-5 and Fe/ZSM-5 (synthesized by incorporating TEBA-Br as template) decreases with increase in SiO_2/M_2O_3 ($M = Al^{3+}$ or Fe^{3+}) ratio.

(4) O-xylene and 1,2,3-trimethyl benzene are excluded from the interior of the Al/ZSM-5 and Fe/ZSM-5 zeolite crystals indicating that effective pore diameter of these zeolites is less than 6.2 Å.

(5) The acidity of H/Al-ZSM-5 and H/Fe-ZSM-5 decreases on increase in SiO_2/M_2O_3 ratio and acidity of the later is weaker than the former.

(6) XPS, EPR and TPD techniques demonstrated that substitution of Fe^{3+} for Al^{3+} in the ZSM-5 type pentasil zeolite framework has been achieved.

CHAPTER - IV

CATALYTIC REACTIONS OVER ZSM-5 PENTASIL ZEOLITES

C O N T E N T S

4.1. INTRODUCTION

Among the various reactions studied over H/ZSM-5 type pentasil zeolites, the conversion of alcohols to hydrocarbons has been receiving increasing attention. This is both because of its industrial importance and complex reaction mechanism that leads to products ranging from C_1 to C_{10} hydrocarbons. Suitable catalyst and reaction parameters can be used to yield desired products in larger amount . Modified H/ZSM-5 zeolite catalyst yields larger amount: of olefins at the expense of other reaction products[168,169]. An increase in reaction temperature increases the aromatics in the C_5^+ fraction in the products[98].

There have been several efforts to selectively produce olefins from methanol. Framework aluminium atoms have been replaced with boron and transition metals[46,170,171] for this purpose. Isomerization of xylenes to p-xylene is another industrially important reaction. In the last two decades, considerable interest has been focussed on the conversion of eight carbon atom alkyl aromatics to xylenes. The demand for these materials, as chemical intermediates, has made it necessary that the petroleum industry produces large quantities to augment their production. The increasing demand for p-xylene has led to both industrial and academic

research in the area of alkyl aromatic isomerization reactions. Zeolite catalyst has been extensively used to isomerize xylenes and increase p-xylene content in C_8 aromatics fraction in the petrochemical industries[172,173].

In this chapter, we report influence of the reaction temperature, SiO_2/M_2O_3 molar ratio and dilution of methanol on the product distribution and product selectivity for the conversion of methanol to olefins and isomerization of commercial C_8 isomer feed over H/AlZSM-5 and H/FeZSM-5 zeolite catalysts.

4.2. EXPERIMENTAL

Catalytic conversions of methanol to olefins and isomerization of xylenes have been carried out in a fixed bed, down flow tubular reactor, at atmospheric pressure. The reactor consists of a fused silica tube, 2 cm in diameter and 35 cm in length provided with a thermowell which carries a thermocouple for sensing the reaction temperature. The reactor was heated with the help of a furnace upto 873 K. The top portion of the reactor serving as a vapouriser-cum-preheater, was packed with inert porcelain beads. The catalytic reactor assembly as shown in Fig. 4.1 also consists of a product receiver system consisting of a coil condenser which is cooled by chilled water.

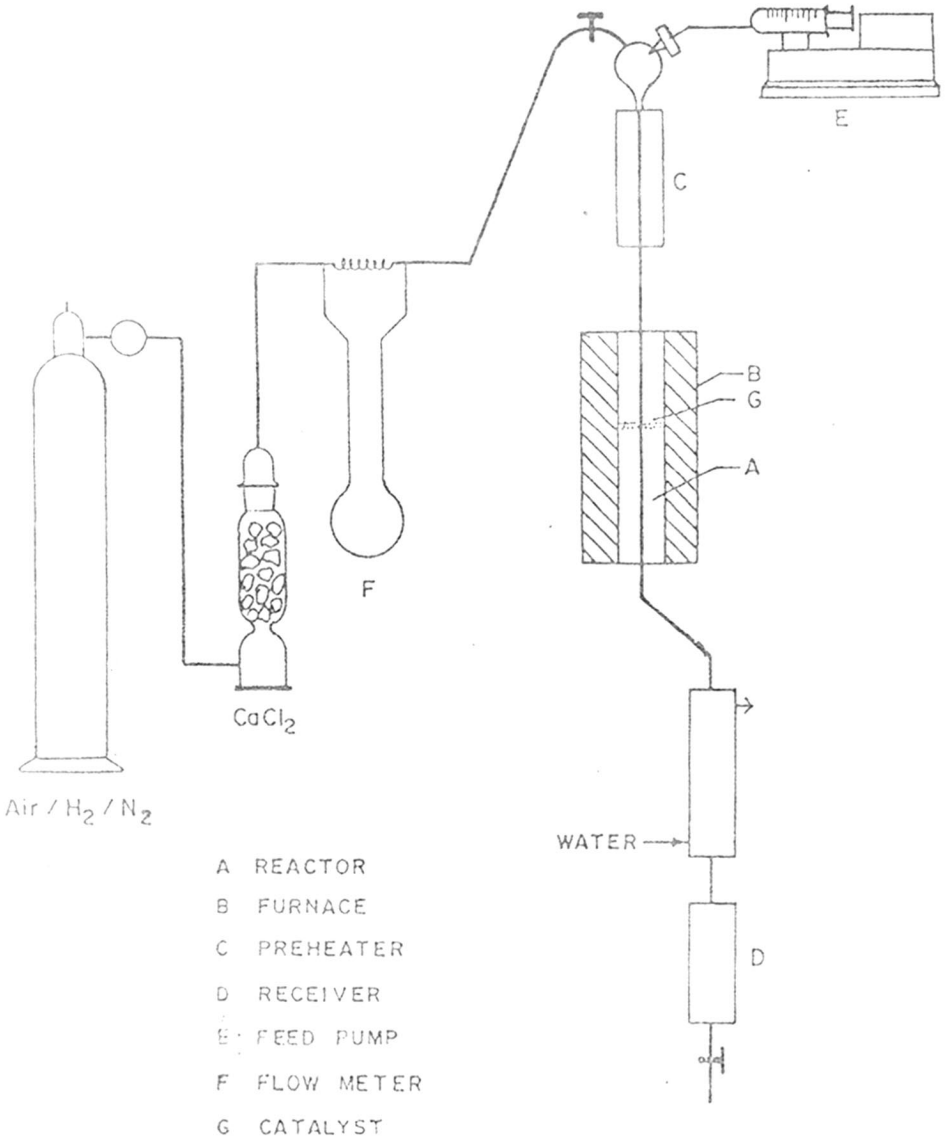

FIG. 4·1. SILICA REACTOR USED FOR CATALYTIC REACTIONS.

The catalyst powder was pressed into 1 cm^2 pellets, sized to 10-22 mesh and a known amount was charged in the reactor column. Prior to reaction, the catalyst was heated in a stream of air at 813 K for 2-3 hours. The catalyst was then flushed with nitrogen and cooled to reaction temperature. The reactant materials methanol/ethanol/commercial C_8 isomer, were fed by a syringe pump (SAGE Instrument, Model 352) at a constant feed rate, vapourised and passed through the catalyst zone, at desired temperature. Since the reaction (conversion of methanol to olefins) is exothermic, the desired temperature had to be obtained by adjusting the furnace temperature.

The reaction products in methanol to olefins reaction were passed through the condenser cooled by chilled water. The condensable liquid products consisting of organic layer and an aqueous layer were collected separately at fixed intervals and weighed. They were then analysed using a 6' x 1/8" column packed with 20% SE-30 on chromosorb AW 80-100 mesh for the organic layer and a porapak-Q column (6' x 1/8") for the aqueous layer on a gas chromatograph (HP Model 5840A, FID Detector). The non-condensable gaseous products (usually C_1-C_5) were passed through a gas sampling tube from which samples could be taken at regular intervals with a gas tight syringe. The

gas samples were analysed using 2 columns, 5' x 1/8" n-octane/porasil C and Porapak-Q in a gas chromatograph.

The catalytic isomerization of commercial C_8 isomer feed was carried out in the same reactor (Fig.4.1). The reaction products were condensed by chilled water and samples collected were analysed by a gas chromatograph (HP 5840A) using a 2 meter long, 1/8" i.d. column packed with 5% diisodecylphthalate + 5% Bentone-34 on chromosorb AW.

4.2.1. Materials

All the chemicals used as feed, such as methanol and ethanol (L.R. grade) were purified by distillation. The commercial C_8 isomer feed was obtained from IPCL, Baroda. A refinery gas test sample HP P/N 5080-8755 obtained from Hewlett Packard was used for identification of gaseous products.

4.3. RESULTS AND DISCUSSION

4.3.1. Conversion of methanol

The reaction of methanol conversion to hydrocarbons especially to olefins was studied over the catalysts H/Fe-ZSM-5 (72) and H/Al-ZSM-5 (75) in the temperature range, 573 to 823 K, at atmospheric pressure and WHSV = 2 hr^{-1}. Tables 4.1 and 4.2 present the data and Fig. 4.2 illustrates the effect of reaction temperature on the product distribution. It is seen (Fig. 4.2) that initially yield of C_5^+ aliphatics and C_1-C_4

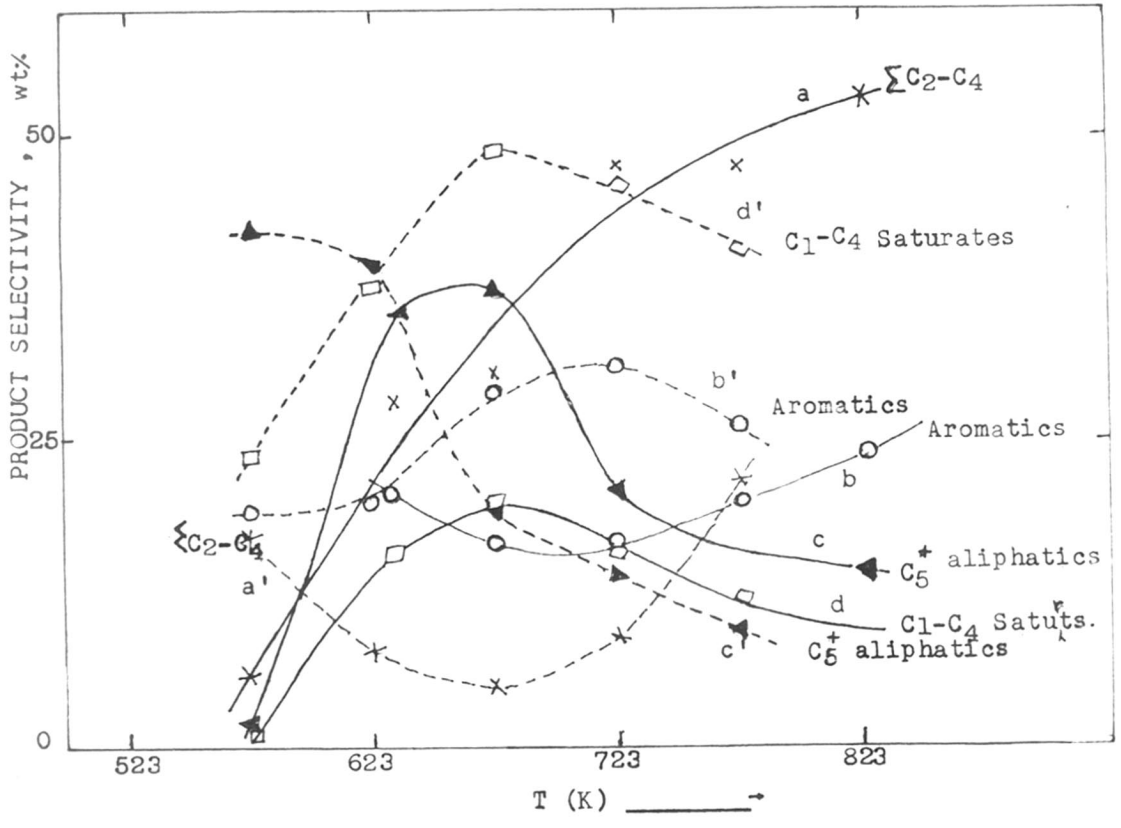

FIG. 4.2. INFLUENCE OF TEMPERATURE ON PRODUCT DISRTIBUTION IN METHANOL CONVERSION REACTION. SiO_2/M_2O_3= 75, WHSV = 2

_____ curve for H/Fe-ZSM-5 Catalyst

------ curve for H/Al-ZSM-5 Catalyst

Table 4.1

Effect of temperature on methanol conversion and product distribution

[Run conditions : Catalyst H/FeZSM-5(72), WHSV = 2.0 hr^{-1}, Temperature (K) at atmospheric pressure]

	Reaction Temp. (K)					
	573	638	673	723	773	828
Conversion wt.%	54.3	83.6	99	100	100	100
DME	92.5	7.4	1.15	0.0	0.0	0.0
Hydrocarbons, wt. %						
Total olefins	5.59	27.71	27.98	47.44	45.36	53.22
C_1-C_4	0.46	15.65	18.67	15.54	12.27	8.7
C_5^+ + Aliphatics	1.47	36.09	37.0	20.7	22.25	13.90
BTX*	-	11.15	9.67	11.33	13.72	16.62
C_9 + C_{10} aromatics	-	9.38	6.73	4.98	6.40	7.60
% Selectivity to aromatics	-	36.3	30.8	44.05	47.5	63.5

* BTX - Benzene, Toluene and Xylene.

Table 4.2

Effect of temperature on methanol conversion and product distribution

[Run conditions: Catalyst H/Al-ZSM-5(75), WHSV = 2.0 hr^{-1}, Temperature (K) at atmospheric pressure]

	Reaction Temp. (K)				
	573	623	673	723	773
Conversion, wt.%	98.3	99.4	99.6	100	100
DME	2.04	0.24	Trace	0.0	0.0
Hydrocarbons, wt, %					
Total C_2-C_4 olefins	16.75	7.72	4.63	8.67	21.62
Ethylene	11.8	1.42	1.30	3.06	8.25
Propylene	2.83	1.52	2.28	4.57	10.42
Butenes	2.12	0.78	1.05	1.04	2.95
C_1-C_4 Saturates	23.57	37.52	48.41	45.74	40.84
C_5^+	59.68	58.74	47.00	45.57	37.52
% Selectivity to aromatics in C_5^+	29.83	31.5	58.8	68.1	70.7

saturates in the case of H/Fe-ZSM-5 catalyst, increases sharply with increase in reaction temperature and is maximum around 673 K (curves C, D) at which the selectivity to aromatics (curve B) is minimum. Above this reaction temperature, it is observed that there is a continuous decrease of C_5^+ and C_1-C_4 fractions, which is accompanied by an increase in the total olefins (curve A) which is maximum at 828 K. The increase in the product selectivity for total olefins and aromatics may be due to the subsequent cracking of higher aliphatics[168] at higher reaction temperatures (above 673 K). The product distribution of methanol reaction over H/Al-ZSM-5 is also illustrated in Fig. 4.2 (curves A', B', C' and D') and data is presented in Table 4.2. In either case, the increase in C_2-C_4 olefins is the result of decrease in C_5^+, especially aliphatics as can be clearly seen in Fig. 4.2. Similarly, the data presented in Tables 4.1 and 4.2 for the reaction of methanol to hydrocarbons bring out a striking difference between the catalytic activities of H/Al-ZSM-5 and H/Fe-ZSM-5 pentasil zeolite catalysts. The data reveal that there is a large increase in the selectivity to olefins at the expense of other products especially aromatics. The low activity of H/Fe-ZSM-5 catalyst at temperatures below 673 K, in comparison with that of H/Al-ZSM-5 (cf. Table 4.2, Fig. 4.2) may be attributed to the presence of weaker acid

sites in H/Fe-ZSM-5 catalyst. As already pointed out (Fig. 3.20, Chapter III), the temperature for desorption of chemisorbed NH_3 for γ-peak is higher and its area is larger for H/Al-ZSM-5, revealing the existence of larger number of stronger acid sites (hydroxyl group acid strength distribution) compared to those in H/Fe-ZSM-5 catalyst. This may be the reason for the larger amount of aromatics in the C_5^+ fraction observed in the case of H/Al-ZSM-5 catalyst, as it is known that the formation of aromatics requires strong acid sites[174,175]. Further, it is evident (cf Table 4.1) that selectivity to olefins in the reaction temperature range 673-773 K over H/Fe-ZSM-5 catalyst is maximum at 723 K. This is comparatively lower than the temperature required for H/Borosilicates[176].

At this stage, it is of interest to review the various mechanisms proposed in the literature for hydrocarbon formation. In the formation of the hydrocarbons from methanol, the mechanism for the initial C-C bond formation has been discussed by several authors[177-180]. According to Chang et al.[98] a methylene diradical is formed by an α-elimination mechanism as a result of strong electrostatic fields and gradients prevailing in the zeolite cages. This diradical then interacts with methanol or dimethyl ether (DME, formed by dehydration) via sp^3 C-H insertion to yield ethylene through protolysis,

$$[:CH_2] + CH_3\text{-}OR \longrightarrow CH_3CH_2\text{-}OR$$

$$CH_3CH_2\text{-}OR \xrightarrow{H^+} C_2H_4 + HOR$$

where R represents a H atom or methyl group.

According to Van Den Berg et al[181] methylethyloxonium ion is a relatively stable ionic intermediate formed after a series of reaction steps subsequent to the reaction of dimethylether (formed by dehydration of methanol) with a Brönsted acid site to form a dimethyloxonium ion. This methylethyloxonium ion can undergo subsequent reactions as shown below

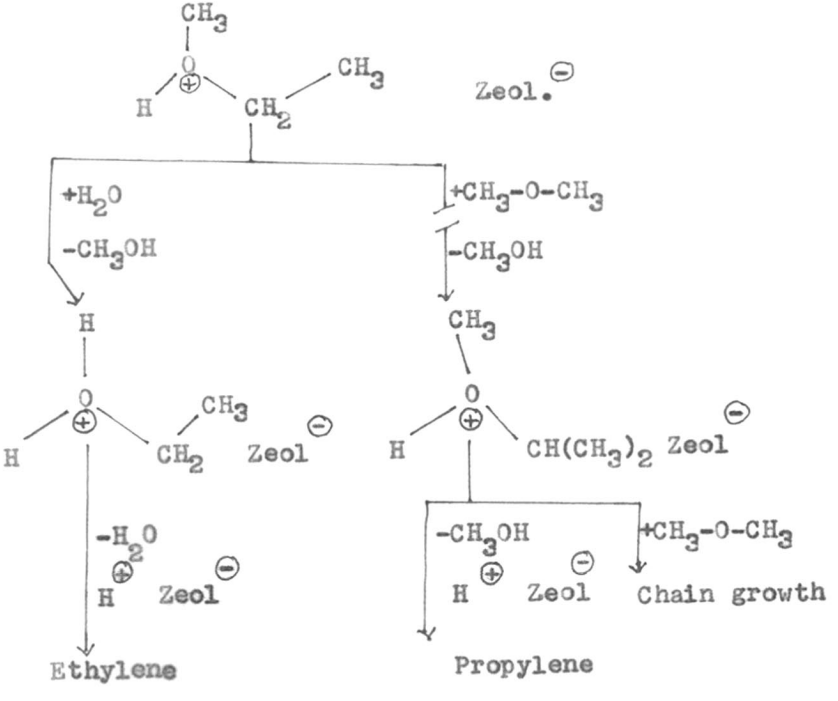

Methylethyloxonium ion can react with the water which is always present or with dimethyl ether. Reaction with water will result in the elimination of CH_3OH and the formation of the ethyloxonium ion. The latter will rapidly eliminate water to form ethylene.

Reaction with dimethyl ether will also result in an elimination of CH_3OH, the dimethylethyloxonium ion being formed in this case. This can undergo rearrangement to give propylene and methanol.

A similar mechanism may hold for the formation of higher molecular weight olefins. For example, a C_4-olefin may be formed from a C_3-surface species by reaction with methanol and dehydration.

The subsequent reactions of the olefins comprising condensation, cyclization, hydrogen transfer, etc. to yield the products observed in the reaction, have been well documented[182,183].

4.3.2. Effect of SiO_2/M_2O_3

Table 4.3 presents the data on the effect of SiO_2/M_2O_3 molar ratio on hydrocarbon distribution and selectivity to aromatics for H/Al-ZSM-5 and H/Fe-ZSM-5 catalysts. It is seen that both the catalysts show the same

Table 4.3

Effect of SiO_2/M_2O_3 on hydrocarbon distribution and selectivity to aromatics in methanol conversion reaction over H/Al-ZSM-5 and H/Fe-ZSM-5 catalysts

[Run conditions: WHSV 2.2 hr^{-1}, reaction temperature (K), SiO_2/M_2O_3 ratio = 75, 200, at atmospheric pressure, feed:methanol]

	Reaction Temperature							
	673				723			
	H/Al-ZSM-5		H/Fe-ZSM-5		H/Al-ZSM-5		H/Fe-ZSM-5	
SiO_2/M_2O_3	75	204	72	193	75	204	72	193
Conversion, methanol wt. %	99.6	100	99	93.8	100	100	100	99.0
DME	-	-	1.0	8.5	-	-	-	2.5
Hydrocarbon distribution								
Total olefins	4.63	10.2	27.98	54.7	8.67	13.1	47.44	65.9
C_1-C_4 saturates	48.41	40.15	18.67	5.2	45.74	39.78	15.54	6.5
C_5^+ Aliphatics	19.4	22.67	37.0	24.8	45.57	47.15	20.70	18.85
Aromatics	27.62	27.0	16.4	10.4	31.03	30.95	16.31	8.75
% Selectivity to aromatics	58.75	54.4	30.8	29.5	68.1	65.6	44.05	31.7

behaviour with regard to product distribution and selectivity to aromatics except with respect to C_5^+ aliphatics when molar ratio (SiO_2/M_2O_3) and reaction temperature are changed. For C_5^+ aliphatics, the trend is reversed for the two catalysts. At increased SiO_2/M_2O_3 ratio there is a decrease in both the number and strength of the acid sites. Since these are responsible for formation of aromatics, the observed effect on aromatics and their selectivity is as expected.

A great advantage of H/Fe-ZSM-5 catalysts is that even dilute aqueous solutions of MeOH can be completely converted with high selectivity to olefins. H/Al-ZSM-5 catalyst gives about 54% olefins as against about 74% olefins over H/Fe-ZSM-5 catalyst, when the same feed i.e. 30% methanol (aqueous solution) is passed over these catalysts at 723 K. Table 4.4 compares the data for product distribution in the conversion of 30% aqueous MeOH over H/Al-ZSM-5 and H/Fe-ZSM-5 catalysts.

H/Fe-ZSM-5 is also a potential catalyst for dehydration of ethanol to ethylene. An additional advantage is its usefulness in converting even more dilute aqueous solutions at comparatively higher space velocities (cf. Table 4.5) than used on the conventional SYNDOL catalyst.

Table 4.4

Product distribution for the conversion of 30% aqueous MeOH over H/Al-ZSM-5 and H/Fe-ZSM5 catalysts

[Run conditions : WHSV 5.0 hr^{-1}, Temp. 723 (K) at atmospheric pressure]

	Catalysts	
	H/Al-ZSM-5	H/Fe-ZSM-5
Conversion, MeOH, wt.%	100	100
DME	-	-
Hydrocarbon distribution, wt.%		
Total olefins	53.75	73.64
Ethylene	19.9	9.4
Propylene	24.1	43.74
Butenes	9.75	20.51
C_1-C_2 saturates	19.58	4.57
C_5^+ aliphatics	14.03	13.78
Aromatics	12.71	8.01
% Selectivity to aromatics	47.53	36.8

Table 4.5

Comparison of H/Fe-ZSM-5 Catalyst performance with commercial SYNDOL catalyst

	SYNDOL[a]	H/Fe-ZSM-5
Dilution	95 vol. %	40%
LHSV hr^{-1}	0.23	5.0
Temp. (K)	591	573
Conversion	99.1	99 +
Selectivity to ethylene	96.8	98.26
Impurities		
H_2 : vol. ppm	670	758
Co_2: vol. ppm	120	340
CH_4: vol. ppm	12	4
C_2H_6: mole %	0.49	?
C_3H_6: mole %	0.03	0.35
C_4 Hydrocarbons mole %	1.0	0.15
Ether mole %	0.05	0.70
Ethanol mole %	0,31	0.08

a : Kochar et al CEP June 1981
0360 7275/81/4926-0066 AIChE

4.3.3. Isomerization of C_8 isofeed

Zeolite ZSM-5 catalysts have been used to isomerize C_8 aromatic hydrocarbons with the aim of increasing the p-xylene content in the product. An industrial catalyst should meet the following objectives:

(i) the reaction should lead to minimum C_8 losses (C_8 aromatics in product (-) C_8 aromatics in feed),

(ii) the conversion of p- and o-xylene as well as the per pass conversion of ethylbenzene (EB) should be reasonably high,

(iii) the catalyst should have chlorine and sulfur tolerance,

(iv) the catalyst must be regenerable without marked loss of performance.

In the above context, activities of H/Fe-ZSM-5 and H/Al-ZSM-5 catalysts have been compared in Table 4.6. The feed consisted of a mixture of C_8 aromatics obtained from Indian Petrochemicals Ltd., Baroda.

The results show that both the catalysts have comparable activity for isomerization of xylene in C_8 isomer feed, except a large difference in the percentage conversion of EB. The H/Al-ZSM-5 catalyst is most active for the cracking of EB with the resultant net gain in xylene being not significant and the C_8 loss considerable, which is attributed to the presence of stronger acid sites in this catalyst.

Table 4.6

Comparison of the performance of H/AlZSM-5 and H/FeZSM-5 catalysts in the conversion of C_8 aromatics to p-xylene

WHSV = 8.0 hr^{-1}, Temp. = 723 K, SiO_2/M_2O_3 = 75

	H/Al-ZSM-5		H/Fe-ZSM-5	
	Isofeed composition wt. %	Prod. distribution wt. %	Isofeed composition wt. %	Prod.distribution wt. %
Aliphatics	2.22	1.31	2.58	3.25
Benzene	1.35	9.74	0.48	3.26
Toluene	2.80	3.59	3.03	3.51
EB	26.21	12.98	26.33	22.21
PX	8.07	14.57	7.47	14.28
MX	54.58	39.54	55.25	40.39
OX	4.72	14.06	4.86	11.54
C_9^+	-	4.3	0.02	1.50
Σ Xyl.	67.37	68.08	67.56	66.21
Σ C_8	93.58	81.06	93.89	88.42
**Δ Xyl.	-	+ 0.52	-	-1.16
**ΔC_8	-	- 12.83	-	-5.16
EB conversion	-	50.70	-	15.26
PATE*	-	86.64	-	87.00

* PATE, para xylene approach to equilibrium

$$= \frac{\text{per cent p-xylene in the product (-) per cent p-xylene in the feed}}{\text{per cent p-xylene at equilibrium (-) per cent p-xylene in the feed}}$$

** Δ = total in the product (-) total in the feed.

4.4. CONCLUSIONS

A comparative study of the activity of H/Al-ZSM-5 and H/Fe-ZSM-5 catalysts for the conversion of methanol to olefins shows that H/Fe-ZSM-5 catalyst gives enhanced selectivity to olefins. This has been correlated with acidity data for the two catalysts.

H/Fe-ZSM-5 catalyst can also convert dilute ethanol to ethylene; the conversion is nearly complete with high selectivity to ethylene even with 30% aqueous ethanol.

H/Fe-ZSM-5 catalyst is also active for isomerization, for instance, conversion of C_8 isomers to p-xylene with minimum loss in total xylene. Its activity for the conversion of EB is, however, low.

S U M M A R Y

The ZSM-5 type pentasil zeolite catalysts recently introduced for hydrocarbon conversion reactions are attracting wide interest in industrial and scientific community. These catalysts have unique properties like shape-selectivity, thermal stability and resistance to coke formation; they can be modified by ion-exchange, acid treatment, and isomorphous substitution methods. Hence the detailed study was undertaken in synthesis of these novel zeolites using sodium-triethyl-n-butylammonium (Na-TEBA) and mixed alkyl amine, alkyl bromide (TEA + n-Bu-Br) as organic templates, in aluminosilicate and ferrosilicate forms. Subsequent characterization was undertaken to study their physico-chemical properties.

It is possible to synthesize ZSM-5 pentasil zeolite with aluminium (Al^{3+}) and ferric (Fe^{3+}) ions substituted in framework silicates. The hydrothermal synthesis procedures under autogenous pressure in temperature range 433 to 473 K have been adopted. Kinetics of nucleation and crystallization for these systems have been studied. In order to describe the crystallization process of the ZSM-5 zeolites, apparent activation energies, both for nucleation as well as crystallization, have been evaluated by the Arrhenius equation. The kinetic data when

fitted to Avrami-Erofeev equation suggested that the reaction in hydrothermal synthesis of ZSM-5 involves both nucleation and subsequent crystal growth mechanism.

The rates of both nucleation and crystal growth of Fe/ZSM-5 crystals are lower than those of Al/ZSM-5 zeolites. The influence of the temperature, pH, SiO_2/M_2O_3 ratio (M = Al^{3+} or Fe^{3+}) on the kinetics of zeolite formation, has been discussed. When Et_3N and n-butyl bromide are used, the zeolite which is formed appears to be a pure crystalline ZSM-5 phase. However, this procedure gives rise to a non-zeolitic phase transformation to α-quartz. The suppression of such transformation to α-quartz during synthesis has been achieved by varying OH^-/H_2O ratio of the initial gel reactant composition. Similarly, the effect of OH^- concentration, organic base concentration, on the formation of these zeolites has been studied. It is concluded that the crystallization rate in both the systems depends on $(TEBA)_2O/SiO_2$ ratio and higher the ratio, faster the crystallization. Although alkalinity strongly affects the nucleation, the crystal growth rate is almost independent of OH^- concentration. The morphology of ZSM-5 zeolite nuclei and crystals has been followed by scanning electron

micrography. It is found that synthesis parameters, such as OH^- concentration, molar ratio and temperature, affect the morphology of ZSM-5 zeolite crystals.

The as-synthesized (C/N) zeolites are heated upto 823 K in air under controlled conditions to decompose the organic cations. The Na form is then converted to NH_4^+ form by repeated ion exchange with NH_4Cl solution. By thermal deammoniation at 823 K, corresponding protonic (H^+) forms of these zeolites are obtained. The catalysts so obtained are characterized by physico-chemical methods described below.

Comparison of x-ray diffraction patterns of Al/ZSM-5 and Fe/ZSM-5 zeolites with published data reveals that the zeolites belong to pentasil family. With increasing SiO_2/M_2O_3 ($M = Al^{3+}$ or Fe^{3+}) ratio the intensity of two peaks at 2θ, 7.9 and 8.8 increases. The separation or spacings (Δ) of two peaks at 2θ, 45.1 and 45.5 is found to be proportional to the Al^{3+} or Fe^{3+} content in the zeolite. The broadening in XRD peaks for Fe/ZSM-5 zeolite is obtained as compared to that in Al/ZSM-5 zeolite. Change in XRD peak area in the range $2\theta = 22^{\circ}$ to 25° can be used to compare the thermal stability of zeolite. H/Al-ZSM-5 and H/Fe-ZSM-5 did not show any structural breakdown when heated upto 1323 K for 5 hours, whereas Na/Al-ZSM-5 and Na/Fe-ZSM-5 showed 30-35%

decrease in crystallinity. It is found that thermal stability increases with increase in SiO_2/M_2O_3 (M = Al^{3+} or Fe^{3+}) ratio. This method can also be used to study the hydrothermal stability of these zeolites.

Differential thermal analysis shows no exothermic effect due to structure breakdown upto 1273 K. Endotherm due to dehydration occurred at about 373 K. The NH_4^+ and Et_3N^+Bu. decomposed oxidatively and were eliminated from the zeolite in the temperature range 523-873 K. The nature of curves obtained by thermogravimetry can thus explain the desorption of physically adsorbed water or decomposition of NH_4^+ cations (below 873 K) and dehydroxylation of surface hydroxyl groups as water beyond 873 K.

Nitrogen adsorption data on both these zeolites is analysed by applying Langmuir, BET and Dubinin equations. BET surface area of Al/ZSM-5(75) is 436 m^2/g and that for Fe/ZSM-5(72) is 419 m^2/g, while Dubinin void volumes are 0.19 cc/g and 0.184 cc/g respectively. Langmuir equation is found to be applicable over a wide pressure range. It is found, from N_2 adsorption and XRD data that micropore volume increases with increase in the crystallinity of the zeolite.

The studies in adsorption and diffusion reveal shape-selectivity, molecular sieving property and hydrophobicity of these zeolites. The relative sorption rates with 6 carbon atom hydrocarbons suggest that the rate of mass transport of hydrocarbons into zeolite crystallites follows the order

n-paraffins > monomethyl paraffins, aromatics > dimethyl paraffins.

Molecules having cross-section greater than 6.4 x 6.9 Å would be excluded from the interior of the zeolite. There is not much difference in the adsorption properties of Al/ZSM-5 and Fe/ZSM-5 zeolites. From the sorption studies it is concluded that

(i) linear aliphatics have an access to both the channel systems in ZSM-5 zeolites,

(ii) iso-aliphatic compounds experience steric hindrance which may restrict their adsorption and diffusion in the sinusoidal channel system,

(iii) aromatic compounds and other methyl substituted aliphatics have strong preference for diffusion in channels of ZSM-5.

A systematic x-ray photoelectron spectroscopy (XPS) study has been done on the samples hydrothermally treated at different temperatures. It can be concluded from the results that the surface of H/Al-ZSM-5 zeolite is enriched with aluminium at increased steam treatment temperature. This is attributed to the migration of framework aluminium ions from the bulk to the external surface of zeolites. XPS spectra of Fe/ZSM-5 shows that Fe ions are in Fe^{3+} state in the zeolite framework. Single O_{1s} peak at 531.5 eV was observed for pure Fe/ZSM-5 while two peaks of O_{1s} at 531.5 and 529.1 eV are observed for sample having occluded Fe_2O_3 species.

Electron paramagnetic resonance spectra (EPR) of Fe/ZSM-5 can identify Fe species in zeolite whether they are

(i) in exchangeable sites of zeolite framework, or

(ii) randomly oriented in hydroxy oxide form, or

(iii) in the silicate framework where they replace some of the SiO_4 tetrahedra.

In order to establish the location of Fe^{3+} in FeZSM-5, EPR spectra were obtained under varying conditions of treatment. The EPR spectra of the samples, as-synthesized, after oxidation in air, after reduction by hydrogen in presence of H_2O or heated in vacuum, were recorded and changes in signals at g = 5.3, 4.3, 2.3, 2.0, were studied. Analysis of the results showed that Fe^{3+} ions are present in Fe/ZSM-5 are mainly in the tetrahedral positions.

The infrared spectra of H/Al-ZSM-5 zeolite in the framework vibration region 300-1200 cm^{-1} are studied. The most intense absorption band occurring at 950-1100 cm^{-1} region related to T-O asymmetric stretching vibrations, is shifted to higher frequency with increase in SiO_2 content. IR spectra of H/Al-ZSM-5 zeolites with varying SiO_2/M_2O_3 ratio showed a quantitative relationship between intensity of absorption band around 1100 cm^{-1} and Al atom fraction (or crystallinity) in the zeolite.

A substitution of iron in the zeolite framework showed the shift in the main asymmetric band towards lower frequency because of longer Fe-O bond distance (1.97 Å) than T-O or Al-O bond distance (1.75 Å). Therefore, band which occurs at around 1100 cm^{-1} shifts towards lower frequency.

Acid strength distribution over Al/ZSM-5 and Fe/ZSM-5 zeolites have been determined by temperature programmed desorption of ammonia. A typical three peak TPD spectrum at around 298-350, 350-600, 600-775 K was obtained for H/Al-ZSM-5. The peaks are ascribed to strongly physisorbed, chemisorbed on crystallite surfaces, on counter cations, and on Brönsted acid sites, respectively. The acid strength distribution of H/Fe-ZSM-5 is similar to H/Al-ZSM-5 except that all the three peaks are shifted to lower temperature. This has been explained on the basis of Paulings

electronegativity principle. The O-H bond strength in Brönsted acid sites of H/Fe/ZSM-5 is stronger than that of H/Al-ZSM-5. Therefore, Brönsted acid site in H/Fe-ZSM-5 is weaker than that of H/Al-ZSM-5 zeolite. The acidity shows the order

H/Al-ZSM-5 > H/Fe-ZSM-5 > H/Silicalite.

The peak temperature of strongest acid sites in both zeolites increases as SiO_2/M_2O_3 ratio decreases which is attributed to the formation of super acid sites.

Catalytic conversion reactions of methanol to olefins and isomerisation of C_8 isomer have been studied over protonic (H^+) forms of Al/ZSM-5 and Fe/ZSM-5 catalysts. The influence of reaction temperature, SiO_2/M_2O_3 ratio and dilution of ethanol with water on the product distribution has been studied and the results are correlated with acidity data for these two catalysts. Comparative study of the catalytic activity in isomerization reactions for both these catalysts with respect to the product distribution reveals that H/Fe-ZSM-5 catalyst gives higher conversion with minimum loss in total xylenes, but its activity for the conversion of EB (ethyl benzene) is low.

In conclusion, the zeolite ZSM-5 can be successfully synthesized using triethyl-n-butylammonium bromide (TEBA-Br) as well as by adding triethylamine and n-butyl bromide in-situ

during synthesis. It is found that the formation of non-zeolitic phase, viz. α-quartz can be suppressed by optimizing the synthesis conditions. Fe^{3+} substitution in SiO_4 tetrahedra to form Fe/ZSM-5 (known as crystalline ferrosilicate) zeolite has been confirmed. The acid strength distribution in pentasil zeolites can be altered to obtain a wide range in product distribution in the conversion of methanol to olefins and/or hydrocarbons as well as isomerization of C_8 isomers. The shape-selective nature of these zeolites also contributes significantly in such hydrocarbon conversion reactions.

---000---

REFERENCES

1. Cronstedt, A., Akad. Handl. Stocholm., 18, 20 (1756)

2. Damour, A., Ann. Mines, 17, 191 (1840).

3. Weigel, O. and Steinhoff, E., Z. Kristallogr., 61, 125 (1925).

4. McBain, J. W., The Sorption of Gases and Vapors by Solids, Chap. 5, Rutledge and Sons, London, 1932.

5. Milton, R. M., in "Molecular Sieves", Soc. Chem. Ind., London (1968) p. 199.

6. Barrer, R. M., "Zeolites and Clay Minerals as Sorbents and Molecular Sieves", Academic Press, London (1978).

7. Breck, D. W., "Zeolite Molecular Sieve", Wiley-Interscience, New York (1974).

8. Breck, D.W., Proceedings of the Conference on the Properties and Applications of Zeolites, Soc. Chem., Ind., London, April 18-20, 1979.

9. Anderson, R. A., ACS Symposium Series, 1977, 40, 637.

10. Rabo, J. A., Bezman, R. D. and Poutsma, M. L., Acta-Phys. Chem., 1978, 24, 39,

11. Rabo, J. A., Ed., "Zeolite Chemistry and Catalysis", Amer. Chem. Soc., Monograph 171 (1976).

12. Sherman, J. D., Adsorption and Ion Exchange Separations, AIChE Symposium Series, 1978, 74, No. 179, 98.

13. Milton, R. M., U.S. Patent 2,882,243 (1959), U.S. Patent 2,882,244 (1959).

14. Fraenkel, D., and Shabtai, J., J. Am. Chem. Soc., 99,7074 (1977)

15. Breck, D. W., U. S. Patent 3,130,007 (1964).

16. Sand, L. B., U. S. Patent 3,436,174 (1969).

17. Anouncement :Chem.and Eng. News, 1962

18. Flanigen, E. M. and Kellberg, E. R., Dutch Patent 6,710,729 (1967).

19. Wadlinger, R. L., Kerr, G. T. and Rosinski, E. J., U. S. Patent 3,308,069 (1967).

20. Argaur, R. J. and Landolt, G.R., U.S.Patent 3,702,886 (1972).

21. Chu, P., U. S. Patent 3,709,979 (1973).

22. Rosinski, E. J. and Rubin, M. K., U.S. Patent, 3,832,449 (1974).

23. Rubin, M. K. Rosinski, E. J. and Plank, C. J., U. S. Patent 4,086,186 (1978).

24. Kokotailo, G. T., and Meier, W. M., Chem. Soc. Special Publication 33, 133 (1979).

25. Flanigen, E. M., Bennett, J. M., Grose, R. W.,

26. Kokotailo, G. T., Lawton, S. L., Olson, D. H. and Meier, W. M., Nature, 272, 437 (1978).

27. Chu, P., U.S. Patent 3,709,979(1973), Morrison, R.A., U.S. Patent 3,856,872 (1974), Keown et al, U.S. Patent 3,751,504 (1973)

28. Zhdanov, S. P., Adv. Chem. Ser., 101, 20 (1971).

29. Flanigen, E. M., Adv. Chem. Ser., 121, 119 (1973).

30. Barrer, R. M. and Denny, P. J., J. Chem. Soc., 971 (1961).

30. a : Kerr, G.T. and Kokotailo, G., J. Amer. Chem. Soc., 83, 4675 (1961).

31. Barrer, R. M., Denny, P. J. and Flanigen, E. M., U. S. Patent 3,306,922 (1967).

32. Kerr, G. T., Inorg. Chem., 5, 1537 (1966); U. S. Patent 3,247,195 (1966).

33. Wadlinger, R. L., Rosinski, E. J. and Plank, C. J., U. S. Patent 3,375,205 (1968).

34. Wadlinger, R. L., Kerr,G.T. and Rosinski, E. J., U. S. Patent 3,308,069 (1967).

35. Ciric, J., U. S. Patent 3,972,983 (1976).

36. Plank, C. J., Rubin, M. K. and Rosinski, E. J., U. S. Patent 4,105,541 (1978).

37. Rubin, M. K., Rosinski, E. J. and Plank, C. J., U. S. Patent 4,086,186 (1978).

38. Parker, L.M. and Bibby, D.M., Zeolite, 3 (1983)

38 a Erdem, A. and Sand, L. B., J. Catal., 60, 241 (1979).

39. Bibby, D. M., Milestone, N.B. and Aldridge, L. P., Nature, 280, 664 (1979).

40. Grose, R. W. and Flanigen, E. M., U. S. Patent 4,104,294 (1978).

41. Grose, R.W. and Flanigen, E. M - unpublished data.

42. Stubican, V. and Ray, R., Amer. Minerol., 47, 116 (1962).

43. Hautefeuille, P., Compt. Rend., 90, 303 and 378 (1880).

44. Perry, A., Compt. Rend., 107, 1150 (1888).

45. Eitel, W., Herlinger, E. and Tromel, G., Nurwiss 18, 469 (1930).

46. Morosi, L., Stabenow, J., Schwarzmann, M., Ger. Patent 2,831,630

47. Barrer, R. M. and Cole, J. F., J. Chem. Soc. A 2475 (1968).

48. Wilson, S.T., Lok, B. M., Massina, C.A., Cannan, T.R., and Flanigen, E. M., J. Am. Chem. Soc., 104, 1146 (1982).

49. Wu, E. L., Lawton, S. L., Olson, D. H., Rohrman, Jr., A. C. and Kokotailo, G.T., J. Phys. Chem., 83, 21, 2777 (1979).

50. Smith, J.V., Acta Crystallogra., 15, 835 (1962).

51. Erdem, A., M.S. Thesis, Worcester Polytechnique Institute, USA, 1978.

52. Culfaz,A., and Sand, L. B., Adv. Chem. Ser., 121, 140 (1973).

53. Chao, N. J., Tasi, T.C., Chen, N.S. and Wang, I., J. Chem. Soc. Faraday Trans. I, 77, 547 (1981).

53 a. Kulkarni, S. B., Shiralkar, V. P., Kotasthane, A. N., Borade, R.B. and Ratnasamy, P., Zeolite, 313 2, 313 (1982).

54. Bibby, D. M., Aldridge, L. P. and Milestone, N.B., J. Cat., 72, 373 (1981).

55. Pollack, S.S., Adkins, J.W., Wetzel, E. L. and Newbury, D., Zeolite, 4 (2) 1984

56. Laves, F., Hafner, S., Norsk, Geol. Tidsski., 42, 57, (1962)

57. Wright, A.C., Rupert, J. P., Granquist, W. T., Am. Mineralogist, 53, 1293, (1968).

58. Zhdanov, S. P., Kiseler, A. V., Lygin, V. I., Titova, T. I., Russ. J. Phys. Chem., 38, 1299 (1964).

59. Flanigen, E. M. and Khatami, H., Adv. Chem. Ser., 101, 201 (1971).

60. Flanigen, E. M., Grose, R.W., Adv. Chem. Ser., 101, 76 (1971).

61. Wu, E. L., Kuhl, G. H., Whyte, T.E. Jr., Venuto, P.B., Adv. Chem. Ser., 101, 490 (1971).

62. Hatada, K., Ono, Y., and Ushik, Y., J. Phys. Chem., 37, 117 (1979).

63. Nagy, J.B., Gigot, M., Gourgue, A. and Derouane, E.G., J. Mol. Catal., 2, 265 (1977).

64. Topsøe, N., Pendersen, K., Derouane, E.G., J. Catal., 70, 41 (1981).

65. Vedrine, J.C., Auroux, A., Bolis, V., Dejaifve, P., Naccache, C., Wierzchowski, P., Derouane, E.G., Nagy, J. B., Gilson, J. P., Van Hooff J. H. C., Van Den Berg, J. P. and Wolthuizen, J. P., J. Catal., 59, 248 (1979).

66. Boxhoorn, G., Van Santen, R. A., Van Erp, W. A., Hays, G.R., Huis, R., and Clague, D. H., J. Chem. Soc., Chem. Comm., 264,(1982)

67. Nagy, J. B., Gabelica, Z. and Derouane, E.G., Zeolite, 3 (1), (1983).

68. Scholle, K. F. M. G. J., Veeman, W.S., Post, J.G. and Van Hooff, J.H.C., Zeolite, 3(3), 214-218 (1983).

69. Boxhoorn, G., Kortbeek, A.G.T.G., Hays, G.R., Alma, N.C.M., Zeolite 4 (1), 15-21 (1984).

70. Lippmaa, E., Mägi, M., Samoson, A., Engelhardt, G., and Grimaa, A.R., J. Am. Chem. Soc., 102, 4889 (1980).

71. Fyfe, C.A., Gobbi, G.C., Klinowski, J., Thomas, J.M. and Ramdas, S., Nature, 296, 530 (1982).

72. Klinowski, J., Thomas, J. M., Fyfe, C.A., Gobbi, G.C., Nature, 296, 533 (1982).

73. Higgins, J.B., Woessnev, D.E., Trewella, J.C. and Schlenker, J. L., Zeolite 4(2), 112-13 (1984).

74. Auroux, A., Bolis, V., Wierzchowski, P.C., Gravelle, P.C. and Vedrine, I.C., J. Chem. Soc. Faraday Trans. I, 75, 2544 (1979)

75. Anderson, J.R., Foger, K., Mole, T., Rajadhyaksha, R. A. and Senders, J.V., J. Catal., 58, 114 (1979).

76. Jacobs, P.A., Utterhoeven, J.B., Steyns, M., Froment, G. and Weitkamp, J., "Proceedings, 5th International Conf. on Zeolites", Naples, Italy, Y Heyden and Sons, London, 607 (1980).

77. Topsøe, N. Y., Pendersen, K. and Derouane, E.G., J. Catal., 70, 41 (1981).

78. Breck, D.W., "Zeolite Molecular Sieves", John Wiley and Sons, New York, 449 (1974).

79. Nakamoti, H. and Takahashi, H., Chemistry Letters, 1013 (1981).

80. Barrer, R. M., Proc. Roy. Soc., A, 167, 392 (1938).

81. Barrer, R. M., Quart. Review, London, 3293 (1949).

82. Barrer, R. M., and Breck, D.W., Trans. Faradays Soc., 46, 853 (1950).

83. Barrer, R. M., and Gibbson, R. M., Trans. Faradays Soc., 59, 2569 (1963).

84. Barrer, R. M., Pure and Appl.Chem., 52, 2143 (1980).

85. Derouane, E.G. and Gabelica, Z., J. Catal., 65, 486 (1980).

86. Jacobs, P.A., Bayer, H. K. and Valyon, J., Zeolite, Vol. 1, 161-168 (1981).

87. Meisel, S. L., McCullough, J. P., Lechthalev, C. H. and Weisz, P.B., ACS meeting, Chicago, I, 11 (1977).

88. Weisz, P.B., Pure and Appl. Chem., 52, 2091 (1980).

89. Olson, D. H., Haag, W. O. and Lago, R. M., J. Catal., 61, 390 (1980)

90. Weisz, P.B. and Frilette, V. J., J. Phys. Chem., 64, 382 (1960)

91. Derouane, E.G., "Catalysis by Zeolite" (Ed. Imelik, B)", 5, (1980).

92. Csicsery, S. M. "Zeolite Chemistry and Catalysis", (Ed. Rabo, J.A.), ACS Monograph 171, 680 (1976)

93. Weisz, P.B., Frilette, V. J. Mattman, R.W. and Mowev, E.B., J. Catal., 1, 307 (1962).

94. Rabo, J. A., Bezman, R.D. and Poustma, M. L., Acta Phys. Chem., 24, 39 (1978).

95. Chen, N. Y., Garwood, W.E., J. Catal., 52, 453 (1978).

96. Chen, N. Y., Kaeding, W.W. and Dwyer, F.G., J. Am. Chem. Soc., 101, 6783 (1979).

97. Chen, N. Y., Garwood, W.E., Haag, W.O. and Schwartz, A. B., - paper presented at Symposium on Advances in Catalytic Chemistry, Oct. 3-5, 1979, Snobird, Utah.

98. Chang, C.C. and Silvestri, A.J., J. Catal., 47, 249 (1977).

99. Weisz, P.B., Haag, W.O. and Rodewald, P.G., Science, 206, 57 (1979).

100. Obermyer, R.T., Mulay, L. N., Oskooie-Tabrize, M. and Rao, V.U.S., J. Appl. Phys., 53(3), 2683-85 (1982).

101. Barrer, R. M. and White, E.A.D., J. Chem. Soc., 156 (1961).

102. Regis, A.I., Sand, L.B., Calmon, C. and Gilwood, M.E., J. Phys. Chem, 64, 1567 (1980).

103. Schwochow, F.E. and Heinze, G.W., Adv. Chem. Ser., 101, 102 (1971).

104. Lok, B. M., Cannan, T.R. and Messina, Zeolite, Vol. 3, 282 (1983).

105. Fyfe, W.S., J. Geol., 61, 553 (1960).

106. Breck, D.W., "Zeolite Molecular Sieve", John Wiley and Sons, N. Y., 1974, p. 267.

107. Sand, L.B., Private communication.

108. Lowe, B.M., Zeolite, Vol. 3, 300-305 (1983).

109. Jacobs, P.A., Derouane, E.G. and Weitkamp, P., J. Chem.Soc. Chem. Communication, 591 (1981).

110. Deelee, H. J., Hearing, J., Riekert, L. and Marosi, L., J. Catal., 71, 27 (1981).

111. Mostowich, R. and Sand, L.B., Zeolite, 2, 143 (1982).

112. a: Avarami, M., J. Chem. Phys., 9, 117 (1941).

b: Erofeev, B.V., C.R. Acad. Sci., USSR, 52, 511 (1946).

113. a: Borade, R.B., "Synthesis and Characterization of ZSM-5 Zeolites" Ph.D. Thesis, Pune Univ., July, 1983.

b: Borade, R.B., Chandwadkar, A.J., Kulkarni, S.B., and Ratnasamy, P., Ind. J. Technology, Vol. 21, 9, 358 (1983).

114. Gamami, M. and Sand, L.B., Zeolite, 3, 155 (1983).

115. Nakamoti, H. and Takahashi, H., Chemistry Letters, 1739 (1981).

116. Derouane, E.G., Nagy, J. B., Gabelica, Z. and Blom, N., Zeolite, 2, 299 (1982).

117. Derouane, E.G., Detremmerie, S., Gabelica, Z. and Blom, N., Appl. Catal., 1, 201 (1981).

118. Flanigen, E.M., Pure and Appl. Chem., 52, 2191 (1980).

119. Rollman, L.D., Inorganic Compounds with unusual Properties", Vol. II, Ed. King, R. B., ACS, New York, 387 (1979).

120. Gabelica, Z., Derouane, E.G. and Blom, N., Appl. Catal., 5, 109 (1988).

120. a: Nastro, A., Sand, L.B., Zeolites, 3, 57 (1983).

121. Howden, M.G., CSIR Report, CENG 413, Southe Africa, 1982.

122. Hagiwara, H., Kiyozurni, Y., Kurita, M., Sato, T., Shimada, H., Suzuki, K., Sahin, S. Nishijima and Todo, N., Chem. Letters, 1653 (1981).

123. Hanawalt, J.D., Rin, H. W. and Frevel, L.K., Ind. Eng. Chem., 10, 457 (1938).

123. a: Nicoletti, M.P. and Van Kirk, J.F., U.S. Patent 4,159,283 (1979); H_a
Hagg, W.O. and R.M. Lago, Eur. Pat. 34,444 (1981).

124. Agashe, M.S., Jose, C.I., J. Chem. Soc., Faraday Trans. II, Vol. 75, 733 (1979).

125. Chao, K. J., Proc. Natl. Sci. Counc., ROC, 3, 233 (1979).

126. Bibby,D.M., Milestone, N.B. and Aldrige, L. P., Nature, 285, 30 (1980).

127. Musker, W. K., J. Amer. Chem. Soc., 86, 960 (1964).

128. Whyte, T.E., Wu, E. L., Keer, G.T. and Venuto, P.B., J. Catal., 20, 88 (1971).

129. Aiello, A. and Barrer, R.M., J. Chem. Soc. A, 1470 (1970).

130. Flanigen, E.M., "Proc. 5th Internatl. Conf. Zeolites", Naples, 1980 (Ed. L.V.C. Rees), Heyden and Sons, London, p. 760 (1980).

131. Von Ballmoos, R., Ph.D. Thesis, Zurich Univ., Zurich, 1981.

132. Gabelica, Z., Derouane, E.G. and Blom, N., ACS Symposium Symposium Series No. 248, on "Catalytic Materials : Relationship between Structure and Reactivity", pp. 220 (1984).

133. Rollmann, L.D., Valyocski, E.W., Eur. Patent, 21674 and 21,675 (1981).

134. McNicol, B. D., Pott, G.T. and Loos, K.R., J. Phys. Chem., 76, 3388 (1972), Adv. Chem. Ser., 121, 153 (1973).

135. Cournoyer, R.A., Kranich, W.L. and Sand, L.B., J. Phys. Chem., 79, 1578 (1975).

136. Kacirek, H. and Lechert, H., J. Phys. Chem., 79, 1589 (1975).

137. Barrer, R. M., J. Chem. Soc., 198 (1959).

138. Dwyer, F.G. and Chu, P., J. Catal., 59, 263 (1979).

139. Tsitsishvili, G.V. and Andronikashvili, T.G., Adv. Chem. Ser., 102, 217 (1971).

140. Ballivet, D., Pichat, P. and Barthomeuf, Adv. Chem. Ser., 121, 469 (1973).

141. Johnson, M.F.L., J. Catal., 52, 425 (1978).

142. Tsitsishvili, G.V., Adv. Chem. Ser., 121, 291 (1973).

143. Smith, J.V., Adv. Chem. Ser., 101, 171 (1971).

144. McDaniel, C.V. and Maher, P.K., "Molecular Sieves", Soc. Chem. Ind., London, 186 (1968).

145. Meisel, S.L., McCullough, J.P., Lechthalev, C. H., and Weisz, P.B., Chem. Tech., 6, 86 (1976).

146. Breck, D. W., "Zeolite Molecular Sieves", John Wiley and Sons, New York, 259 (1974).

147. Babu, G. P., Ph. D. Thesis, Pune University, India (1983).

148. Olson, D. H., Kokotailo, G.T., Lowton, S. L., and Meier, W. M., J. Phy. Chem., 85, 2238 (1981).

149. Keer, G. T., Adv. Chem. Ser., 121, 219 (1973).

150. Temper, J. F., Delafosse, D. and Contoux, J.P., ACS Symp. Ser., 40, 76 (1977).

151. Vedrine, J.C., Dufoux, M., M Naccache, C. and Imelik, B., J. Chem. Soc. Faraday Trans. I,, 74, 440 (1972).

152. Kulkarni, S. J., Badrinarayanan, S. and Kulkarni, S. B., J. Catal., 75, 423 (1982).

153. Van Ballmoss, R. and Meier, W.M., Nature, 289, 782 (1981).

154. Wagner, C.D., Anal.Chem., 44, 1050 (1972).

154. a: Stencel, J. M., Diehl, J.R., Douglas, L. J., Spitler, C.A., Crowford, J.E. and Nelson, G.A., Colloids and Surfaces, 4, 331 (1982).

155. Derouane, E.G., Mestdagh, M. and Vielyove, L., J. Catal., 33, 169 (1974).

156. McNicol, B.D. and Pott, G.T., J. Catal., 25, 223 (1972).

157. Wichterlova, B., Zeolite, 1, 181 (1981).

158. Wichterlova, B. and Jiru, P., React. Kinet. Catal., Lett., 13, 197 (1980).

159. Castev, T. Jr., Newell, G.S., Holton, W.C. and Silchtev, C.P., J. Chem. Phys., 32, 668 (1980).

160. Griffith, J.S., J. Mol. Phys., 8, 213 (1964).

161. Lahodny-Sarac, O. and White, J. L., J. Phys. Chem., 75, 2408 (1971).

162. Flanigen, E. M., Khatami, H. and Szymanski, H.A., Adv. Chem. Ser., 101, 201 (1971).

163. Pichat, P., Beaumont, R. and Barthomeuf, D., J.Chem. Soc. Faraday Trans. I, 70, 1402 (1974).

164. Jacobs, P.A., J. Phys. Chem., 86, 3050 (1982).

165. Sayed, O. M. B., Kydd, R.A., Cooney, R. P., J. Catal., 88, 137 (1984).

166. Lone, K. G., Echevskii, G.V. and Nosyreva, G. N., J. Catal., 85, 287 (1984).

167. Scholle, K. E. M. G. J., J. Phy. Chem., 88, 5 (1984).

168. Keading, W. W., Butter, S.A., J. Catal., 61, 155 (1980).

169. Balkrishnan, I., Rao, B.S., Hegde, S.G., Kotasthane, A. N., Kulkarni, S.B. and Ratnasamy, P., J. Molecular Catalysis, 17, 261 (1982).

170. Murthy, K. R., Halgeri, A.B. and Prasad Rao, T.S.R., Ind. J. Technology, 21, 379 (1983).

171. Ione, K. G., Vostrikova, L.A., Pestrova, A.V., Mustikhin, V. M., Proceedings of 8th International Congress on Catalysis, Berlin, 2-6 July, 1984.

172. G. Prakash Babu, Kulkarni, S.B. and Ratnasamy, P., J. Catal., 79, 215 (1983).

173. Morrison, R.A., U. S. Patent, 3,856,872 (1974).

174. Jacobs, P. A., Leeman, H. E., Uytterhoeven, J. B., J. Catal., 33, 17 and 31 (1974).

175. Jacobs, P.A., Declerck, L. J., Uytterhoeven, J. B., J. Chem. Soc. Faraday Tran. I, 71, 1545 (1975).

176. Tarramasso, M., Perego, G. and Notari, B., Proc. 5th Intnatl. Conf. on Zeolites, Ed. L.V. C. Rees, Heyden, London, 1980.

177. Derouane, E. G., Nagy, J. B., Dejaifve, P., Van Hooff, J. H. C., Spekman, B. P., Vedrine, J. C., Naccahe, C., J. Catal., 40 (1978).

178. Anderson, J. R., Foger, K., Mole, T., Rajadhyaksha, R. A. and Sanders, J. V., J. Catal., 58, 114 (1979).

179. Pearson, D. E., J. Chem. Soc., Chem. Commun., p.397 (1974).

180. Olah, G.A., Schlosberg, R. H., J. Am. Chem. Soc., 90, 2726 (1968).

181. Van den Berg, J. P., Wolthuizen, J. P. and Van Hooff J. H. C., Proc. Vth Conf. Zeolites, Naples, Italy, 1980, p. 649.

182. Venuto, P.B., and Landis, P. S. L., Adv. Catal., 18, 259 (1968).

183. Pines, H., The Chemistry of Catalytic Hydrocarbons, Academic, New York, 1981.

---000---